NORSAR Scientific Report No. 1-2006

Semiannual Technical Summary

1 July - 31 December 2005

Frode Ringdal (ed.)

Kjeller, January 2006

REPORT DOCUMENTATION PAGE

Form Approved
OMB No. 0704-0188

1. REPORT DATE *(DD-MM-YYYY)*	2. REPORT TYPE	3. DATES COVERED *(From - To)*
15-02-2006	Semiannual Technical Summary	1 July - 31 December 2005

4. TITLE AND SUBTITLE
Semiannual Technical Summary, 1 July - 31 December 2005

5a. CONTRACT NUMBER
F08650-01-C-0055

5b. GRANT NUMBER

5c. PROGRAM ELEMENT NUMBER
NDC Support / R&D

6. AUTHOR(S)
Frode Ringdal (Ed.)

5d. PROJECT NUMBER
T/0155, NORSAR Phase 3

5e. TASK NUMBER
SOW Task 4.3

5f. WORK UNIT NUMBER
CDRL sequence nos. A001-A004

7. PERFORMING ORGANIZATION NAME(S) AND ADDRESS(ES)
Stiftelsen NORSAR
Post Box 53
NO-2027 Kjeller
Norway

8. PERFORMING ORGANIZATION REPORT NUMBER
Scientific Report No. 1-2006

9. SPONSORING/MONITORING AGENCY NAME(S) AND ADDRESS(ES)
AFTAC/TTS, 1030 South Highway A1A MS 1000, Patrick AFB, FL 32925-3002

Army Space and Missile Defense Command , 1515 Wilson Blvd., Suite 720
Arlington, VA 22209

10. SPONSOR/MONITOR'S ACRONYM(S)
AFTAC/TTS & USASMDC

11. SPONSOR/MONITOR'S REPORT NUMBER(S)

12. DISTRIBUTION/AVAILABILITY STATEMENT
Approved for public release; distribution unlimited

13. SUPPLEMENTARY NOTES

14. ABSTRACT

This report describes the research activities carried out at NORSAR under Contract No. F085650-01-C-0055 for the period 1 July-31 December 2005. In addition, it provides summary information on operation and maintenance (O&M) activities at the Norwegian National Data Center (NDC) during the same period. Research activities described in this report are largely funded by the United States Government, and the United States also covers the cost of transmission of selected data to the United States NDC. The O&M activities, including operation and transmission links within Norway and to Vienna, Austria, are being funded jointly by the CTBTO/PTS and the Norwegian Government, with the understanding that the funding of O&M activities for primary stations in the International Monitoring System (IMS) will gradually be transferred to the CTBTO/PTS. The O&M statistics presented in this report are included for the purpose of completeness, and in order to maintain consistency with earlier reporting practice.
(cont.)

15. SUBJECT TERMS
NORSAR, Norwegian Seismic Array

16. SECURITY CLASSIFICATION OF:			17. LIMITATION OF ABSTRACT	18. NUMBER OF PAGES	19a. NAME OF RESPONSIBLE PERSON
a. REPORT	b. ABSTRACT	c. THIS PAGE			SSgt Joshua W. Bricker, AFTAC/TTS
U	U	U	SAR	85	19b. TELEPHONE NUMBER *(Include area code)* (321) 494-9471

Reset

Standard Form 298 (Rev. 8/98)
Prescribed by ANSI Std. Z39.18

Abstract (cont.)

The NOA Detection Processing system has been operated throughout the period with an uptime of 100%. A total of 2,481 seismic events have been reported in the NOA monthly seismic bulletin during the reporting period. On-line detection processing and data recording at the NDC of data from ARCES, FINES, SPITS and HFS data have been conducted throughout the period. Processing statistics for the arrays for the reporting period are given.

A summary of the activities at the Norwegian NDC and relating to field installations during the reporting period is provided in Section 4. Norway is now contributing primary station data from two seismic arrays: NOA (PS27) and ARCES (PS28), one auxiliary seismic array SPITS (AS72), and one auxiliary three-component station (JMIC). These data are being provided to the IDC via the global communications infrastructure (GCI). Continuous data from the three arrays are in addition being transmitted to the US_NDC. The performance of the data transmission to the US_NDC has been satisfactory during the reporting period.

Summaries of five scientific and technical contributions are presented in Chapter 6 of this report.

Section 6.1 is entitled "Research in Regional Seismic Monitoring". It summarizes a presentation at the 27th Seismic Research Review, giving an overview of selected topics in the continuing research effort at NORSAR aimed at improving seismic monitoring tools at regional distances. The first topic is the use of the large-aperture NORSAR array for automatic processing of regional phases. We describe a new processing system which represents a significant improvement over previous processing systems for this large array, and opens up interesting possibilities for improved automatic detection and location using local or regional networks. The second topic is a continued study of combining seismic and infrasonic recordings for detection and characterization of seismic events at local and regional distances. Here, we present results from analysis of several recent surface explosions in the Kola peninsula near the Norwegian border. The third topic concerns an initial investigation of the potential of obtaining improved detection of small seismic events by the use of waveform correlation in conjunction with array processing. We present examples of use of the array-based correlation technique in detecting the small (m_b=2.5) aftershock of the 16 August 1997 Kara Sea event..

Section 6.2 is entitled "Surface Wave Tomography for the Barents Sea and Surrounding Regions - Part II". This paper is a continuation of an initial study presented in the previous Semiannual Technical Summary. Existing global and regional tomographic models have limited resolution in the European Arctic due to the small number of seismic stations, relatively low regional seismicity, and limited knowledge of the crustal structure. During the last decades, new seismic stations have been permanently or temporarily installed in and around this region. The substantial data set of new surface group-velocity measurements combined with already existing data has provided the opportunity for constructing a new 3D shear-velocity model of the crust and upper mantle down to about 250 km beneath the European Arctic. This model has higher spatial and depth resolution than previous models and clarifies or reveals important features of the tectonic setting in the region: continent-ocean boundary, a dipping slab-like high velocity zone in the upper mantle and the lithospheric structure under the deep sedimentary basin.

Section 6.3 is entitled "Infrasound data processing using Apatity and ARCES array data". In this study, we have focused on developing basic infrasonic processing software for the Apatity

infrasonic array and for the ARCES seismic array. In the case of ARCES, there are currently no infrasonic sensors available, but the seismic sensors have proved useful as an initial substitute for detecting and processing infrasonic signals from explosions at local and regional distances. We have also developed an algorithm for associating detected infrasonic phases (either by ARCES or Apatity) to regional seismic events generated in the on-line Generalized Beamforming process which is currently in experimental operation at NORSAR. We have developed an initial set of association criteria, and applied them to about one full year (2005) of data. We found that 944 infrasound signals could be associated with 651 different events of the GBF bulletin. For these 651 events, 333 events could be associated only with infrasound signals observed at the Apatity infrasound array, 250 events could be associated only with infrasound signals observed at the ARCES seismic array and 68 events could be associated with infrasound signals at both arrays.

Section 6.4 contains a continued study of combining seismic and infrasonic recordings for detection and characterization of seismic events at local and regional distances. We present results from an analysis of 108 surface explosions in northern Finland in 2001-2005. Infrasonic signals from these explosions were well recorded on the infrasound array in Apatity and also clearly recorded on the seismic sensors at the ARCES and Apatity arrays. Applying waveform cross-correlation to the ARCES seismic array data we found extremely high correlation coefficients for this data set. This indicates that these explosions are all very closely spaced, probably within an area of some hundreds of meters in diameter. We have used this database to study the stability of slowness estimates for both seismic and infrasonic phases, using ARCES and Apatity array recordings. Our analysis of seismic P-phase observations confirm the stability of fixed-frequency band f-k analysis previously noted by several investigators. Furthermore, by analyzing various sub-configurations of the ARCES array, we find that the scatter (standard deviation) in the azimuth estimates for the explosions is about inversely proportional to array aperture. When carrying out a similar analysis of infrasonic data, we find some interesting differences. In contrast to the case for the seismic P-waves, the azimuth scatter found by our f-k estimation process does not decrease when the array aperture increases. Furthermore, the average azimuth remains the same both with varying array aperture and with varying filter bands. This is also in contrast to what we have observed for the seismic P-waves.

Section 6.5 contains a study of moment tensor inversion for regional seismic events in Fennoscandia and adjacent regions. We have investigated various algorithms to accomplish robust moment tensor inversions for regional events with magnitudes of 4.0 – 4.5, and applied these programs to three regional earthquakes observed in Fennoscandia. In general, surprisingly good results were obtained for the regional moment tensor inversion of two of the earthquakes (the 14 April 2004 Jan Mayen and the 04 July 2003 Svalbard events), although the azimuthal coverage is generally not very good when using only regional data directly available at NORSAR. In case of the 07 April 2004 Flisa earthquake, moment tensor inversions proved to be more difficult. It appears that more stations may have to be used to better constrain the auxiliary plane. Even short-period stations may be included, since due to its small size, the high-frequency content of the recordings is unusually large compared to the Jan Mayen and Svalbard events. The velocity model for Fennoscandia used at first turned out to be too simple for this regional inversion and had to be adjusted by trial-and-error fitting of synthetic to observed seismograms to improve the modelling of surface wave dispersion.

AFTAC Project Authorization	:	T/0155/PKO
ARPA Order No.	:	4138 AMD # 53
Program Code No.	:	0F10
Name of Contractor	:	Stiftelsen NORSAR
Effective Date of Contract	:	1 Feb 2001 (T/0155/PKO)
Contract Expiration Date	:	28 February 2006
Project Manager	:	Frode Ringdal +47 63 80 59 00
Title of Work	:	The Norwegian Seismic Array (NORSAR) Phase 3
Amount of Contract	:	$ 2,933,442.58
Period Covered by Report	:	1 July - 31 December 2005

The research presented in this report was supported by the Army Space and Missile Defense Command and was monitored by AFTAC, Patrick AFB, FL32925, under contract no. F08650-01-C-0055. Other sponsors are acknowledged where appropriate.

The operational activities of the seismic field systems and the Norwegian National Data Center (NDC) are currently jointly funded by the Norwegian Government and the CTBTO/PTS, with the understanding that the funding of IMS-related activities will gradually be transferred to the CTBTO/PTS.

NORSAR Contribution No. 970

Table of Contents

Page

1 Summary

This report describes the research activities carried out at NORSAR under Contract No. F08650-01-C-0055 for the period 1 July - 31 December 2005. In addition, it provides summary information on operation and maintenance (O&M) activities at the Norwegian National Data Center (NDC) during the same period. Research activities described in this report are largely funded by the United States Government, and the United States also covers the cost of transmission of selected data to the US NDC. The O&M activities, including operation of transmission links within Norway and to Vienna, Austria are being funded jointly by the CTBTO/PTS and the Norwegian Government, with the understanding that the funding of O&M activities for primary stations in the International Monitoring System (IMS) will gradually be transferred to the CTBTO/PTS. The O&M statistics presented in this report are included for the purpose of completeness, and in order to maintain consistency with earlier reporting practice.

The seismic arrays operated by the Norwegian NDC comprise the Norwegian Seismic Array (NOA), the Arctic Regional Seismic Array (ARCES) and the Spitsbergen Regional Array (SPITS). This report presents statistics for these three arrays as well as for additional seismic stations which through cooperative agreements with institutions in the host countries provide continuous data to the NORSAR Data Processing Center (NDPC). These additional stations include the Finnish Regional Seismic Array (FINES) and the Hagfors array in Sweden (HFS).

The NOA Detection Processing system has been operated throughout the period with an uptime of 100%. A total of 2,481 seismic events have been reported in the NOA monthly seismic bulletin during the reporting period. On-line detection processing and data recording at the NDC of data from ARCES, FINES, SPITS and HFS data have been conducted throughout the period. Processing statistics for the arrays for the reporting period are given.

A summary of the activities at the Norwegian NDC and relating to field installations during the reporting period is provided in Section 4. Norway is now contributing primary station data from two seismic arrays: NOA (PS27) and ARCES (PS28), one auxiliary seismic array SPITS (AS72), and one auxiliary three-component station (JMIC). These data are being provided to the IDC via the global communications infrastructure (GCI). Continuous data from the three arrays are in addition being transmitted to the US_NDC. The performance of the data transmission to the US_NDC has been satisfactory during the reporting period.

So far among the Norwegian stations, the NOA and the ARCES array (PS27 and PS28 respectively) and the radionuclide station at Spitsbergen (RN49) have been certified. Provided that adequate funding continues to be made available (from the PTS and the Norwegian Ministry of Foreign Affairs), we envisage continuing the provision of data from these and other Norwegian IMS-designated stations in accordance with current procedures. The IMS infrasound station at Karasjok (IS37) is expected to be built in the fall of 2006, provided that the local authorities grant the permissions required for the establishment of the station.

Summaries of five scientific and technical contributions are presented in Chapter 6 of this report.

Section 6.1 is entitled “Research in Regional Seismic Monitoring”. It summarizes a presentation at the 27th Seismic Research Review, giving an overview of selected topics in the continuing research effort at NORSAR aimed at improving seismic monitoring tools at regional distances. The first topic is the use of the large-aperture NORSAR array for automatic processing of regional phases. We have recently completed a new processing system for incorporating

regional seismic phases detected by the large NORSAR array into the Generalized Beamforming process currently in use at NORSAR for on-line automatic detection and location of seismic events in the European Arctic. The system employs a multitaper method to calculate continuous spectra of the waveforms and detects changes in spectral content consistent with regional phases propagating across the array. It represents a significant improvement over previous processing systems for this large array, and opens up interesting possibilities for improved automatic detection and location using local or regional networks.

The second topic is a continued study of combining seismic and infrasonic recordings for detection and characterization of seismic events at local and regional distances. We present results from analysis of several recent surface explosions in the Kola peninsula near the Norwegian border. We used the recordings to make a location estimate based upon the infrasonic detections (on the seismic sensors) at these two arrays, and found that the locations matched closely the locations obtained through standard seismic data analysis. This indicates an interesting potential for joint two-array infrasonic processing, and this concept will be further developed once the IMS infrasound array near ARCES has been established (expected in 2006).

The third topic concerns an initial investigation of the potential of obtaining improved detection of small seismic events by the use of waveform correlation in conjunction with array processing. We present examples on the power of the array-based correlation technique, demonstrating that waveform correlation could be used to detect the small aftershock (m_b=2.5) following the 16 August 1997 Kara Sea event, not only at the Spitsbergen array (distance 1100 km), but even at the large NORSAR array situated more than 2300 km from the epicenter.

Section 6.2 is entitled “Surface Wave Tomography for the Barents Sea and Surrounding Regions - Part II”. This paper is a continuation of an initial study presented in the previous Semiannual Technical Summary. Existing global and regional tomographic models have limited resolution in the European Arctic due to the small number of seismic stations, relatively low regional seismicity, and limited knowledge of the crustal structure. During the last decades, new seismic stations have been permanently or temporarily installed in and around this region. The substantial data set of new surface group-velocity measurements combined with already existing data has provided the opportunity for constructing a new 3D shear-velocity model of the crust and upper mantle down to about 250 km beneath the European Arctic.

This model has higher spatial and depth resolution than previous models and clarifies or reveals important features of the tectonic setting in the region: continent-ocean boundary, a dipping slab-like high velocity zone in the upper mantle and the lithospheric structure under the deep sedimentary basin.

Ritzwoller *et al.* (2003) derived source specific travel-time corrections (SSSCs) based on a 3D tomographic surface-wave model. The new 3D velocity model presented here may be used for refining these corrections for regional P and S waves propagating through the larger Barents Sea region.

Section 6.3 is entitled “Infrasound data processing using Apatity and ARCES array data”. In this study, we have focused on developing basic infrasonic processing software for the Apatity infrasonic array and for the ARCES seismic array. In the case of ARCES, there are currently no infrasonic sensors available (the plans are to install an infrasound array in 2006), but the seismic sensors have proved useful as an initial substitute for detecting and processing infrasonic signals from explosions at local and regional distances.

We have also developed an algorithm for associating detected infrasonic phases (either by ARCES or Apatity) to regional seismic events generated in the on-line Generalized Beamforming process which is currently in experimental operation at NORSAR. The following association criteria were used to correlate seismic events with presumed, corresponding infrasound signals:

- The epicentral distance of the event must be within 500 km from the array.
- The possible onset time of the infrasound signals was set to be within the time window spanned by group velocities between 0.2 and 0.7 km/s.
- The difference between the event backazimuth and the backazimuth observed for the infrasound signal should not be larger than 20 degrees.

Applying these rules to about one full year of data (the year 2005), we found that 944 infrasound signals could be associated with 651 different events of the GBF bulletin. For these 651 events we obtained the following statistics:

- 333 events could be associated only with infrasound signals observed at the Apatity infrasound array.
- 250 events could be associated only with infrasound signals observed at the ARCES seismic array.
- 68 events could be associated with infrasound signals at both arrays, the ARCES seismic array and the Apatity infrasound array.

We plan in the future to compare in more detail the infrasound observations with analyst reviewed event locations. This will require a review by an analyst of each infrasound signal, in order to confirm their validity and to identify possible misassociations if appropriate.

Section 6.4 contains a continued study of combining seismic and infrasonic recordings for detection and characterization of seismic events at local and regional distances. We present results from an analysis of 108 surface explosions in northern Finland in 2001-2005. These explosions were presumably carried out for the purpose of destroying old ammunition, and generated unusually strong infrasonic signals in addition to seismic signals. These infrasonic signals were well recorded on the infrasound array in Apatity and also clearly recorded on the seismic sensors at the ARCES and Apatity arrays.

Waveform cross-correlation applied to ARCES seismic array data results in extremely high correlation coefficients for this data set. This indicates that these explosions are all very closely spaced, probably within an area of some hundreds of meters in diameter. The waveform cross-correlation method has also been used to determine very accurate origin times for the explosions. This database will be highly valuable for various studies related to obtaining improved accuracy in detecting and characterizing seismic events using regional array recordings at local distances.

In the present paper, we have used this database to study the stability of slowness estimates for both seismic and infrasonic phases, using ARCES and Apatity array recordings. Our analysis of seismic P-phase observations confirm the stability of fixed-frequency band f-k analysis previously noted by several investigators. Furthermore, by analyzing various sub-configurations of the ARCES array, we find that the scatter (standard deviation) in the azimuth estimates for the explosions is about inversely proportional to array aperture.

When carrying out a similar analysis of infrasonic data, we find some interesting differences. In contrast to the case for the seismic P-waves, the azimuth scatter found by our f-k estimation process does not decrease when the array aperture increases. Furthermore, the average azimuth remains the same both with varying array aperture and with varying filter bands. This is also in contrast to what we have observed for the seismic P-waves.

Section 6.5 contains a study of moment tensor inversion for regional seismic events in Fennoscandia and adjacent regions. Although moment tensor inversion is routinely applied by miscellaneous institutions for teleseismic events, it is rarely exerted in the case of weaker regional events with magnitudes of about 4.0. The reason for this is that regional earthquakes possess higher frequencies and reliable regional velocity models of crust and upper mantle are required. In this study we have investigated various algorithms to accomplish robust moment tensor inversions for regional events with magnitudes of 4.0 – 4.5, and applied these programs to three regional earthquakes observed in Fennoscandia.

In general, surprisingly good results were obtained for the regional moment tensor inversion of two of the earthquakes (the 14 April 2004 Jan Mayen and the 04 July 2003 Svalbard events), although the azimuthal coverage is generally not very good when using only regional data directly available at NORSAR. The most critical working step is the alignment of seismograms and Green's functions along with determining the length of the phase phase analysis window. The longer the phase analysis window, the more information is contained, but at the same time, the risk of overlapping with further phases not aligned correctly in time due to an insufficient velocity model is larger.

In case of the 07 April 2004 Flisa earthquake, moment tensor inversions proved to be more difficult. It appears that more stations may have to be used to better constrain the auxiliary plane. Even short-period stations may be included, since due to its small size, the high-frequency content of the recordings is unusually large compared to the Jan Mayen and Svalbard events.

The velocity model for Fennoscandia used at first turned out to be too simple for this regional inversion and had to be adjusted by trial-and-error fitting of synthetic to observed seismograms to improve the modelling of surface wave dispersion.

Frode Ringdal

2 Operation of International Monitoring System (IMS) Stations in Norway

2.1 PS27 — Primary Seismic Station NOA

The mission-capable data statistics were 100%, the same as for the previous reporting period. The net instrument availability was 99.473%.

There were no outages of all subarrays at the same time in the reporting period.

Monthly uptimes for the NORSAR on-line data recording task, taking into account all factors (field installations, transmissions line, data center operation) affecting this task were as follows:

		Mission Capable	Net instrument availability
July	:	100%	99.799%
August	:	100%	99.982%
September	:	100%	98.199%
October	:	100%	99.706%
November	:	100%	99.210%
December	:	100%	99.688%

J. Torstveit

NOA Event Detection Operation

In Table 2.1.1 some monthly statistics of the Detection and Event Processor operation are given. The table lists the total number of detections (DPX) triggered by the on-line detector, the total number of detections processed by the automatic event processor (EPX) and the total number of events accepted after analyst review (teleseismic phases, core phases and total).

	Total DPX	Total EPX	Accepted Events		Sum	Daily
			P-phases	Core Phases		
July	7,119	950	457	94	551	17.8
Aug	7,701	809	311	49	360	11.6
Sep	9,815	832	303	51	354	11.8
Oct	11,360	1,133	540	47	587	18.9
Nov	9,912	768	255	58	313	10.4
Dec	11,839	836	253	63	316	10.2
	57,746	5,328	2,119	362	2,481	13.5

Table 2.1.1. *Detection and Event Processor statistics, 1 July - 31 December 2005.*

NOA detections

The number of detections (phases) reported by the NORSAR detector during day 182, 2005, through day 365, 2005, was 57,746, giving an average of 313 detections per processed day (184 days processed).

B. Paulsen

U. Baadshaug

2.2 PS28 — Primary Seismic Station ARCES

The mission-capable data statistics were 99.287%, as compared to 98.197% for the previous reporting period. The net instrument availability was 99.105%.

The main outages in the period are presented in Table 2.2.1.

Day	Period
23/10	12.00 -
24/10	- 16.00
25/10	13.22 - 13.44

Table 2.2.1. *The main interruptions in recording of ARCES data at NDPC, 1 July - 31 December 2005.*

Monthly uptimes for the ARCES on-line data recording task, taking into account all factors (field installations, transmission lines, data center operation) affecting this task were as follows:

		Mission Capable	Net instrument availability
July	:	100%	99.958%
August	:	100%	100 %
September	:	99.990%	99.990%
October	:	95.840%	94.860%
November	:	99.963%	99.963%
December	:	99.930%	99.974%

The lower than normal uptime of ARCES is mainly due to problems with the UPS (power supply) during 23-26 October. This problem has been corrected.

J. Torstveit

Event Detection Operation

ARCES detections

The number of detections (phases) reported during day 182, 2005, through day 365, 2005, was 196,469, giving an average of 1068 detections per processed day (184 days processed).

Events automatically located by ARCES

During days 182, 2005, through 365, 2005, 8534 local and regional events were located by ARCES, based on automatic association of P- and S-type arrivals. This gives an average of 46.4 events per processed day (179 days processed). 54% of these events are within 300 km, and 82% of these events are within 1000 km.

U. Baadshaug

2.3 AS72 — Auxiliary Seismic Station Spitsbergen

The mission-capable data for the period were 100% the same as for the previous reporting period. The net instrument availability was 99.086%.

There were no outages of all instruments at the same time in the reporting period.

Monthly uptimes for the Spitsbergen on-line data recording task, taking into account all factors (field installations, transmissions line, data center operation) affecting this task were as follows:

		Mission Capable	Net instrument availability
July	:	100%	100%
August	:	100%	94.857%
September	:	100%	99.997%
October	:	100%	99.740%
November	:	100%	99.963%
December	:	100%	99.992%

J. Torstveit

Event Detection Operation

Spitsbergen array detections

The number of detections (phases) reported from day 182, 2005, through day 365, 2005, was 416,772, giving an average of 2265 detections per processed day (184 days processed).

Events automatically located by the Spitsbergen array

During days 182, 2005, through 365, 2005, 38,009 local and regional events were located by the Spitsbergen array, based on automatic association of P- and S-type arrivals. This gives an average of 206.6 events per processed day (184 days processed). 74% of these events are within 300 km, and 89% of these events are within 1000 km.

U. Baadshaug

2.4 AS73 — Auxiliary Seismic Station at Jan Mayen

The IMS auxiliary seismic network includes a three-component station on the Norwegian island of Jan Mayen. The station location given in the protocol to the Comprehensive Nuclear-Test-Ban Treaty is 70.9˚N, 8.7˚W.

The University of Bergen has operated a seismic station at this location since 1970. A so-called Parent Network Station Assessment for AS73 was completed in April 2002. A vault at a new location (71.0^{o}N, 8.5^{o}W) was prepared in early 2003, after its location had been approved by the PrepCom. New equipment was installed in this vault in October 2003, as a cooperative

effort between NORSAR and the CTBTO/PTS. Continuous data from this station are being transmitted to the NDC at Kjeller via a satellite link installed in April 2000. Data are also made available to the University of Bergen.

J. Fyen

2.5 IS37 — Infrasound Station at Karasjok

The IMS infrasound network will include a station at Karasjok in northern Norway. The coordinates given for this station are 69.5˚N, 25.5˚E. These coordinates coincide with those of the primary seismic station PS28.

A site survey for this station was carried out during June/July 1998 as a cooperative effort between the Provisional Technical Secretariat of the CTBTO and NORSAR. The site survey led to a recommendation on the exact location of the infrasound station. The appropriate application forms have been sent to the local authorities to obtain the permissions needed to establish the station. Station installation is expected to take place in the fall of 2006, provided that such permissions are granted in a timely manner.

S. Mykkeltveit

2.6 RN49 — Radionuclide Station on Spitsbergen

The IMS radionuclide network includes a station on the island of Spitsbergen. This station is also among those IMS radionuclide stations that will have a capability of monitoring for the presence of relevant noble gases upon entry into force of the CTBT.

A site survey for this station was carried out in August of 1999 by NORSAR, in cooperation with the Norwegian Radiation Protection Authority. The site survey report to the PTS contained a recommendation to establish this station at Platåberget, near Longyearbyen. The infrastructure for housing the station equipment was established in early 2001, and a noble gas detection system, based on the Swedish “SAUNA” design, was installed at this site in May 2001, as part of PrepCom’s noble gas experiment. A particulate station (“ARAME” design) was installed at the same location in September 2001. A certification visit to the station took place in October 2002, and the particulate station was certified on 10 June 2003. The equipment at RN49 is being maintained and operated in accordance with a contract with the CTBTO/PTS.

S. Mykkeltveit

3 Contributing Regional Seismic Arrays

3.1 NORES

NORES has been out of operation since lightning destroyed the station electronics on 11 June 2002.

J. Torstveit

3.2 Hagfors (IMS Station AS101)

Data from the Hagfors array are made available continuously to NORSAR through a cooperative agreement with Swedish authorities.

The mission-capable data statistics were 99.993% as compared to 99.996% for the previous reporting period. The net instrument availability was 99.993%.

There were no outages of all instruments in the reporting period.

Monthly uptimes for the Hagfors on-line data recording task, taking into account all factors (field installations, transmissions line, data center operation) affecting this task were as follows:

		Mission Capable	Net instrument availability
July	:	100%	100%
August	:	100%	100%
September	:	99.965%	99.965%
October	:	99.993%	99.993%
November	:	100%	100%
December	:	100%	100%

J. Torstveit

Hagfors Event Detection Operation

Hagfors array detections

The number of detections (phases) reported from day 182, 2005, through day 365, 2005, was 148,358, giving an average of 806 detections per processed day (184 days processed).

Events automatically located by the Hagfors array

During days 182, 2005, through 365, 2005, 4571 local and regional events were located by the Hagfors array, based on automatic association of P- and S-type arrivals. This gives an average of 24.8 events per processed day (184 days processed). 70% of these events are within 300 km, and 90% of these events are within 1000 km.

U. Baadshaug

3.3 FINES (IMS station PS17)

Data from the FINES array are made available continuously to NORSAR through a cooperative agreement with Finnish authorities.

The mission-capable data statistics were 100%, the same as for the previous reporting period. The net instrument availability was 96.469%.

Monthly uptimes for the FINES on-line data recording task, taking into account all factors (field installations, transmissions line, data center operation) affecting this task were as follows:

		Mission Capable	Net instrument availability
July	:	100%	93.703%
August	:	100%	97.358
September	:	100%	96.599
October	:	99.999%	91.285%
November	:	100%	99.982
December	:	100%	99.993%

J. Torstveit

FINES Event Detection Operation

FINES detections

The number of detections (phases) reported during day 182, 2005, through day 365, 2005, was 47,945, giving an average of 261 detections per processed day (184 days processed).

Events automatically located by FINES

During days 182, 2005, through 365, 2005, 2360 local and regional events were located by FINES, based on automatic association of P- and S-type arrivals. This gives an average of 12.8 events per processed day (184 days processed). 81% of these events are within 300 km, and 91% of these events are within 1000 km.

U. Baadshaug

3.4 Regional Monitoring System Operation and Analysis

The Regional Monitoring System (RMS) was installed at NORSAR in December 1989 and has been operated at NORSAR from 1 January 1990 for automatic processing of data from ARCES and NORES. A second version of RMS that accepts data from an arbitrary number of arrays and single 3-component stations was installed at NORSAR in October 1991, and regular operation of the system comprising analysis of data from the 4 arrays ARCES, NORES, FINES and

GERES started on 15 October 1991. As opposed to the first version of RMS, the one in current operation also has the capability of locating events at teleseismic distances.

Data from the Apatity array was included on 14 December 1992, and from the Spitsbergen array on 12 January 1994. Detections from the Hagfors array were available to the analysts and could be added manually during analysis from 6 December 1994. After 2 February 1995, Hagfors detections were also used in the automatic phase association.

Since 24 April 1999, RMS has processed data from all the seven regional arrays ARCES, NORES, FINES, GERES (until January 2000), Apatity, Spitsbergen, and Hagfors. Starting 19 September 1999, waveforms and detections from the NORSAR array have also been available to the analyst.

Phase and event statistics

Table 3.5.1 gives a summary of phase detections and events declared by RMS. From top to bottom the table gives the total number of detections by the RMS, the number of detections that are associated with events automatically declared by the RMS, the number of detections that are not associated with any events, the number of events automatically declared by the RMS, and finally the total number of events worked on interactively (in accordance with criteria that vary over time; see below) and defined by the analyst.

New criteria for interactive event analysis were introduced from 1 January 1994. Since that date, only regional events in areas of special interest (e.g, Spitsbergen, since it is necessary to acquire new knowledge in this region) or other significant events (e.g, felt earthquakes and large industrial explosions) were thoroughly analyzed. Teleseismic events of special interest are also analyzed.

To further reduce the workload on the analysts and to focus on regional events in preparation for Gamma-data submission during GSETT-3, a new processing scheme was introduced on 2 February 1995. The GBF (Generalized Beamforming) program is used as a pre-processor to RMS, and only phases associated with selected events in northern Europe are considered in the automatic RMS phase association. All detections, however, are still available to the analysts and can be added manually during analysis.

	Jul 05	Aug 05	Sep 05	Oct 05	Nov 05	Dec 05	Total
Phase detections	151,880	157,416	183,672	172,681	152,602	140,494	958,745
- Associated phases	4,981	4,772	7,176	6,955	5,050	4,391	33,325
- Unassociated phases	146,899	152,644	176,496	175726	147,552	136,103	925,420
Events automatically declared by RMS	953	988	1,460	1,440	1,003	872	6,716
No. of events defined by the analyst	75	65	89	75	73	50	427

Table 3.5.1. RMS phase detections and event summary 1 July - 31 December 2005.

U. Baadshaug

B. Paulsen

4 NDC and Field Activities

4.1 NDC Activitities

NORSAR functions as the Norwegian National Data Center (NDC) for CTBT verification. Six monitoring stations, comprising altogether 113 field sensors, will be located on Norwegian territory as part of the future IMS as described elsewhere in this report. The four seismic IMS stations are all in operation today, and all of them are currently providing data to the CTBTO on a regular basis. The radionuclide station at Spitsbergen was certified on 10 June 2003, whereas the infrasound station in northern Norway will need to be established within the next few years. Data recorded by the Norwegian stations is being transmitted in real time to the Norwegian NDC, and provided to the IDC through the Global Communications Infrastructure (GCI). Norway is connected to the GCI with a frame relay link to Vienna.

Operating the Norwegian IMS stations continues to require increased resources and additional personnel both at the NDC and in the field. The PTS has established new and strictly defined procedures as well as increased emphasis on regularity of data recording and timely data transmission to the IDC in Vienna. This has led to increased reporting activities and implementation of new procedures for the NDC operators. The NDC carries out all the technical tasks required in support of Norway's treaty obligations. NORSAR will also carry out assessments of events of special interest, and advise the Norwegian authorities in technical matters relating to treaty compliance.

Verification functions; information received from the IDC

After the CTBT enters into force, the IDC will provide data for a large number of events each day, but will not assess whether any of them are likely to be nuclear explosions. Such assessments will be the task of the States Parties, and it is important to develop the necessary national expertise in the participating countries. An important task for the Norwegian NDC will thus be to make independent assessments of events of particular interest to Norway, and to communicate the results of these analyses to the Norwegian Ministry of Foreign Affairs.

Monitoring the Arctic region

Norway will have monitoring stations of key importance for covering the Arctic, including Novaya Zemlya, and Norwegian experts have a unique competence in assessing events in this region. On several occasions in the past, seismic events near Novaya Zemlya have caused political concern, and NORSAR specialists have contributed to clarifying these issues.

International cooperation

After entry into force of the treaty, a number of countries are expected to establish national expertise to contribute to the treaty verification on a global basis. Norwegian experts have been in contact with experts from several countries with the aim of establishing bilateral or multilateral cooperation in this field. One interesting possibility for the future is to establish NORSAR as a regional center for European cooperation in the CTBT verification activities.

NORSAR event processing

The automatic routine processing of NORSAR events as described in NORSAR Sci. Rep. No. 2-93/94, has been running satisfactorily. The analyst tools for reviewing and updating the solutions have been continually modified to simplify operations and improve results. NORSAR is currently applying teleseismic detection and event processing using the large-aperture NORSAR array as well as regional monitoring using the network of small-aperture arrays in Fennoscandia and adjacent areas.

Communication topology

Norway has implemented an independent subnetwork, which connects the IMS stations AS72, AS73, PS28, and RN49 operated by NORSAR to the GCI at NOR_NDC. A contract has been concluded and VSAT antennas have been installed at each station in the network. Under the same contract, VSAT antennas for 6 of the PS27 subarrays have been installed for intra-array communication. The seventh subarray is connected to the central recording facility via a leased land line. The central recording facility for PS27 is connected directly to the GCI (Basic Topology). All the VSAT communication is functioning satisfactorily. As of 10 June 2005, AS72 and RN49 are connected to NOR_NDC through a VPN link.

Jan Fyen

4.2 Status Report: Provision of data from Norwegian seismic IMS stations to the IDC

Introduction

This contribution is a report for the period July - December 2005 on activities associated with provision of data from Norwegian seismic IMS stations to the International Data Centre (IDC) in Vienna. This report represents an update of contributions that can be found in previous editions of NORSAR's Semiannual Technical Summary. It is noted that as of 31 December 2005, two of the Norwegian seismic stations providing data to the IDC have been formally certified.

Norwegian IMS stations and communications arrangements

During the reporting interval 1 July - 31 December 2005, Norway has provided data to the IDC from the four seismic stations shown in Fig. 4.2.1. PS27 —NOA is a 60 km aperture teleseismic array, comprised of 7 subarrays, each containing six vertical short period sensors and a three-component broadband instrument. PS28 — ARCES is a 25-element regional array with an aperture of 3 km, whereas AS72 — Spitsbergen array (station code SPITS) has 9 elements within a 1-km aperture. AS73 — JMIC has a single three-component broadband instrument.

The intra-array communication for NOA utilizes a land line for subarray NC6 and VSAT links based on TDMA technology for the other 6 subarrays. The central recording facility for NOA is located at the Norwegian National Data Center (NOR_NDC).

Continuous ARCES data are transmitted from the ARCES site to NOR_NDC using a 64 kbits/s VSAT satellite link, based on BOD technology.

Continuous SPITS data were transmitted to NOR_NDC via a VSAT terminal located at Platåberget in Longyearbyen (which is the site of the IMS radionuclide monitoring station

RN49 installed during 2001) up to 10 June 2005. The central recording equipment for the SPITS array has been moved to the University of Spitsbergen (UNIS). A 512 hps SHDSL link has been established between UNIS and NOR_NDC. Both AS72 and RN49 data are now transmitted to NOR_NDC over this link using VPN technology.

A minimum of seven-day station buffers have been established at the ARCES and SPITS sites and at all NOA subarray sites, as well as at the NOR_NDC for ARCES, SPITS and NOA.

The NOA and ARCES arrays are primary stations in the IMS network, which implies that data from these stations is transmitted continuously to the receiving international data center. Since October 1999, this data has been transmitted (from NOR_NDC) via the Global Communications Infrastructure (GCI) to the IDC in Vienna. Data from the auxiliary array station SPITS — AS72 have been sent in continuous mode to the IDC during the reporting period. AS73 — JMIC is an auxiliary station in the IMS, and the JMIC data have been available to the IDC throughout the reporting period on a request basis via use of the AutoDRM protocol (Kradolfer, 1993; Kradolfer, 1996). In addition, continuous data from all three arrays is transmitted to the US_NDC.

Uptimes and data availability

Figs. 4.2.2 and 4.2.3 show the monthly uptimes for the Norwegian IMS primary stations ARCES and NOA, respectively, for the period 1 July - 31 December 2005, given as the hatched (taller) bars in these figures. These barplots reflect the percentage of the waveform data that is available in the NOR_NDC data archives for these two arrays. The downtimes inferred from these figures thus represent the cumulative effect of field equipment outages, station site to NOR_NDC communication outage, and NOR_NDC data acquisition outages.

Figs. 4.2.2 and 4.2.3 also give the data availability for these two stations as reported by the IDC in the IDC Station Status reports. The main reason for the discrepancies between the NOR_NDC and IDC data availabilities as observed from these figures is the difference in the ways the two data centers report data availability for arrays: Whereas NOR_NDC reports an array station to be up and available if at least one channel produces useful data, the IDC uses weights where the reported availability (capability) is based on the number of actually operating channels.

Use of the AutoDRM protocol

NOR_NDC's AutoDRM has been operational since November 1995 (Mykkeltveit & Baadshaug, 1996). The monthly number of requests by the IDC for JMIC data for the period July - December 2005 is shown in Fig. 4.2.4.

NDC automatic processing and data analysis

These tasks have proceeded in accordance with the descriptions given in Mykkeltveit and Baadshaug (1996). For the period July - December 2005, NOR_NDC derived information on 476 supplementary events in northern Europe and submitted this information to the Finnish NDC as the NOR_NDC contribution to the joint Nordic Supplementary (Gamma) Bulletin, which in turn is forwarded to the IDC. These events are plotted in Fig. 4.2.5.

Data access for the station NIL at Nilore, Pakistan

NOR_NDC continued to provide access to the seismic station NIL at Nilore, Pakistan, through a VSAT satellite link between NOR_NDC and Pakistan's NDC in Nilore.

Current developments and future plans

NOR_NDC is continuing the efforts towards improving and hardening all critical data acquisition and data forwarding hardware and software components, so as to meet the requirements related to operation of IMS stations.

The NOA array was formally certified by the PTS on 28 July 2000, and a contract with the PTS in Vienna currently provides partial funding for operation and maintenance of this station. The ARCES array was formally certified by the PTS on 8 November 2001, and a contract with the PTS is in place which also provides for partial funding of the operation and maintenance of this station. Provided that adequate funding continues to be made available (from the PTS and the Norwegian Ministry of Foreign Affairs), we envisage continuing the provision of data from all Norwegian seismic IMS stations without interruption to the IDC in Vienna.

U. Baadshaug
S. Mykkeltveit
J. Fyen

References

Kradolfer, U. (1993): Automating the exchange of earthquake information. *EOS, Trans., AGU*, 74, 442.

Kradolfer, U. (1996): AutoDRM — The first five years, *Seism. Res. Lett.*, 67, 4, 30-33.

Mykkeltveit, S. & U. Baadshaug (1996): Norway's NDC: Experience from the first eighteen months of the full-scale phase of GSETT-3. *Semiann. Tech. Summ., 1 October 1995 - 31 March 1996*, NORSAR Sci. Rep. No. 2-95/96, Kjeller, Norway.

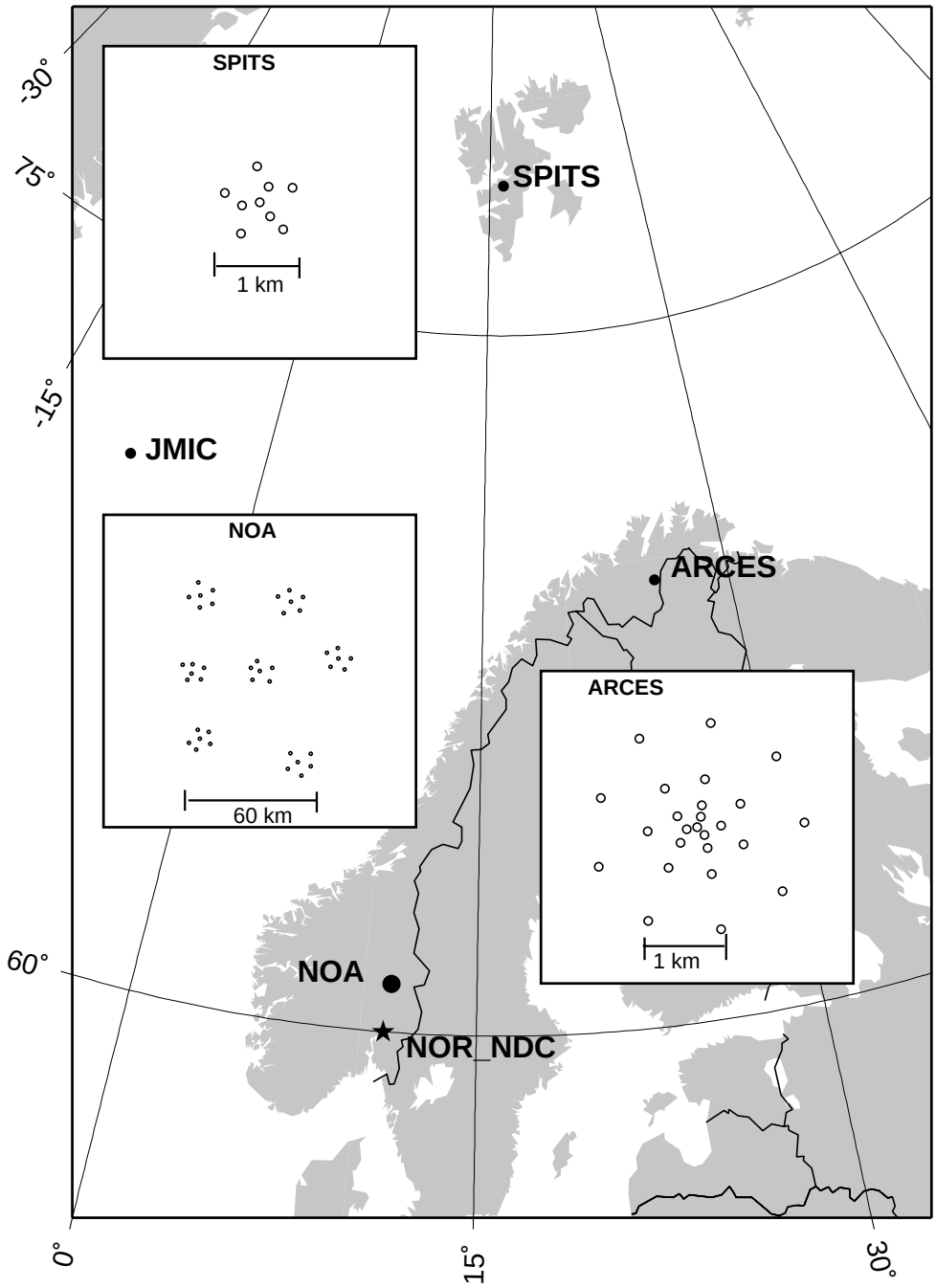

Fig. 4.2.1. The figure shows the locations and configurations of the three Norwegian seismic IMS array stations that provided data to the IDC during the period July - December 2005. The data from these stations and the JMIC three-component station are transmitted continuously and in real time to the Norwegian NDC (NOR_NDC). The stations NOA and ARCES are primary IMS stations, whereas SPITS and JMIC are auxiliary IMS stations.

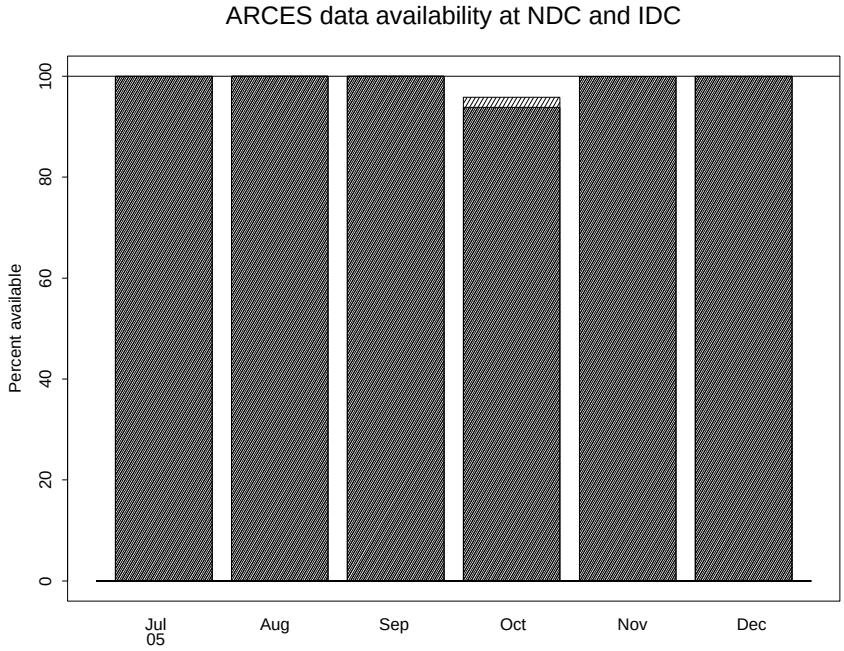

Fig. 4.2.2. The figure shows the monthly availability of ARCES array data for the period July - December 2005 at NOR_NDC and the IDC. See the text for explanation of differences in definition of the term "data availability" between the two centers. The higher values (hatched bars) represent the NOR_NDC data availability.

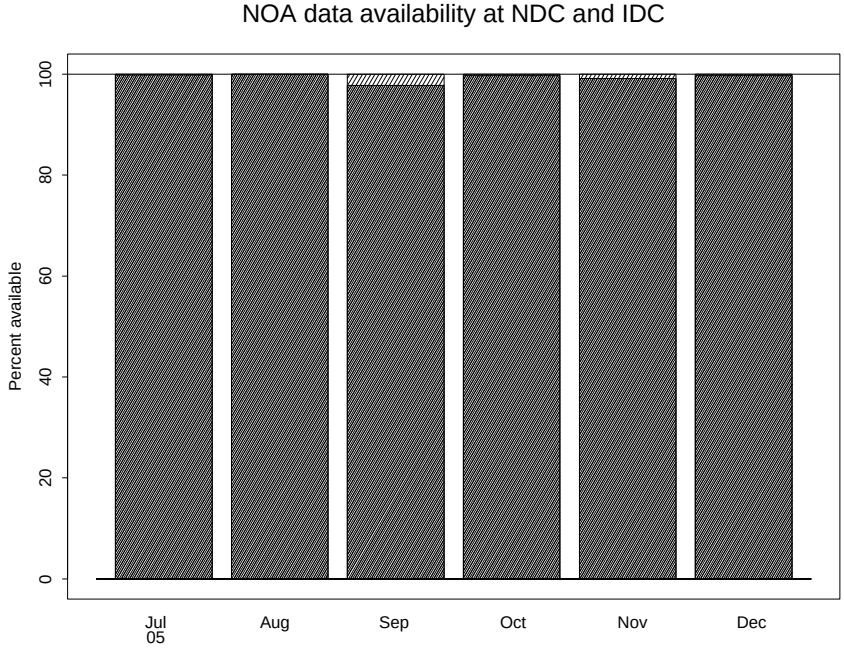

Fig. 4.2.3. The figure shows the monthly availability of NORSAR array data for the period July - December 2005 at NOR_NDC and the IDC. See the text for explanation of differences in definition of the term "data availability" between the two centers. The higher values (hatched bars) represent the NOR_NDC data availability.

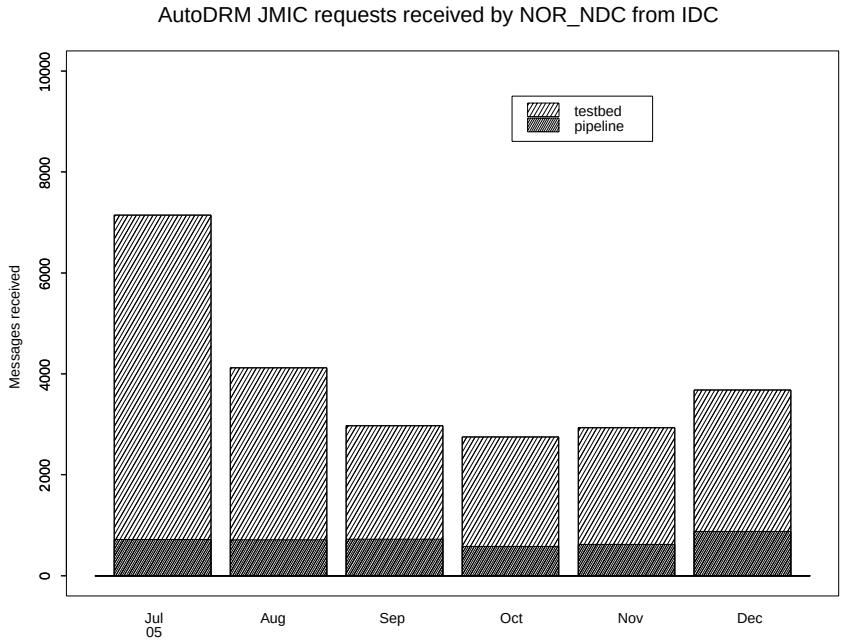

Fig. 4.2.4. The figure shows the monthly number of requests received by NOR_NDC from the IDC for JMIC waveform segments during July - December 2005.

Reviewed Supplementary events

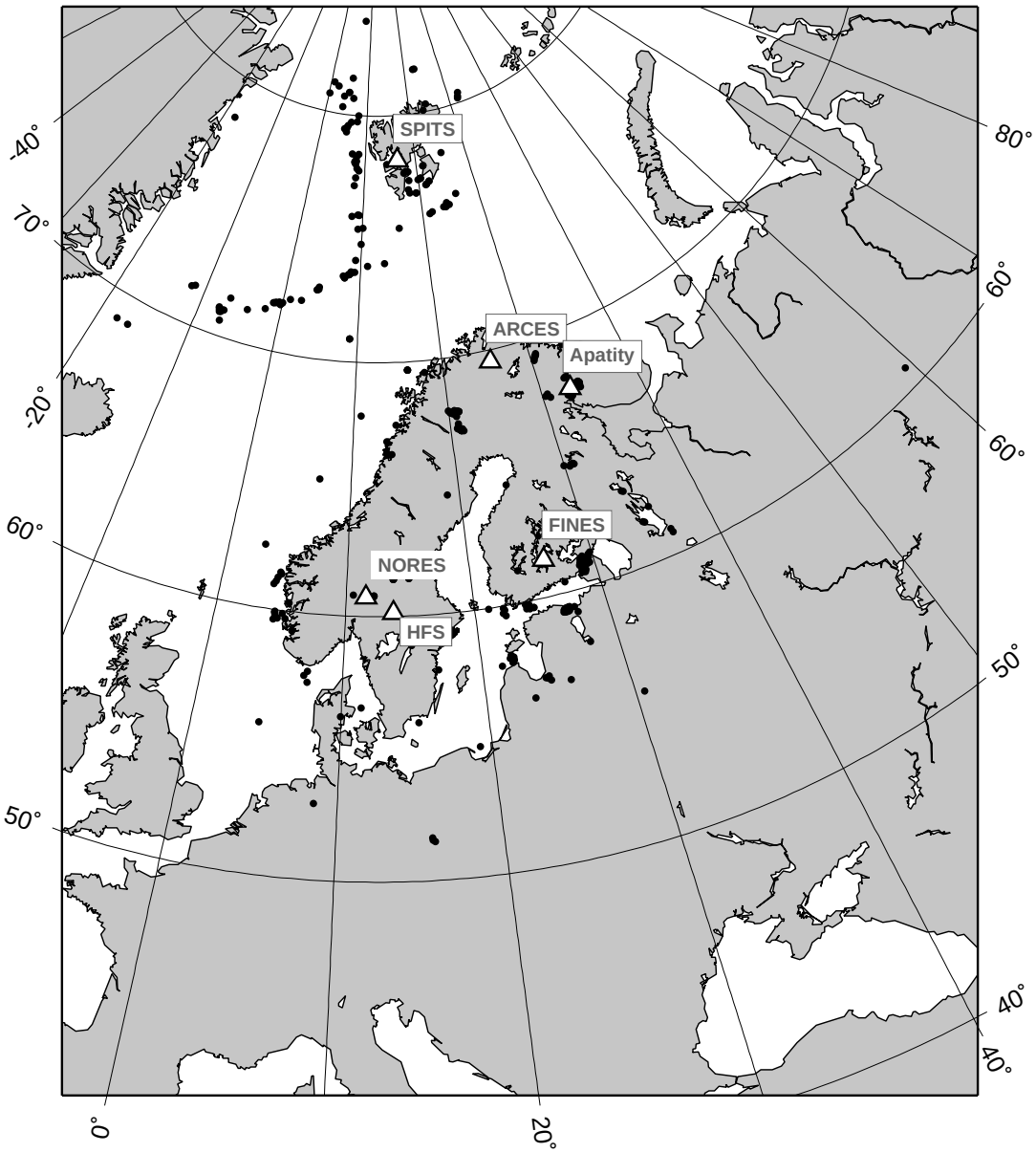

Fig. 4.2.5. The map shows the 476 events in and around Norway contributed by NOR_NDC during July - December 2005 as supplementary (Gamma) events to the IDC, as part of the Nordic supplementary data compiled by the Finnish NDC. The map also shows the main seismic stations used in the data analysis to define these events.

4.3 Field Activities

The activities at the NORSAR Maintenance Center (NMC) at Hamar currently include work related to operation and maintenance of the following IMS seismic stations: the NOA teleseismic array (PS27), the ARCES array (PS28) and the Spitsbergen array (AS72). Some work has also been carried out in connection with the seismic station on Jan Mayen (AS73), the radionuclide station at Spitsbergen (RN49), and preparations for the infrasound station at Karasjok (IS37). NORSAR also acts as a consultant for the operation and maintenance of the Hagfors array in Sweden (AS101).

NORSAR carries out the field activities relating to IMS stations in a manner generally consistent with the requirements specified in the appropriate IMS Operational Manuals, which are currently being developed by Working Group B of the Preparatory Commission. For seismic stations these specifications are contained in the Operational Manual for Seismological Monitoring and the International Exchange of Seismological Data (CTBT/WGB/TL-11/2), currently available in a draft version.

All regular maintenance on the NORSAR field systems is conducted on a one-shift-per-day, five-day-per-week basis. The maintenance tasks include:

- Operating and maintaining the seismic sensors and the associated digitizers, authentication devices and other electronics components.
- Maintaining the power supply to the field sites as well as backup power supplies.
- Operating and maintaining the VSATs, the data acquisition systems and the intra-array data transmission systems.
- Assisting the NDC in evaluating the data quality and making the necessary changes in gain settings, frequency response and other operating characteristics as required.
- Carrying out preventive, routine and emergency maintenance to ensure that all field systems operate properly.
- Maintaining a computerized record of the utilization, status, and maintenance history of all site equipment.
- Providing appropriate security measures to protect against incidents such as intrusion, theft and vandalism at the field installations.

Details of the daily maintenance activities are kept locally. As part of its contract with CTBTO/PTS NORSAR submits, when applicable, problem reports, outage notification reports and equipment status reports. The contents of these reports and the circumstances under which they will be submitted are specified in the draft Operational Manual.

P.W. Larsen
K.A. Løken

4.4 Spitsbergen array refurbishment

As part of this contract, NORSAR has refurbished the Spitsbergen array to satisfy the IMS technical specifications. The refurbishment included upgrading 5 of the array sites to comprise three-component seismometers instead of the original vertical sensors. Both before and after this refurbishment, the Spitsbergen array configuration conforms to the minimum IMS requirement for a new seismic array, having 9 short-period vertical seismometers and one three-component broadband sensor.

As reported in NORSAR Sci. Rep. No. 1 and 2-2004, Guralp Systems was selected as the main vendor for the seismometers, digitizers and data acquisition system. See NORSAR Scientific Report No. 1-2005 for details of the refurbishment.

The station has provided 100% mission capable data availability throughout the reporting period.

The sensors at sites SPB3, SPB4 and SPB5 are all initially installed in sand. During August 2005, the remaining sensors were also installed in sand. For the current flat acceleration response, the sensitivity for periods longer than 10 seconds may be too low to satisfy CTBTO requirements for a broadband sensor. This issue will be investigated further.

J. Fyen

5 Documentation Developed

Bungum, H. and O. Olesen (2005): The 31st of August 1819 Lurøy earthquake revisited. Nor. J. Geology, 85, 245-252.

Bungum, H., C. Lindholm & J. I. Faleide (2005): Postglacial seismicity offshore mid-Norway with emphasis on spatio-temporal-magnitudal variations. Marine and Petroleum Geology, 22, 137-148.

Bungum, H., O. Ritzmann, N. Maercklin, J.-I. Faleide, W.D. Mooney & S.T. Detweiler (2005): A new three-dimensional model for the crust and upper mantle in the Barents Sea region. EOS 86(16), 160-161.

Bungum, H., T. Kværma, S. Mykkeltveit, N. Maercklin, M. Roth, K. Åstebol, D. B. Harris & S. Larsen (2005): Energy partitioning for seismic events in Fennoscandia and NW Russia. **In**: Proceedings, 27th Seismic Research Review, Ground-based nuclear explosion monitoring technologies, Rancho Mirage, California, LA-UR-05-6407, 529–538.

Bungum, H., N. Maercklin, O. Ritzmann, J. I. Faleide, Ch. Weidle, A. Levshin, J. Schweitzer, W. D. Mooney & S. T. Detweiler (2005): Development of a three-dimensional velocity model for the crust and upper mantle in the greater Barents Sea region. **In**: Proceedings, 27th Seismic Research Review, Ground-based nuclear explosion monitoring technologies, Rancho Mirage, California, LA-UR-05-6407, 13–22.

Douglas, J., H. Bungum & F. Scherbaum (2006): Ground-motion prediction equations for southern Spain and southern Norway using the composite model perspective. J. Earthq. Eng., 10(1), 1-40.

Gibbons, S. J., T. Kværna, & F. Ringdal (2005). Monitoring of seismic events from a specific source region using a single regional array: a case study. J. Seismology, 9, 277-294.

Harris, D. B., F. Ringdal, E. Kremenetskaya, S. Mykkeltveit, D. Rock, N. Maercklin, J. Schweitzer, T. Hauk & J. Lewis (2005): Ground Truth collection for mining explosions in northern Fennoscandia and northwestern Russia. **In**: Proceedings, 27th Seismic Research Review: Ground-based nuclear explosion monitoring technologies, Rancho Mirage, California, LA-UR-05-6407, 31–41.

Kværna, T., S.J. Gibbons, F. Ringdal & D.B. Harris (2005): Integrated Seismic Event Detection and Location by Advanced Array Processing. **In:** Proceedings, 27th Seismic Research Review, Ground-based Nuclear Explosion Monitoring Technologies, Rancho Mirage, California, September 2005, 927-936.

Kühn, D. & J. Schweitzer (2006): Moment tensor (MT) inversion for regional events in Fennoscandia and adjacent areas. **In:** Semiannual Technical Summary, 1 July - 31 December 2005, NORSAR Sci. Rep. 1-2006, Kjeller, Norway.

Levshin, A., J. Schweitzer , Ch. Weidle, N. Shapiro, N. Maercklin & M. Ritzwoller (2006): Surface wave tomography for the Barents Sea and surrounding regions — Part II. **In:** Semiannual Technical Summary, 1 July - 31 December 2005, NORSAR Sci. Rep. 1-2006, Kjeller, Norway.

Levshin, A., J. Schweitzer, Ch. Weidle, N. Maercklin, N. Shapiro & M. H. Ritzwoller (2005): Surface wave tomography of the European Arctic. EOS Trans., Am. Geophys. Un., Fall Meet. Suppl., 86(52), abstract S51E-1053 (poster).

Lindholm, C.D., M. Roth, H. Bungum & J.I. Faleide (2005): Probabilistic and deterministic seismic hazard results and influence of the sedimentary Møre Basin, NE Atlantic. Marine and Petroleum Geology, 22, 149-160.

Maercklin, N., S. Mykkeltveit, J. Schweitzer, D. Rock, & D. B. Harris (2005): Data from deployment of temporary seismic stations in northern Norway and Finland. Report UCRL-SR-209656. Lawrence Livermore National Laboratory. Livermore, California.

Oye, V. & W. L. Ellsworth, 2005. Orientation of three-component geophones in the San Andreas Fault Observatory at Depth Pilot Hole, Parkfield, California. Bull. Seism. Soc. Am., 95, 2, 751-758, doi: 10.1785/0120040130.

Oye V., H, Bungum & M. Roth (2005): Source parameters and scaling relations for mining related seismicity within the Pyhasalmi ore mine, Finland. Bull. Seism. Soc. Am., 95, 3, 1011-1026.

Pettenati, F., L. Sirovich, H. Bungum, and J. Schweitzer (2005): Source inversion of regional intensity patterns of five earthquakes from south-western Norway. Boll. Geof. Teor. e Appl., 46(2-3), 111-134.

Ringdal, F. (2005): Semiannual Technical Summary, 1 January - 30 June 2005. NORSAR Sci. Rep. 2-2005, Kjeller, Norway, August 2005.

Ringdal, F. & S.J. Gibbons (2006): Seismic/Infrasonic Processing: Case study of explosions in north Finland. **In:** Semiannual Technical Summary, 1 July - 31 December 2005, NORSAR Sci. Rep. 1-2006, Kjeller, Norway.

Ringdal, F., S.J. Gibbons, T. Kværna, V. Asming, Y. Vinogradov, S. Mykkeltveit & J. Schweitzer (2006): Research in regional seismic monitoring. **In:** Semiannual Technical Summary, 1 July - 31 December 2005, NORSAR Sci. Rep. 1-2006, Kjeller, Norway.

Ringdal, F., S. Gibbons , T. Kværna, V. Asming, Y. Vinogradov, S. Mykkeltveit & J. Schweitzer: Research in Regional Seismic Monitoring. 27th Seismic Research Review — Ground-based nuclear monitoring technologies. Rancho Mirage, California, September 20 - 22, 2005, LA-UR-05-6407, Proceedings, CD Version file 2 - 16, **Volume 1**, 423-432.

Ringdal, F., S.J. Gibbons & D.B. Harris (2005): Adaptive Waveform Correlation Detectors for Arrays: Algorithms for Autonomous Calibration. **In:** Proceedings of the 27th Seismic Research Review, Ground-based Nuclear Explosion Monitoring Technologies, Rancho Mirage, California, September 2005, 413-422.

Schweitzer, J., F. Ringdal, T. Kværna, V. Asming & Y. Vinogradov (2006): Infrasound data processing using Apatity and ARCES array data. **In:** Semiannual Technical Summary, 1 July - 31 December 2005, NORSAR Sci. Rep. 1-2006, Kjeller, Norway.

6 Summary of Technical Reports / Papers Published

6.1 Research in regional seismic monitoring

(Paper presented at the 27th Seismic Research Review)

This project represents a continuing research effort aimed at improving seismic monitoring tools at regional distances, with emphasis on the Barents/Kara Sea region, which includes the former Novaya Zemlya test site. The tasks comprise development and improvement of detection, location and discrimination algorithms as well as experimental on-line monitoring using tools such as regional Generalized Beamforming (GBF) and Threshold Monitoring (TM). It also includes special studies of mining events, for which detailed ground truth information is being provided by the Kola Regional Seismological Centre (KRSC). These studies are documented in the NORSAR Semiannual Technical Summaries. In this paper, we present three of these investigations in more detail.

The first topic is the use of the large-aperture NORSAR array for automatic processing of regional phases. Such processing is notoriously difficult, due to the low coherency across the large array of the high-frequency regional phases, and has not been successfully implemented in the past. We have recently completed a new processing system for incorporating regional seismic phases detected by the large NORSAR array into the Generalized Beamforming process currently in use at NORSAR for on-line automatic detection and location of seismic events in the European Arctic. The system employs a multitaper method to calculate continuous spectra of the waveforms and detects changes in spectral content consistent with regional phases propagating across the array. It represents a significant improvement over previous processing systems for this large array, and opens up interesting possibilities for improved automatic detection and location using local or regional networks.

The second topic is a continued study of combining seismic and infrasonic recordings for detection and characterization of seismic events at local and regional distances. We present results from an analysis of several recent surface explosions in the Kola peninsula near the Norwegian border. These explosions were carried out for the purpose of destroying old ammunition, and generated unusually strong infrasonic signals in addition to seismic signals. Not unexpectedly, the infrasonic signals were well recorded on the infrasound array in Apatity, but more interestingly, they were also clearly recorded on the seismic sensors at the ARCES and Apatity arrays (both at about 250 km distance from the source area). We used the recordings to make a location estimate based upon the infrasonic detections (on the seismic sensors) at these two arrays, and found that the locations matched closely the locations obtained through standard seismic data analysis. This indicates an interesting potential for joint two-array infrasonic processing, and this concept will be further developed once the IMS infrasound array near ARCES has been established (expected in 2006).

The third topic concerns an initial investigation of the potential of obtaining improved detection of small seismic events by the use of waveform correlation in conjunction with array processing. We present examples on the power of the array-based correlation technique, demonstrating that waveform correlation could be used to detect the small aftershock (m_b=2.5) following the 16 August 1997 Kara Sea event, not only at the Spitsbergen array (distance 1100 km), but even at the large NORSAR array situated more than 2300 km from the epicenter. We also discuss some other potential applications of this technique, which we will develop further over the next three years in a separate joint research project with LLNL.

6.1.1 Objective

This work represents a continued effort in seismic and infrasonic monitoring, with emphasis on studying earthquakes and explosions in the Barents/Kara Sea region, which includes the former Russian nuclear test site at Novaya Zemlya. The overall objective is to characterize the seismicity of this region, to investigate the detection and location capability of regional seismic networks and to study various methods for screening and identifying seismic events in order to improve nuclear explosion monitoring capability. Another objective is to carry out special studies of mining events, for which detailed ground truth information is being provided by the Kola Regional Seismological Centre (KRSC).

6.1.2 Research Accomplished

NORSAR and Kola Regional Seismological Centre (KRSC) of the Russian Academy of Sciences have for many years cooperated in the continuous monitoring of seismic events in North-West Russia and adjacent sea areas. The research has been based on data from a network of sensitive regional arrays which has been installed in northern Europe during the last decade in preparation for the CTBT monitoring network. This regional network, which comprises stations in Fennoscandia, Spitsbergen and NW Russia provides a detection capability for the Barents/Kara Sea region that is close to $m_b = 2.5$ (Ringdal, 1997).

The research carried out during this effort is documented in detail in several contributions contained in the NORSAR Semiannual Technical Summaries. In the present paper we will limit the discussions to some recent results of interest in the general context of regional monitoring of seismic events in the European Arctic.

Developing NORSARs regional processing system

NORSAR has for a number of years carried out processing and analysis of seismic events in the European Arctic, using the regional array network in Fennoscandia and NW Russia. The regional processing system at the NORSAR Data Center comprises the following steps:

- Automatic single array processing, using a suite of bandpass filters in parallel and a beam deployment that covers both P and S type phases for the region of interest.
- An STA/LTA detector applied independently to each beam, with broadband f-k analysis for each detected phase in order to estimate azimuth and phase velocity.
- Single-array phase association for initial location of seismic events, and also for the purpose of chaining together phases belonging to the same event, so as to prepare for the subsequent multiarray processing.
- Multi-array event detection, using the Generalized Beamforming (GBF) approach (Ringdal and Kværna, 1989) to associate phases from all stations in the regional network
- Interactive analysis of selected events, resulting in a reviewed regional seismic bulletin, which includes hypocentral information, magnitudes and selected waveform plots.

Until recently, the large aperture NORSAR array in southern Norway has not been incorporated in this process, since a sufficiently reliable regional processing system has not been available for an array this size. The NORSAR array was designed in the late 1960s to detect low-yield underground nuclear explosions at teleseismic distances (Bungum et. al., 1971). The instruments, covering an aperture of approximately 100 km, were spaced to minimise the coherency of microseisms and thus provide an optimal SNR-gain for teleseismic signals

between 0.5 and 2.0 Hz using classical beamforming with suitable steering parameters. After 1980, the focus in nuclear explosion monitoring turned towards the observation and interpretation of regional seismic phases and this motivated the development of the NORES regional seismic array and numerous subsequent arrays based upon this design (Mykkeltveit et. al., 1990). The GBF system provides fully automatic event locations by the association of phase detections made by the network of regional seismic arrays in Fennoscandia and Spitsbergen and the absence of detections from the NORES array (since June 2002) has led to a substantially worse detection and location capability for Southern and Western Norway. A spatial reconfiguration of the NORSAR array to facilitate the processing of high-frequency regional phases using traditional regional array processing methods has been deemed undesirable because of the exciting possibilities which the large aperture NORSAR array represents in terms of detection of low-magnitude events using full waveform methods and because of the unique opportunity to study the variation of site effects over this large heterogeneous region. The vast majority of underground nuclear explosions occurred before the most of the regional arrays were built and the 35 year long database of high quality digital seismic data from the NORSAR array provides a unique and invaluble reference.

Traditional array processing methods are entirely inadequate to process high frequency regional phases over the NORSAR array due to the signal incoherence. The low attenuation in Fennoscandia means that many regional signals are best observed at high frequencies; signals become incoherent over the NORSAR subarrays (aperture of the order 10 km) above approximately 3 Hz. It was noted many years ago by Ringdal et. al., 1972, however, that high frequency signals could be detected with a high SNR over the NORSAR array despite the incoherence of the actual waveforms by forming incoherent beams with the envelopes of filtered waveforms.

Attempts to estimate propagation parameters from such a procedure have subsequently failed due to the very different time-histories recorded at the different sites. The multitaper method of *Thomson (1982)* facilitates the calculation of low-variance estimates for the amplitude density spectrum, *A(f)*, over relatively short time windows and recent improvements in CPU power mean that it is now trivial to compute running "spectrograms" (i.e. *A(f)* as a continuous function of time) in real-time for the entire NORSAR array. In particular, the function $D(f,t) = \log_{10}(A(f)_{t+}) - \log_{10}(A(f)_{t-})$ measures the ratio between the energy in a time-window immediately following time t and the energy in a time-window immediately prior to time t. Fig. 6.1.1 shows the functions *A(f)* and *D(f,t)* for two channels of the NORSAR array for a regional event. The *D(f,t)* function reaches a maximum value in the vicinity of the phase arrival time with variation determined by how emergent the signal is and how the amplitude at each site varies with time. However, the form of the *D(f,t)* function is a far more stable indicator of the arrival of a phase than the SNR of a waveform filtered in a given frequency band. Under the traditional power detectors of the kind proposed by *Freiburger (1963)*, frequency bands are chosen a priori and are not necessarily optimal for a given signal; the *D(f,t)* function only attains significant values for the frequencies at which an SNR is observed. A time window length of 3.0 seconds was deemed ideal for the identification of regional phases at NORSAR; the sought after phases generally have a frequency content between 2.0 and 16.0 Hz and this length of time window is generally sufficient to ensure that the maximum value comes close to the phase onset time even for quite emergent signals.

These functions of time and frequency can be beamformed in the same way as seismograms using the plane wave delays appropriate for regional phases; although the NORSAR array is too large for the true validity of such propagation models, the deviations from plane waves

generally cancel out under the beamforming process resulting in a maximum value which typically fits the arrival time at the NB200 central array element with a surprising consistency. The detection process is executed by calculating a scalar function of time which is a mean of D(f,t) in a frequency band appropriate for the aniticipated phase Following a detection reduction algorithm, the slowness of the detected phase is estimated by beamforming the differentiated spectrograms on a dense grid; the slowness results for the northern Norway event displayed in Fig. 6.1.1 are shown in Fig. 6.1.2. For each of the phases shown, the slowness estimate is close to that anticipated from the reviewed event location.

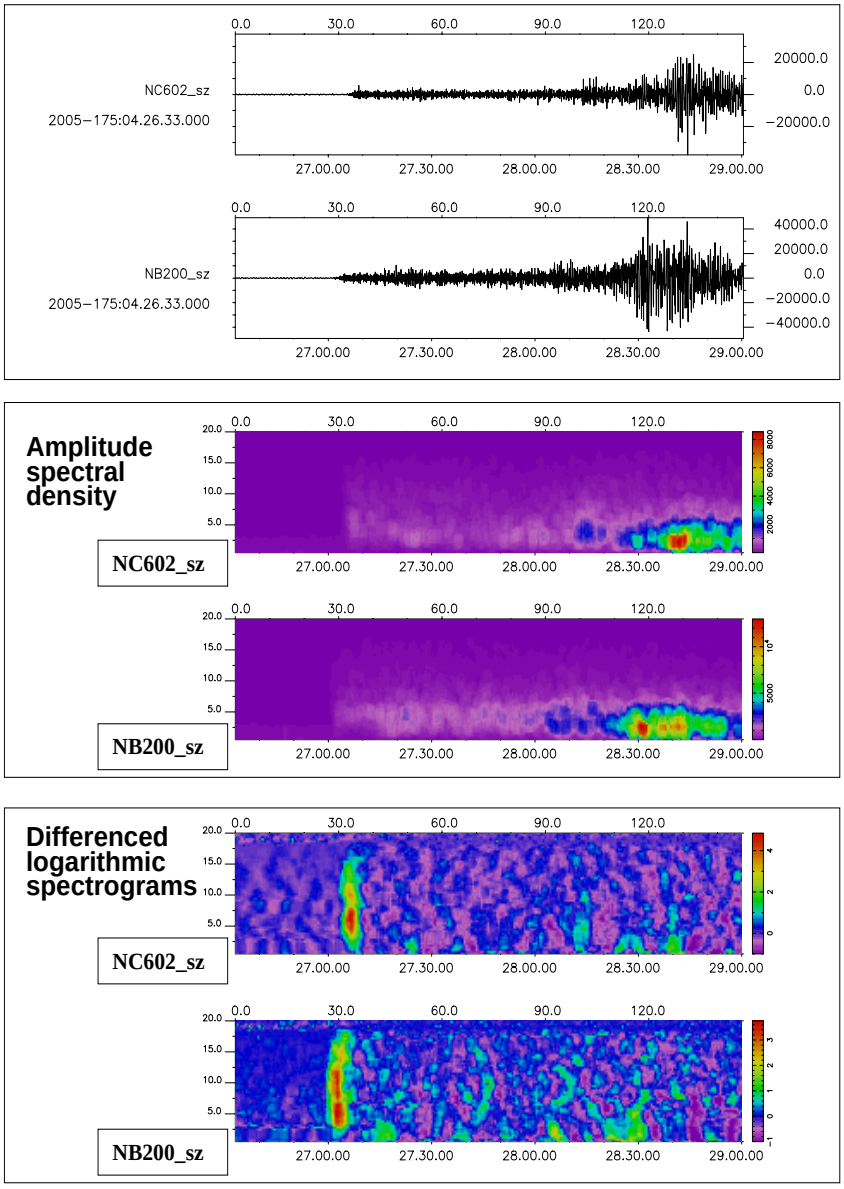

Fig. 6.1.1. Seismograms from two elements of the NORSAR array (top panel) for an earthquake in Northern Norway (distance approximately 610 km) with corresponding spectrograms, A(f), (center panel) and the function $D(f,t) = \log_{10}(A(f)_{t+}) - \log_{10}(A(f)_{t-})$ *(lower panel).*

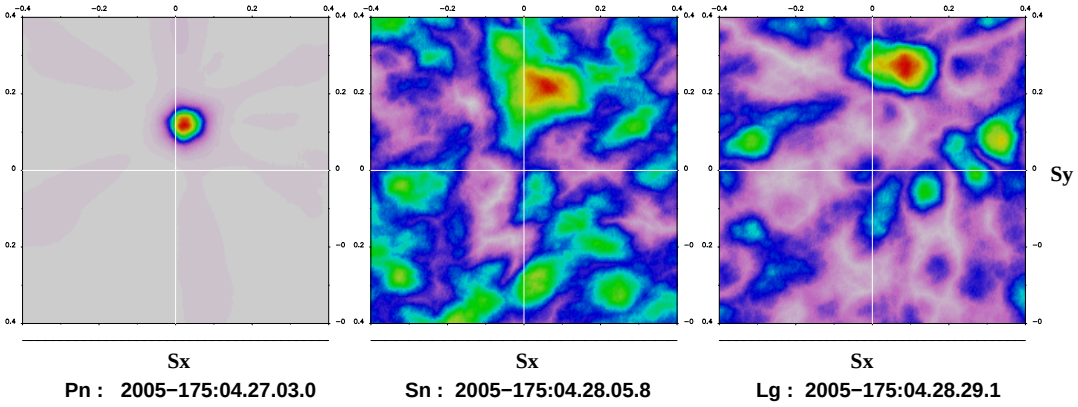

Fig. 6.1.2. Slowness estimates from the large aperture NORSAR array for the Pn, Sn, and Lg phases from the North Norway event on June 24th 2005 using spectrogram beamforming at the times indicated. The automatic location estimate incorporating these phase detections, together with detections from the regional arrays in Fennoscandia, is found on http://www.norsar.no/NDC/bulletins/gbf/2005/GBF05175.html

Such detections from the NORSAR array have been incorporated in the GBF system since March 16, 2005, and, despite the unconventional method employed, have contributed significantly to the automatic detection capability in this region and have reduced considerably the analyst workload. Since operations began, an average of 40 detections per day have been registered for regional, far regional and some teleseismic events. Most teleseismic events are missed since the waveforms are bandpass filtered above 1.8 Hz; such signals should be captured by the traditional processing of the NORSAR array. Although the number of detections made is far smaller than for the regional arrays, the large aperture of the array, combined with a conservative detection threshold, ensures that almost all detections are the result of genuine regional phases and the vast majority are subsequently associated with phases from the regional arrays. Local Rg detections which can often dominate the detection lists from the other arrays are not made since such phases would not excite all seven subarrays at times consistent with regional body waves or Lg phases. Given that the energy contrast is so low for many coda phases, few are detected using this process; waveform coherence with the appropriate steering parameters is required to achieve a sufficient SNR for detection. This is regrettable in that the rich information available to a regional array is lost, but, for the GBF, the NORSAR contributions have in many cases provided the best constraints on the solution since the detections made are almost inevitably the first P- and first S- phases at these sites.

Combined seismic-infrasonic processing

We have continued our studies of combining seismic and infrasonic recordings for detection and characterization of seismic events at local and regional distances, following up the work of Vinogradov and Ringdal (2003). We present results from an analysis of five recent surface explosions in the Kola peninsula near the Norwegian border. These co-located explosions were carried out for the purpose of destroying old ammunition, and generated unusually strong infrasonic signals in addition to seismic signals. Not unexpectedly, the infrasonic signals were well recorded on the infrasound array in Apatity, but more interestingly, they were also clearly recorded on the seismic sensors at the ARCES and Apatity arrays (both at about 250 km distance from the source area). Fig. 6.1.3 shows selected seismometer recordings from the

ARCES array for one of the explosions, with the seismic waves and the sound waves indicated on the figure.

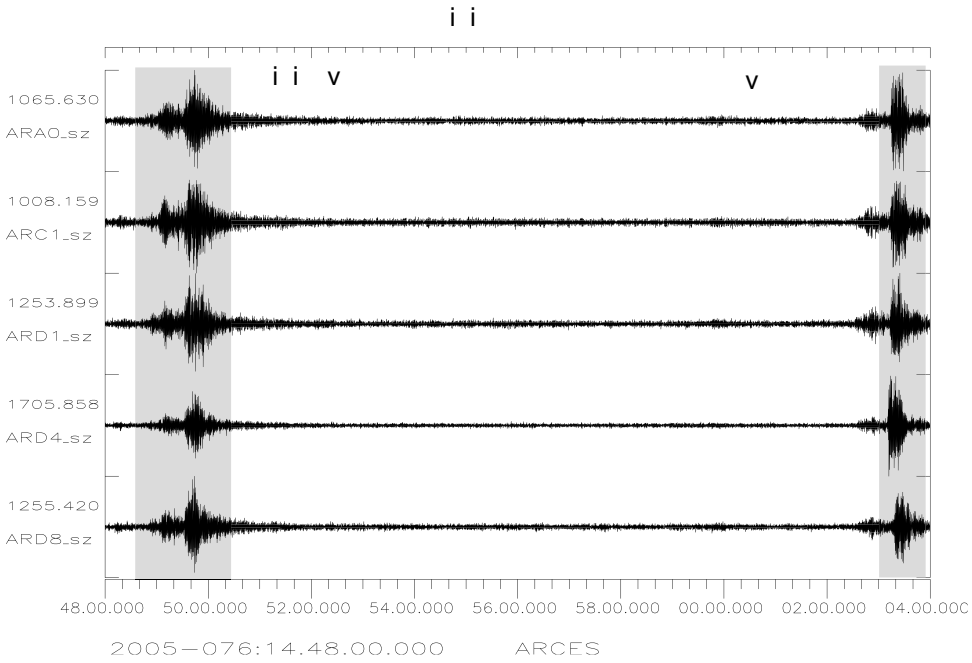

Fig. 6.1.3. ARCES waveforms for one of the explosions discussed in the text. Note the clear recording of both the seismic P and And S waves and the sound waves, which appear about 14 minutes later.

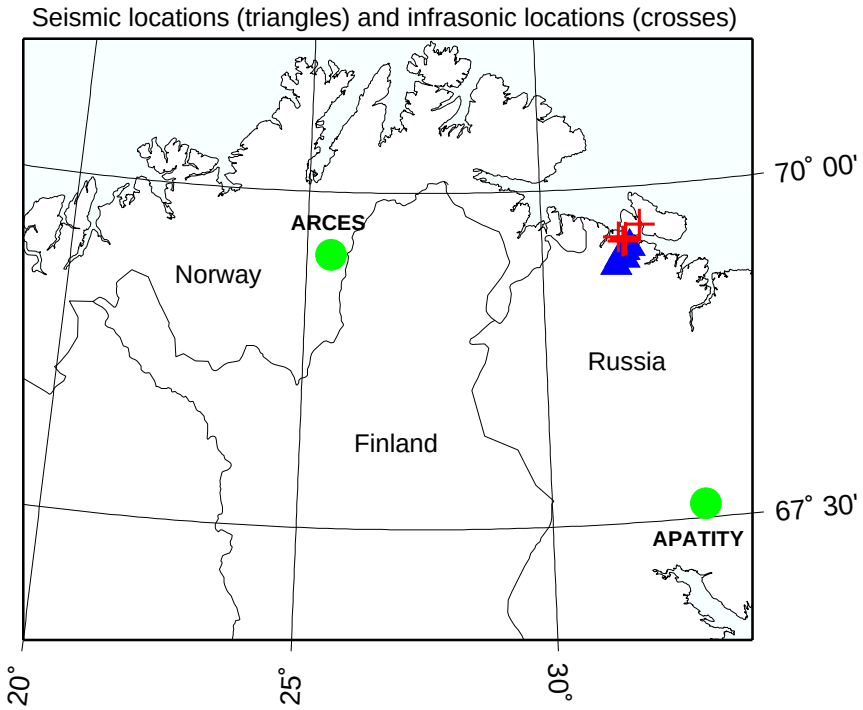

Fig. 6.1.4. The map shows results from locating the five explosions described in the text. The triangles are locations based on standard interactive analysis of the seismic data from the ARCES and APATITY arrays, whereas the crosses are locations obtained using only the estimated azimuths of the sound waves recorded by the two arrays.

Although we do not know the exact coordinates of the explosion site, we used this opportunity to investigate the stability of azimuth estimates of sound waves, using various subconfigurations of the ARCES array. It turned out that the estimates were very stable, even for the smallest subset of the array (the four-element A-ring, with a diameter of about 300 m). The estimates ranged from 82 to 86 degrees, with no significant change in the stability with the size of the selected array subset. For the 3-element APATITY infrasound array, (diameter 300 m), the estimates were likewise stable, ranging from 346 to 351 degrees.

We used the estimated azimuths (from the infrasonic waves) for the two arrays to locate the five events, and compared the recordings to those obtained using standard seismic analysis. As can be seen from Fig. 6.1.4, the locations match quite closely. This indicates an interesting potential for joint two-array infrasonic processing, and this concept will be further developed once the IMS infrasound array near ARCES has been established (expected in 2006).

Array-based waveform correlation

We have carried out an initial investigation of the potential of obtaining improved detection of small seismic events by the use of waveform correlation in conjunction with array processing. As an example of the power of using arrays in the waveform correlation process, we describe briefly some results from detecting an aftershock of the well known Kara Sea event of 16 August 1997. This small aftershock (m_b=2.5), occurred about 4 hours after the main event, and was detected by only one IMS station (the Spitsbergen array) by conventional processing (see map in Fig. 6.1.5). This array was situated about 1280 km from the event, and had several P-phase detections with a relatively low SNR, but no S-phase detection. The event could therefore not be located automatically, and was identified as an aftershock through careful analyst inspection.

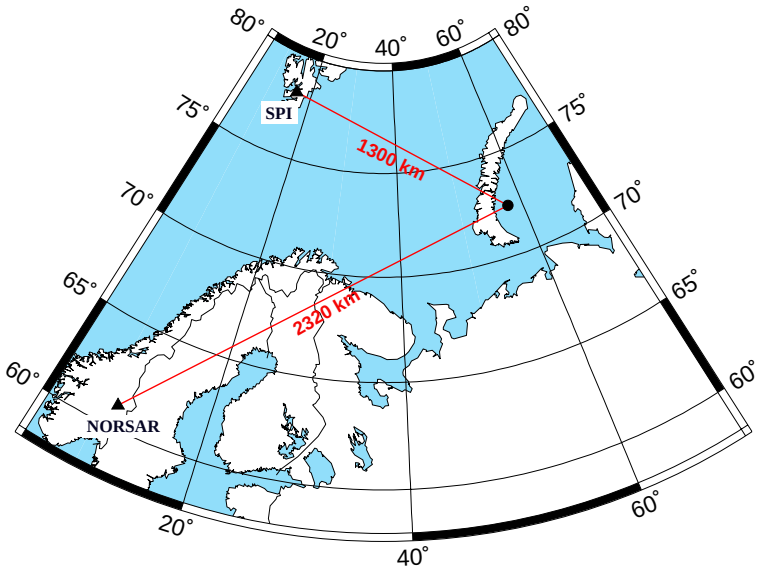

Fig. 6.1.5. The location of the NORSAR and Spitsbergen arrays in relation to the site of the 16 August 1997 Kara Sea events (main shock of m_b=3.5 and aftershock of m_b=2.5)

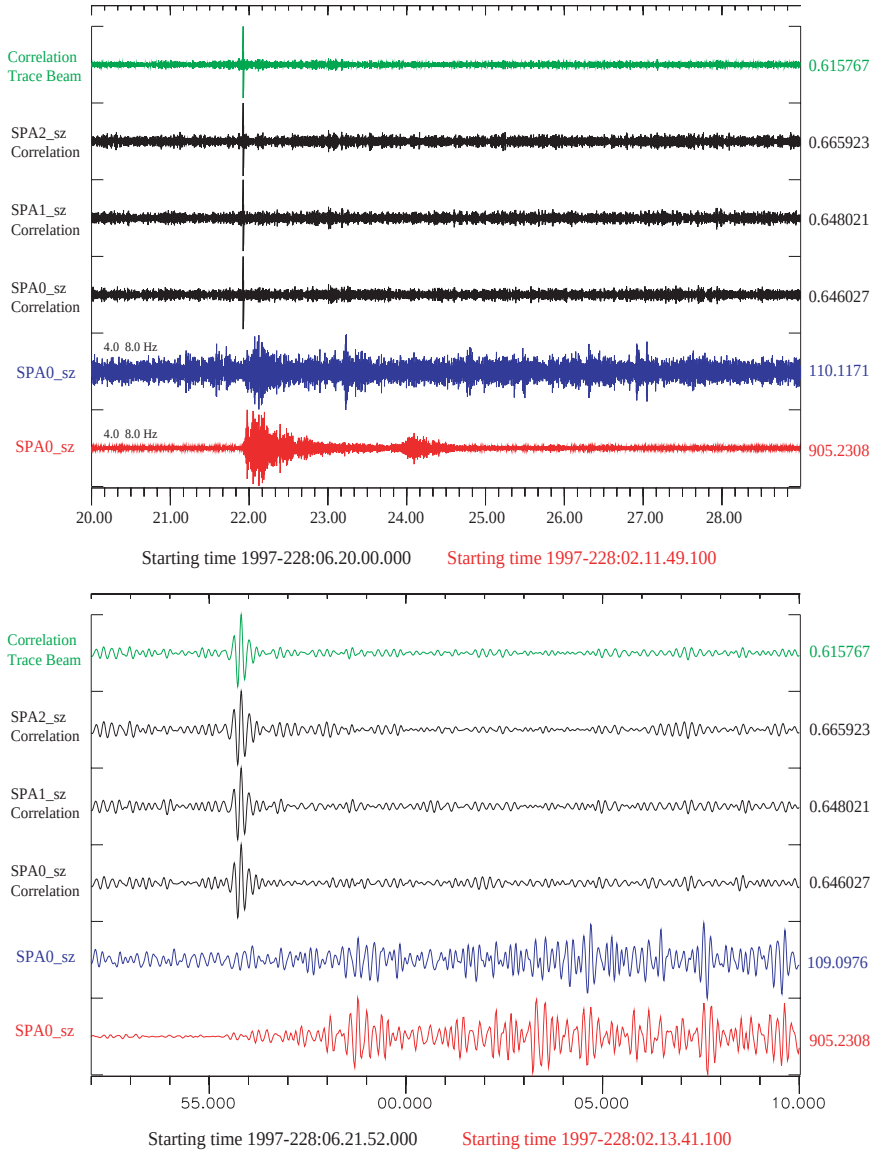

Fig. 6.1.6. Detection of an aftershock from the 16 August 1997 Kara Sea event using waveform correlation on the short period vertical channels of the Spitsbergen array. Each channel was bandpass filtered between 4.0 and 8.0 Hz and a 60 second long data segment was extracted from the master event signal (shown in red for SPA0 sz) with the first data segment beginning at 1997-228:02.13.44.913. The data containing the presumed aftershock was filtered in the same band (shown in blue for SPA0) and a trace of fully normalized correlation coefficients was calculated for each channel. The green channel is the summation of the 9 correlation coefficient traces. A clear peak is observed on the correlation beam at a time 1997-228:06.21.55.815. The lower panel is a zoom-in of the upper panel.

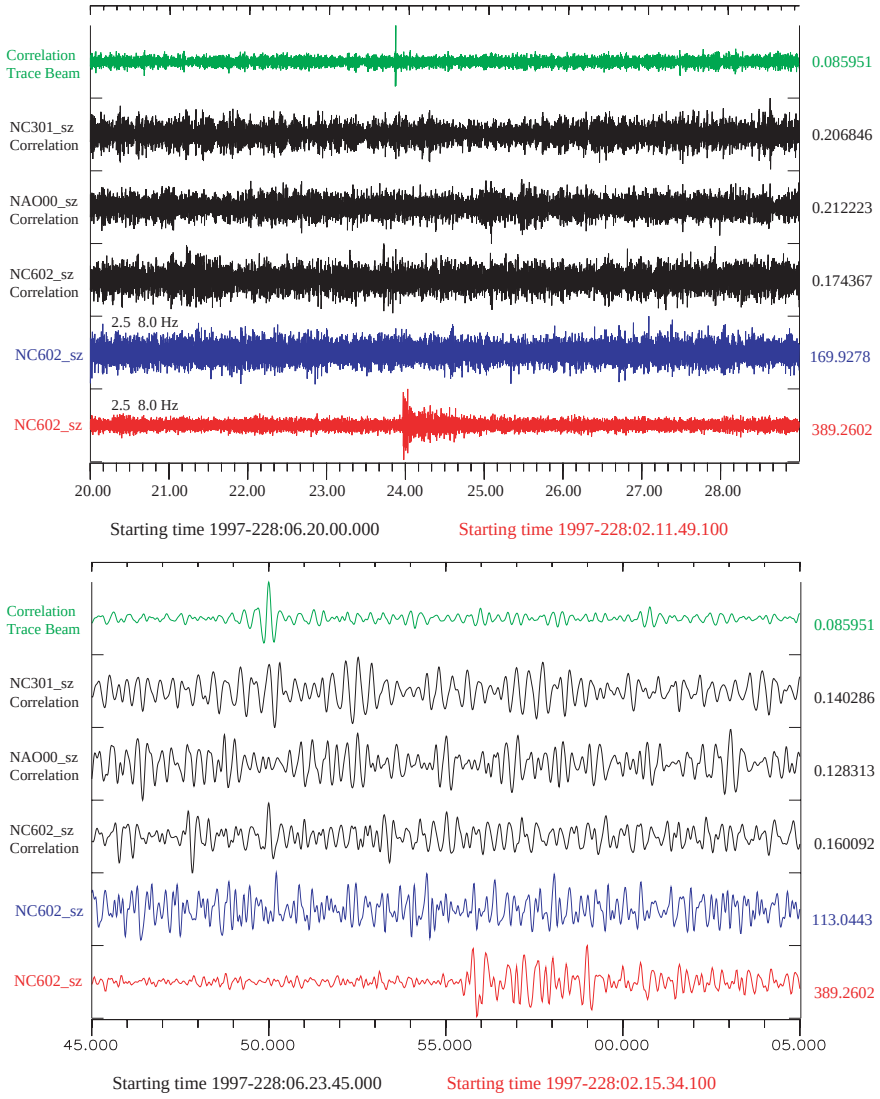

Fig. 6.1.7. Detection of the Kara Sea event aftershock by waveform correlation using the NORSAR array. The frequency band applied in this calculation is 2.5 - 8.0 Hz. The time windows containing the master event signal are staggered by several seconds to account for the significant time delays across the array; the first master event time-window begins at 1997-228:02.15.39.087 for instrument NC301. The signal at this far more distant array is buried in the noise to a far greater extent than at SPI and in no filter band could this signal be detected with a conventional STA/LTA detector. While the SPI signal is very coherent over the array in the frequency band for which the SNR is optimal facilitating a reasonable SNR gain by conventional beamforming; this is not the case for the NOA signal. In contrast to the correlation displayed in Fig. 6.1.3, the individual sensor correlation traces do not indicate clear simultaneous maxima. However, the beam (formed by applying the appropriate time-shifts to the individual correlation traces) displays a clear peak at time 1997-228:06.23.49.999.

We applied an array correlation procedure to both the small-aperture Spitsbergen array and the large-aperture NORSAR array (at a distance of more than 2300 km), using the main event as a master waveform. The results for the small aftershock are shown in Figs. 6.1.6 and 6.1.7. Both

figures show very distinct correlation peaks for the aftershock at times indicative of two co-located events. The Spitsbergen array (Fig. 6.1.6) has clear peaks both for the individual sensors and on the beam. The results from the large NORSAR array (Fig. 6.1.7) are even more impressive, and illlustrate one of the main strengths of the correlation/beamforming process; the individual correlation traces are coherent across the array even when the actual waveforms are not. The correlation/beamforming process therefore provides an SNR gain far greater than that achieved by conventional beamforming. In fact, the event cannot even be seen on the NORSAR individual sensor correlation traces, whereas it is clearly visible on the beam of these traces. We plan to develop the array-based correlation method further over the next three years in a separate joint research project with LLNL.

6.1.3 Conclusions and recommendations

We have implemented a new processing system for incorporating regional seismic phases detected by the large NORSAR array into the Generalized Beamforming process currently in use at NORSAR for on-line automatic detection and location of seismic events in the European Arctic. The system represents a significant improvement over previous processing systems for large arrays, and we recommend that this metod be further developed for improving automatic detection and location using local or regional networks.

We have obtained some interesting results when comparing location estimates based on seismic and infrasonic recordings of surface explosions at local and regional distances. Using ARCES and Apatity array recordings of a set of explosions near the Norwegian-Russian border, we have found that the infrasonic locations (using azimuths only) match closely the locations obtained through standard seismic data analysis. This indicates an interesting potential for joint two-array infrasonic processing, and we recommend that this concept be further developed once the IMS infrasound array near ARCES has been established (expected in 2006).

We have documented a significant potential of obtaining improved detection of small seismic events by the use of waveform correlation in conjunction with array processing. We have demonstrated that waveform correlation could be used to detect the small aftershock (m_b=2.5) following the 16 August 1997 Kara Sea event, not only at the Spitsbergen array (distance 1100 km), but even at the large NORSAR array situated more than 2300 km from the epicenter. We recommend that further studies be undertaken on potential applications of this technique, which we will develop further over the next three years in a separate joint research project with LLNL.

F. Ringdal
S. J. Gibbons
T. Kværna
V. Asming
Yu. Vinogradov
S. Mykkeltveit
J. Schweitzer

References

Bungum, H., E. S. Husebye and F. Ringdal (1971) The NORSAR array and preliminary results of data analysis, *Geophys. J. R. Astr. Soc., 25*, 115-126.

Freiburger, W. F.(1963). An approximation method in signal detection, *Quart. J. App. Math.*, 20, 373-378.

Mykkeltveit, S., F. Ringdal, T. Kværna and R. W. Alewine (1990). Application of regional arrays in seismic verification research, *Bull. Seism. Soc. Am.*, **80**, 1777-1800.

Ringdal, F. (1997): Study of low-magnitude seismic events near the Novaya Zemlya nuclear test site, *Bull. Seism. Soc. Am. 87 No. 6*, 1563-1575.

Ringdal, F. and T. Kværna (1989). A multichannel processing approach to real time network detection, phase association and threshold monitoring, *Bull. Seism. Soc. Am.*, **79**, 1927-1940.

Ringdal, F., E. S. Husebye and A. Dahle (1972). Event detection problems using a partially coherent seismic array, NORSAR Tech. Rep. 45, Kjeller, Norway.

Thomson, D. J. (1982). Spectrum Estimation and Harmonic Analysis, *Proc. IEEE,* 70 , 1055-1096.

Vinogradov, Yu. and F. Ringdal (2003). Analysis of infrasound data recorded at the Apatity array, *Semiannual Technical Summary 1 July - 31 December 2002*, NORSAR Sci. Rep. 1-2003, Kjeller, Norway.

6.2 Surface Wave Tomography for the Barents Sea and Surrounding Regions – Part II

6.2.1 Introduction

In a previous study (Part I; Levshin et al., 2005a) a new dataset of surface-wave observations from more than 150 local and regional events with travel paths through the greater Barents Sea region was compiled and group-velocity dispersion curves were measured for Love and Rayleigh waves in the period range 14 – 160 s. This large amount of new group-velocity measurements was used to enlarge the already existing data base compiled at the University of Colorado and to increase the path density in the region under investigation (Levshin *et al.*, 2001). This combined data set of group-velocity observations was inverted for 2D group-velocity maps (Barmin *et al.*, 2001; Ritzwoller *et al.*, 2002; Levshin *et al.*, 2005a). Pasyanos (2005) recently published another set of group-velocity maps for Eurasia and the European Artic, which show very similar large scale features in the greater Barents Sea region but which have far less resolution for smaller scale anomalies in that area.

As mentioned in Levshin *et al.* (2005a), it was planned to invert the new group velocity maps for Love and Rayleigh waves for a new 3D velocity model of the European Arctic. This paper summarizes the results of this inversion.

6.2.2 Inversion of the 3D tomographic S-velocity model

The 2D group-velocity maps derived from the new dataset of Love and Rayleigh wave group-velocity observations were the main input for a new 3D inversion for S-wave velocities. Due to the small number of short period surface-wave observations however, the resolution is limited for details in the structure of the crust, in particular in its upper most part. In addition, surface waves of higher frequencies are much more influenced by scattering at lateral heterogeneities in the crust.

To improve the inversion with respect to that, we applied a new crustal model of the Barents Sea and its surrounding areas, which had been derived in a joint project between the University of Oslo, NORSAR, and the USGS (Bungum *et al.*, 2005). This model with its detailed information on crustal thickness and sedimentary basins in the area helps to constrain the tomographic inversion based on surface wave data particularly in the shallow parts of the resulting model of crustal and upper mantle S-wave velocities.

Therefore, for the 3D inversion of the surface-wave data this crustal model was applied as an initial model. The upper crust with its information on sedimentary coverage of the greater Barents Sea region was used as constraint and not altered during the inversion. The lower crust and the Moho depth were also taken from the recent crustal model but this part of the model was also inverted for. Since the crustal model of Bungum *et al.* (2005) is a P-wave velocity model, the corresponding S velocities were calculated with the P-to-S velocity transformation as used in CRUST2.0 (Bassin *et al.*, 2000; http://mahi.ucsd.edu/Gabi/rem.dir/crust/crust2.html).

For the upper mantle part, the Colorado University (CU) model of Shapiro & Ritzwoller (2002) was used as initial model down to a depth of 250 km (see also http://ciei.colorado.edu/~nshapiro/MODEL/index.html). Below 300 km, we applied the Harvard model J362D28 (Antolik *et*

al., 2003) as input model. A smooth transition was used between these two models in the depth range from 250 to 300 km.

The 3D inversion method follows the technique described in detail by Shapiro & Ritzwoller (2002). The resulting 3D shear-velocity model of the crust and upper mantle beneath the European Arctic provides higher resolution and accuracy than previous models. In addition, the 3D S-velocity model was converted into a 3D P-velocity model using temperature-velocity relations for mantle material as described in Goes *et al.* (2000) and Shapiro & Ritzwoller (2004).

The inversion results are presented as deviations in shear-wave speed from the average S-wave speed in each layer of the model (in percent). Fig. 6.2.1 shows the new model in several horizontal slices in the range from 60 to 280 km depth. The new model reveals substantial variations in shear-wave speeds in the upper mantle across the region. Of particular note are clarified images of the mantle expression of first-order tectonic regimes like the mid-Atlantic ridge, the continental-ocean transition in the Norwegian Sea or a thickened crust beneath Novaya Zemlya (Fig. 6.2.2).

An extended region of increased velocity beneath the Barents Sea is dipping eastwards and suggests higher densities and thus an optional explanation for the evolution of the deep sedimentary basin in that region. This dipping structure is best seen along vertical profiles showing the velocity distribution over the entire modeled depth range. Fig. 6.2.2 presents four such profiles and in addition the velocity variations in 40 km depth, which reveal approximately the lateral change in the velocities relevant for Sn propagation. Engdahl & Schweitzer (2004a; 2004b) described pronounced differences in travel times and waveform shapes on NORSAR array recordings of nuclear explosions conducted both at the northern and at the southern nuclear test side on Novaya Zemlya. This observation may be explained by multipathing effects due to the dipping high velocity body.

6.2.3 Conclusions

The substantial data set of new surface group-velocity measurements combined with already existing data has provided the opportunity for constructing a new 3D shear-velocity model of the crust and upper mantle down to about 250 km beneath the European Arctic.

This model has higher spatial and depth resolution than previous models and clarifies or reveals important features of the tectonic setting in the region: continent-ocean boundary, a dipping slab-like high velocity zone in the upper mantle and the lithospheric structure under the deep sedimentary basin.

Ritzwoller *et al.* (2003) derived source specific travel-time corrections (SSSCs) based on 3D tomographic surface-wave model. The new 3D velocity model presented here may be used for refining these corrections for regional P and S waves propagating through the larger Barents Sea region.

Acknowledgements

For this study we requested and retrieved broadband and long periodic data from the Norwegian National Seismic Network (NNSN, University in Bergen), Kola Regional Seismological Center (KRSC, Apatity), Danmarks og Grønlands Geologiske Undersøgelse (GEUS, Copenhagen), Totalförsvarets forskningsinstitut (FOI, Stockholm), British Geological Service (BGS, Edinburgh), the Finish National Seismic Network (FNSN, University of Helsinki), and the international network operators and data centers IRIS and GEOFON. That they all made their data available for this study is gratefully acknowledged.

Anatol Levshin, University of Colorado
Johannes Schweitzer
Christian Weidle, University of Oslo
Nikolai Shapiro, University of Colorado
Nils Maercklin
Mike Ritzwoller, University of Colorado

References

Antolik, M., Y.J. Gu, A.M. Dziewonski & G. Ekström (2003). A new joint model of compressional and shear velocity in the mantle. *Geophys. J. Intl.* **153**, 443-466.

Barmin, M.P., M.H. Ritzwoller, & A.L. Levshin (2001). A fast and reliable method for surface wave tomography. *Pure Appl. Geophys.* **158**, 1351-1375.

Bassin, C., G. Laske, & G. Masters (2000). The current limits of resolution for surface wave tomography in North America. *EOS Trans. AGU* **81**(48), F879, Abstract S12A-03.

Bungum, H., O. Ritzmann, N. Maercklin, J.I. Faleide, W.D. Mooney, & S.T. Detweiler (2005). Three-dimensional model for the crust and upper mantle in the Barents Sea region. *EOS Trans. AGU* **86**, 160-161.

Engdahl, E.R. & J. Schweitzer (2004a). Observed and predicted travel times of Pn and P phases recorded at NORSAR from regional events. In: Semiannual Technical Summary, 1 January – 30 June 2004, *NORSAR Scientific Report* **2-2004**, 51-56.

Engdahl, E.R. & J. Schweitzer (2004b). Observed and predicted travel times of Pn and P phases recorded at NORSAR from regional events. *Eos Trans. AGU* **85** (47), Abstract S13B-1050.

Goes, S., R. Govers & R. Vacher (2000). Shallow mantle temperatures under Europe from P and S wave tomography. *J. Geophys. Res.* **105**, 11,153-11,169.

Levshin, A.L., M.H. Ritzwoller, M.P. Barmin, A. Villaseñor & C.A. Padgett (2001). New constraints on the Arctic crust and uppermost mantle: surface wave group velocities, P_n, and S_n. *Phys. Earth Planet. Int.* **123**, 185-204.

Levshin, A., Ch. Weidle & J. Schweitzer (2005a). Surface wave tomography for the Barents Sea and surrounding regions. In: Semiannual Technical Summary, 1 January – 30 June 2005, *NORSAR Scientific Report* **2-2005**, 37-48.

Levshin, A., J. Schweitzer, Ch. Weidle, N. Maercklin, N. Shapiro & M. Ritzwoller (2005b). Surface wave tomography of the European Artic, *Eos Trans. AGU* **86 (52)**, Fall Meeting Supplement, Abstract S51E-1053.

Pasyanos, M.E. (2005). A variable resolution surface wave dispersion study of Eurasia, North Africa, and surrounding regions. *J. Geoph. Res.* **110**, B12301, doi:10.1029/2005JB003749, 22 pp.

Ritzwoller M.H., N.M. Shapiro, M.P. Barmin & A.L. Levshin (2002). Global surface wave diffraction tomography. J. Geoph. 107(B12), 2335, ESE 4-1 – 4-13, doi:10.1029/2002JB001777.

Ritzwoller, M.H., N.M. Shapiro, A.L. Levshin, E.A. Bergman & E.R. Engdahl (2003). The ability of a global 3-D model to locate regional events. *J. Geophys. Res.* **108**(B7), 2353, ESE 9-1 – 9-24.

Shapiro, N.M. & M.H. Ritzwoller (2002). Monte-Carlo inversion for a global shear velocity model of the crust and upper mantle. *Geophys. J. Int.* **151**, 88-105.

Shapiro, N.M. & M.H. Ritzwoller (2004). Thermodynamic constraints on seismic inversions. *Geophys. J. Int.* **157**, 1175-1188, doi:10.1111/j.l365-246X.2004.02254.x.

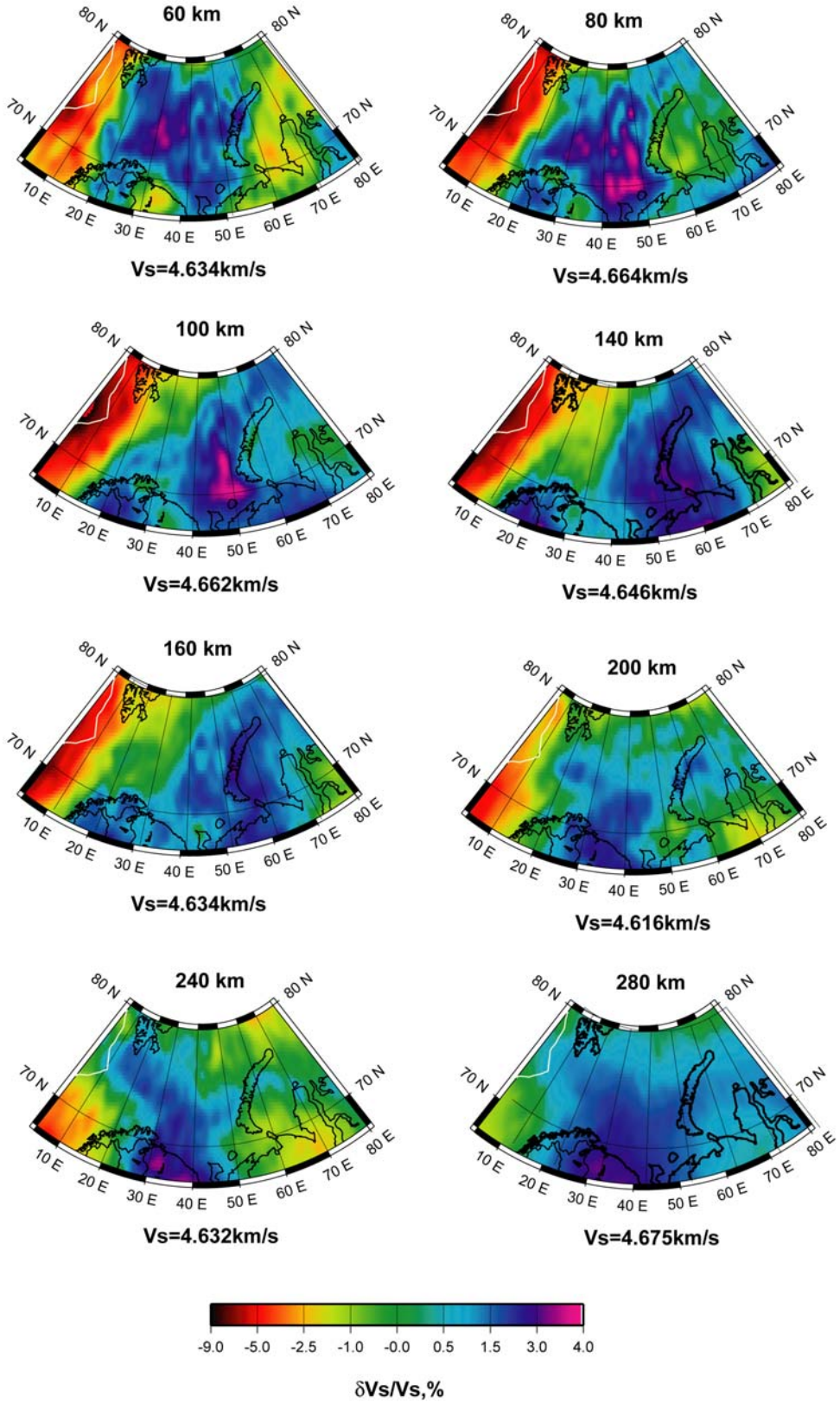

Fig. 6.2.1. Results of the 3D tomographic inversion, shear wave velocities in percentage relative to the average velocity; shown are the S velocities in different depths. The mean S velocity is given for each map separately.

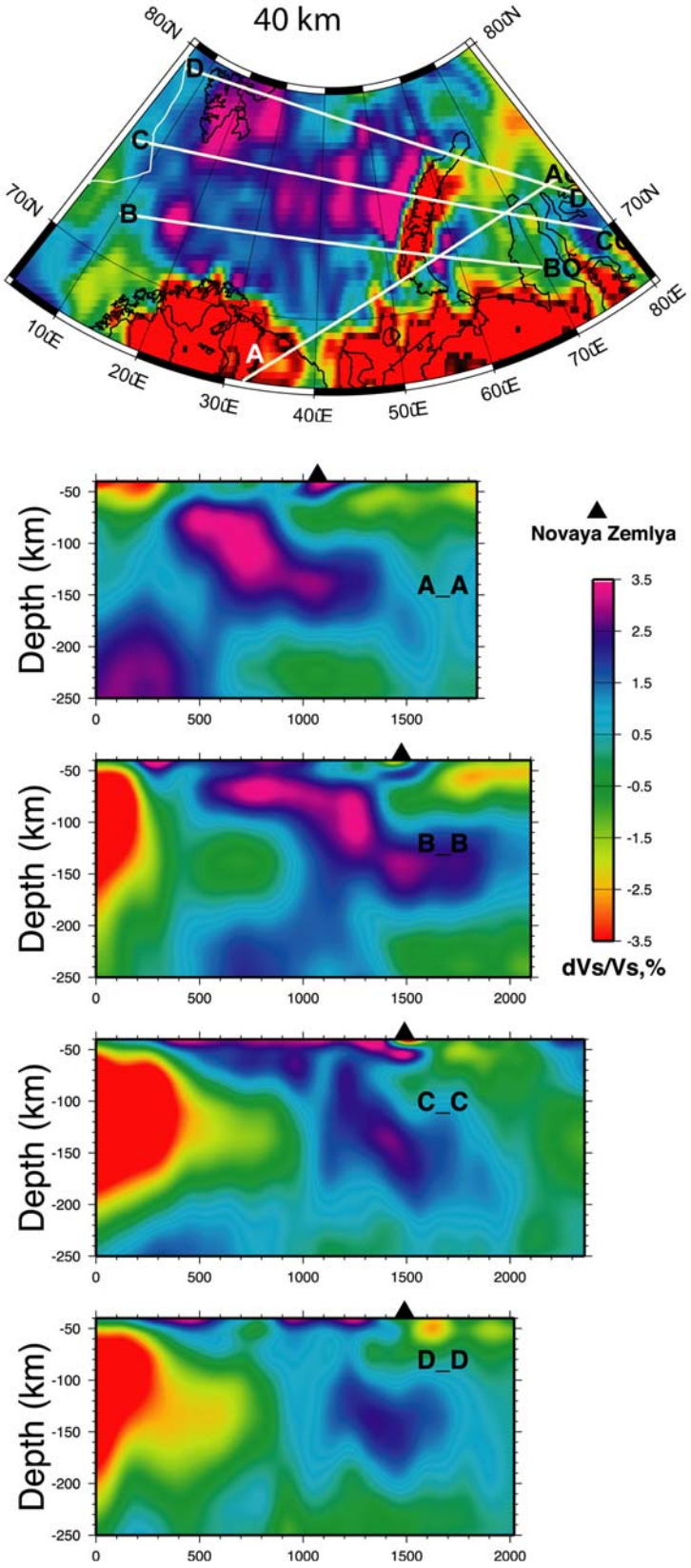

Fig. 6.2.2. On top are shown the relative S velocities in 40 km depth with respect to the mean velocity and the location of four transects. The four lower figures show the S-velocity perturbations along these transects.

6.3 Infrasound data processing using Apatity and ARCES array data

6.3.1 Introduction

In this study, we have focused on developing basic infrasonic processing software for the Apatity infrasonic array and for the ARCES seismic array. In the case of ARCES, there are currently no infrasonic sensors available (the plans are to install an infrasound array in 2006), but the seismic sensors have proved useful as an initial substitute for detecting and processing infrasonic signals from explosions at local and regional distances.

We have also developed an algorithm for associating detected infrasonic phases (either by ARCES or Apatity) to regional seismic events generated in the on-line Generalized Beamforming process which is currently in experimental operation at NORSAR. The current status of these developments is summarized in the following.

6.3.2 Infrasound data processing using Apatity array data

The Apatity infrasound array is a three-element array co-located with the nine-element Apatity short-period regional seismic array, installed in 1992 on the Kola Peninsula, Russia by the Kola Regional Seismological Centre (KRSC). The three infrasound sensors (MB1, MB2, and MB3) are located close to the seismic array sites A1, A2, and A3 (Fig. 6.3.1).

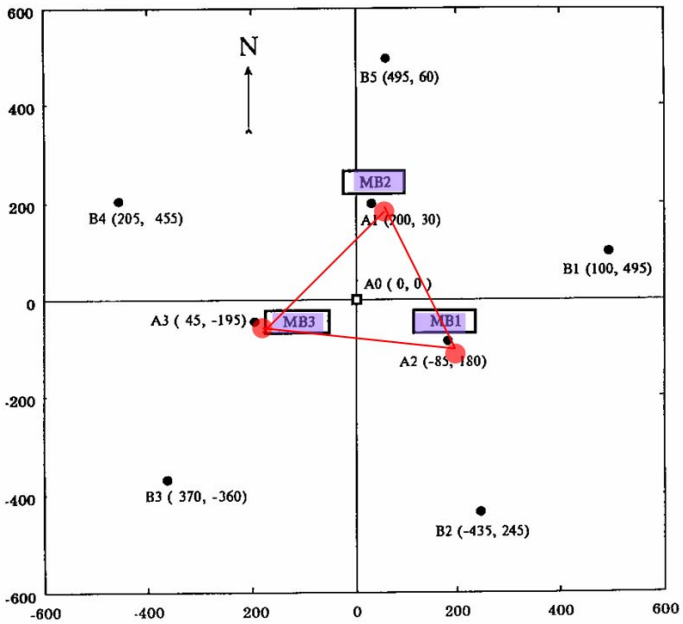

Fig. 6.3.1. Map of the Apatity seismic array with the location of the three infrasound sensors MB1, MB2, and MB3 (Baryshnikov, 2004). The axis coordinates are in meters relative to the array center.

The infrasound array was installed in June 2002, and since then, its continuous data stream has been included in the data stream from the seismic sensors transmitted to KRSC. In 2003, the originally installed K-304-AM microbarometers were exchanged with CHAPARRAL Model 5 microbarometers, for further details see Baryshnikov (2004). At all three infrasound array sites, star-like tube-systems have been installed to filter out acoustic noise.

With only 3 sensors in the array, the SNR gain by beamforming is small (√3). Nevertheless, we used beamforming and filtering in this initial study as a basis for detecting infrasound signals. Whenever an infrasound signal is observed by all three sensors, standard array techniques like fk-analysis can be efficiently used to measure backazimuth and apparent velocity of the signal. These measurements have to be interpreted very carefully, since the array-response function of a three element array has many sidelobes. Fig. 6.3.2 shows the array response of the Apatity infrasound array for a signal with a dominant period of 5 Hz, which is within the frequency range usually observed for regional infrasound signals.

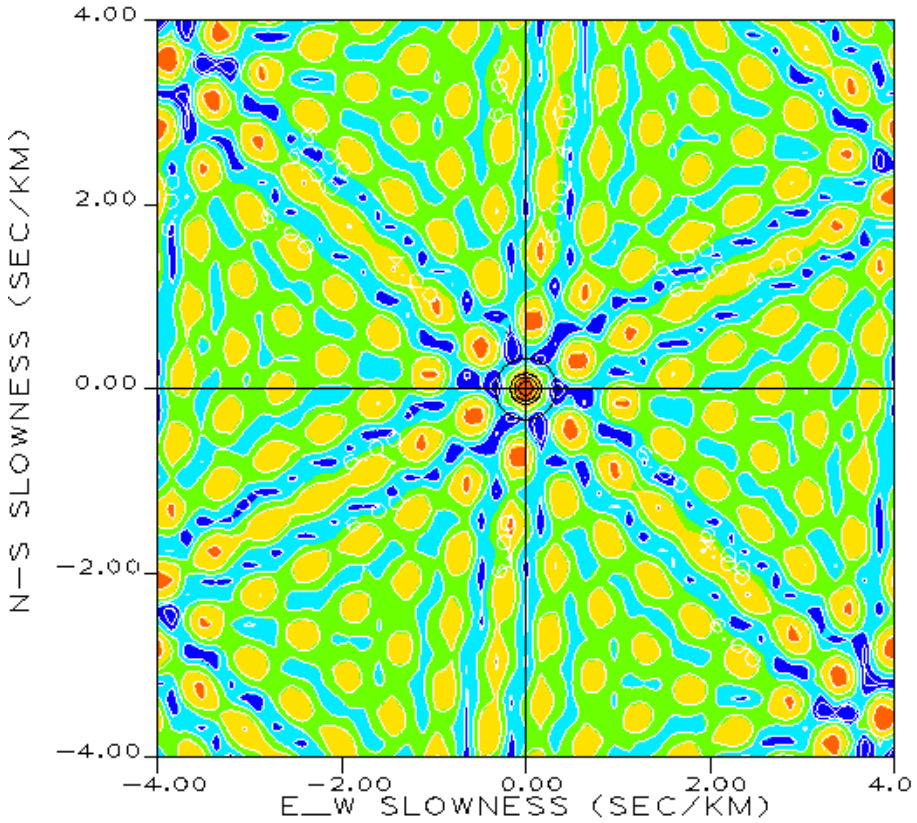

Fig. 6.3.2. The array response of the Apatity 3-element infrasound array for a signal with a dominant frequency of 5 Hz.

Signal detector for Apatity array data

Infrasound signals have usually dominant frequencies in the same range as seismic signals, and tools developed for detecting and analyzing seismic signals at seismic arrays can also be used for processing infrasound signals. This approach was used to develop an initial detector for the Apatity infrasound array:

To cover the range of incidence angles expected for infrasound signals, array beams were deployed with three different apparent velocities (0.33, 0.45, and 0.55 km/s).

For each of these apparent velocities, beams were deployed for 12 different backazimuths (0, 30, 60, 90, 120, 150, 180, 210, 240, 270, 300, and 330 degrees).

Each of these 36 beams are filtered with eight different bandpass filters in the frequency ranges 0.8 – 2.0, 1.5 – 3.0, 2.0 – 4.0, 2.5 – 8.0, 3.0 – 6.0, 4.0 – 8.0, 6.0 – 12.0, and 8.0 – 16.0 Hz.

This deployment resulted in a total of 288 beams.

During testing, it became clear that larger noise bursts at one of the three sensors very often cause spurious detections on the beams. Such noise bursts are quite frequent and the number of such detections is therefore quite high. To reduce the number of such noise detections, the detection threshold of the STA/LTA detector was initially set as high as 10.0. With this setting, smaller signals will be missed, but this largely reduces the number of noise detections.

All data from 2005 were processed using these detector settings. This resulted in a total of 69,227 detections, which averages to 189.7 detections /day.

Fk-analysis for Apatity array data

As already mentioned, the largest fraction of infrasound detections is caused by noise bursts at one of the array sensors. Such detections are not of particular interest in our context and should therefore be identified and discarded. By comparing the observed amplitudes in the detection-filter band at the individual sensors, all detections based on large amplitudes at a single sensor are removed from any further analysis. Fig. 6.3.3 shows an example of such a signal.

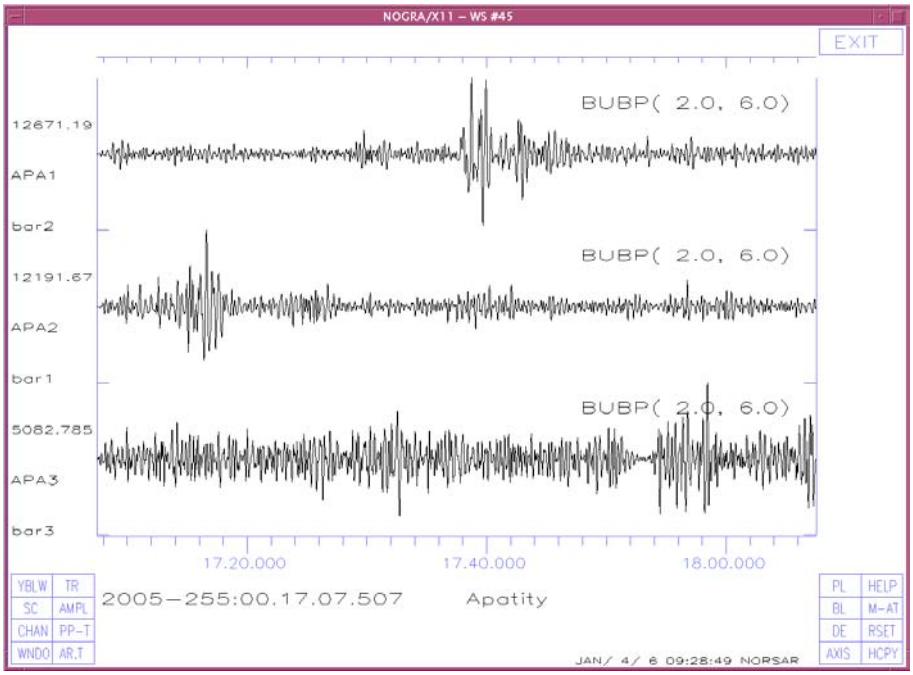

Fig. 6.3.3. Typical observation of single sensor noise bursts at the the Apatity infrasound array.

Before fk-analysis, the data are Butterworth bandpass filtered. The frequency range of this bandpass filter is based on the detection filter, but is widened to include a larger frequency range. The amount of such widening is SNR-dependent. For the fk-analysis a signal-window length between 3 and 15 s is used, and the minimum noise-length window before the estimated onset time is set to 0.5 s.

However, even after checking the amplitudes many noise burst detections remain in the detection lists and the results of the fk-analysis must be further evaluated. It is known that infrasound signals are highly coherent across arrays. Fig. 6.3.4 shows a data example for such a highly coherent infrasound signal. This coherency can be used as an additional parameter to select reliable infrasound signals. The following evaluation procedure has been implemented:

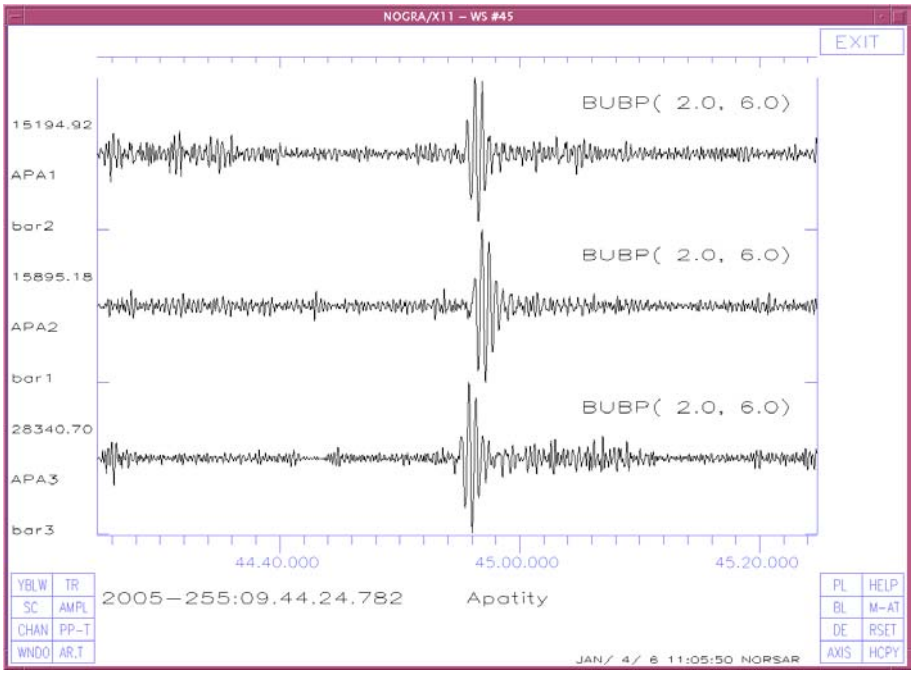

Fig. 6.3.4. A typical infrasound signal recorded at the three infrasound sensors of the Apatity infrasound array.

- The backazimuth and apparent velocity estimated by fk-analysis are used to calculate a beam trace.
- This beam trace is cross-correlated with all three single traces and backazimuth and apparent velocity are recalculated by fitting a plane-wave to the relative onset times on the single traces.
- These wavefront parameters and the cross-correlation values are then compared with the results of the fk-analysis.
- Each fk-analysis (and cross-correlation analysis) is performed for 7 slightly changed window positions/length to find the best slowness estimate, i.e., the highest relative power and cross-correlation value.
- If the highest cross-correlation values exceed a certain threshold, the corresponding plane wave fit is used to determine the wavefront parameters, otherwise the best f-k result is used.
- Following the rule used at the IDC in Vienna, whenever the apparent velocity is between 0.27 and 0.66 km/s, the phase is assumed to be an infrasound (IS) observation.

By this implementation, 8,556 infrasound signals were found for 2005, which gave on average 23.4 detections per day. For the 8,382 infrasound signals detected until the 17th of December 2005 we show histograms with the distribution of apparent velocities (Fig. 6.3.5) and the backazimuth values (Fig. 6.3.6). It is obvious that the largest number of infrasound signals correlates with pronounced backazimuth directions and that most of the signals have apparent velocities between 0.3 and 0.4 km/s.

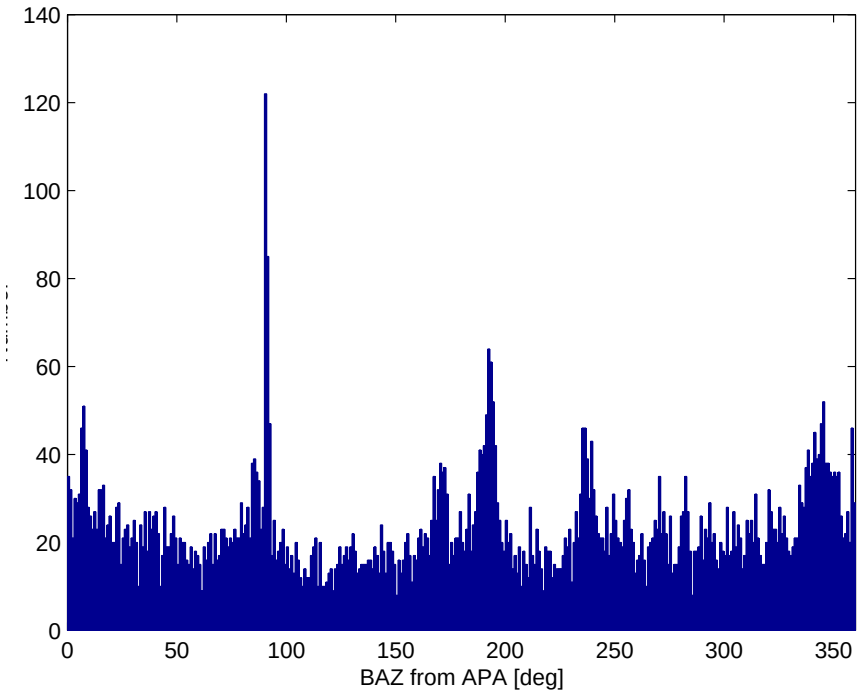

Fig. 6.3.5. Distribution of 8,556 backazimuth observations of infrasound signals observed with the Apatity infrasound array during 1st January – 17th December 2005.

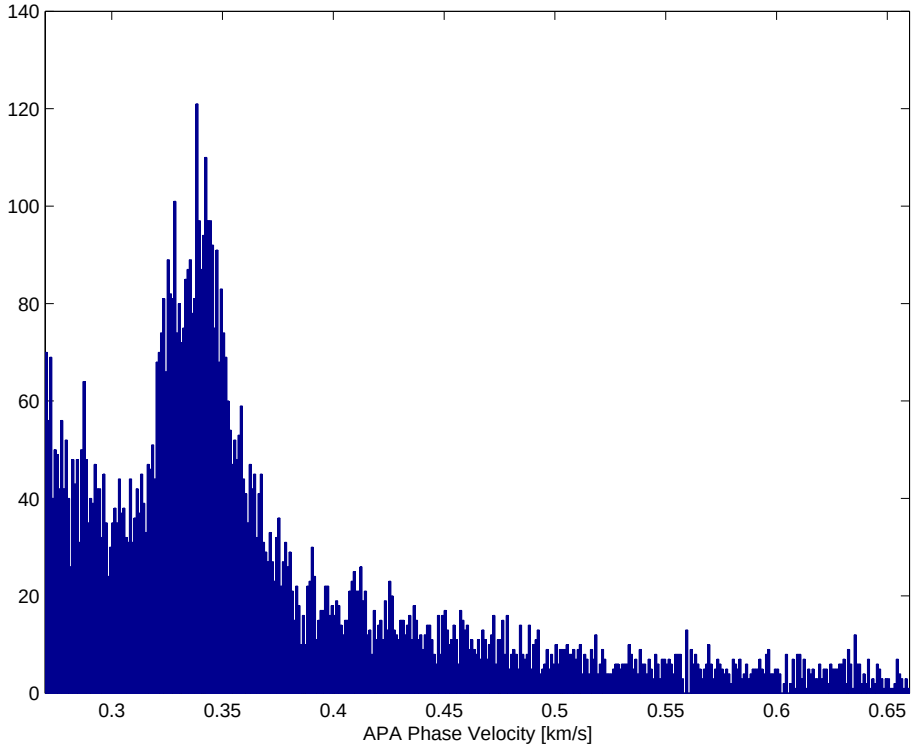

Fig. 6.3.6. Distribution of 8,556 apparent velocity observations of infrasound signals observed with the Apatity infrasound array during 1st January – 17th December 2005.

6.3.3 Infrasound data processing using ARCES array data

Description of the ARCES Array

The 25 element ARCES array is as the Apatity array a short-period regional seismic array, located in the European Arctic. ARCES has no infrasound sensors but because of special installation conditions, many of its seismic sensors are also sensitive to infrasound signals. The main reason for this sensitivity is that the seismometers of the array are standing directly on bedrock, which appears at the Earth's surface in this part of Norway. The seismometers and the associated electronic equipment are protected against the harsh arctic weather conditions by being installed inside closed vaults, but many examples can be found for which sound waves from e.g. large explosions couple into the ground and thereby produce acoustic signals recorded by the seismic sensors (e.g., Ringdal & Schweitzer, 2005).

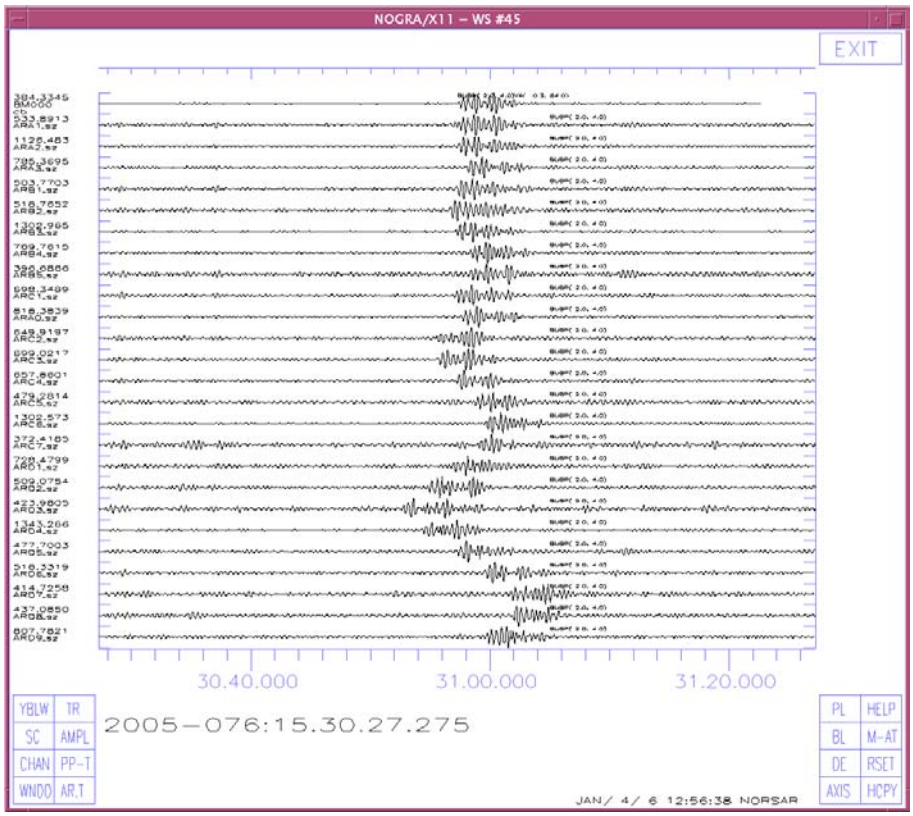

Fig. 6.3.7. An example for an acoustic signal recorded by the seismic instruments of the ARCES array.

The ARCES array consists of 25 sites located on concentric circles with a maximum aperture of 3 km. The observed coupling of acoustic signals into the ground is not equally effective for all sites and large amplitude differences can be observed. However, if recorded, the infrasound signals are highly coherent across the array just like we have observed for data from the Apatity infrasound array. Fig. 6.3.7 shows such a signal recorded at the ARCES array.

With its much higher number of sites and larger aperture, the ARCES array has much better capabilities to measure the wavefront parameters backazimuth and apparent velocity compared to the Apatity array.

Signal detector for ARCES array data

The beam deployment for an infrasound detector at ARCES has to cover the interesting apparent velocity range for all backazimuths. Because of the larger aperture of the array and thereby longer travel times needed by infrasound signals to cross the array, an enormous number of detection beams is needed to cover the whole parameter space. To keep the number of detection beams within a reasonable range, the ARCES D-ring is not used for this initial detector deployment. Two different array configurations have been defined:

- One with 16 ARCES sites comprising the center instrument, the A-, B- and C-ring.
- One with only the A-sites of ARCES (A0, A1, A2, and A3), which is similar to the Apatity infrasound array configuration. However, when comparing the array responses of the different configurations (Figs. 6.3.2 and 6.3.8), it is obvious that the additional element in the center of ARCES improves the array response by reducing disturbing sidelobes.

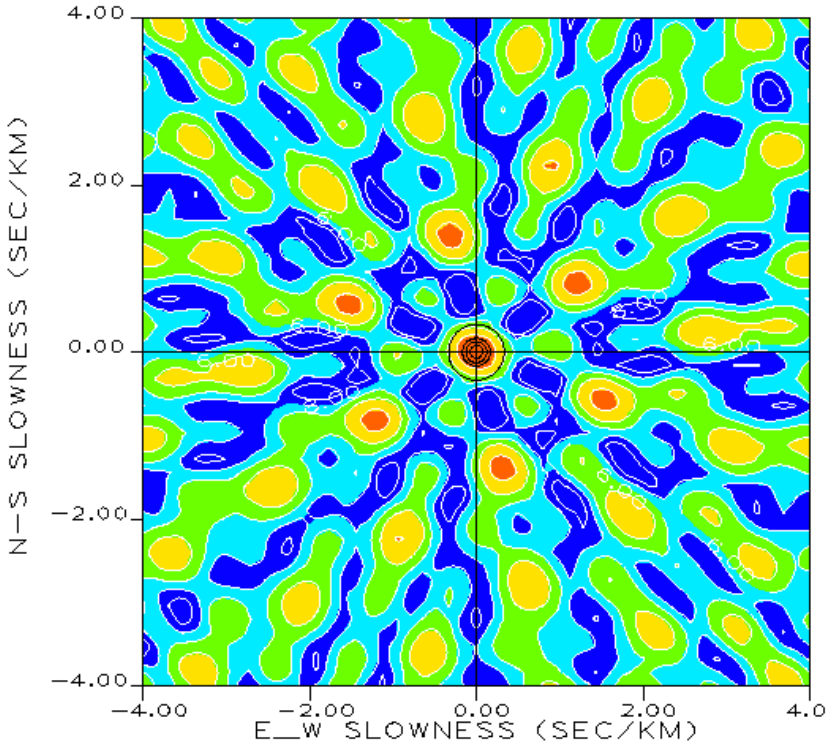

Fig. 6.3.8. The ARCES array responses for a 5 HZ signal for the four element configuration (A-sites only)

For these two configurations altogether 672 detection beams were deployed:

- To cover the range of incidence angles expected for infrasound signals, array beams were deployed with eight different apparent velocities (0.283, 0.306, 0.333, 0.365, 0.405, 0.454, 0.516, 0.599 km/s) for the larger array configuration (A0, A-, B-, and C-ring)and four different apparent velocities (0.283, 0.333, 0.405, and 0.516 km/s) for the smaller array configuration. (A0 and A-ring).
- For each of these apparent velocities, beams were deployed for 36 different backazimuths (0, 10, 20, 30, …. 340, and 350 degrees) for the larger array configuration and 12 different backazimuths (5, 35, 65, …. 305, and 335 degrees) for the smaller array configuration.

- Each of the 288 beams for the larger configuration are filtered with two different bandpass filters in the frequency ranges 2.0 – 4.0 and 3.0 – 6.0 Hz.
- Each of the 48 beams for the larger configuration are filtered with two different bandpass filters in the frequency ranges 3.0 – 6.0, and 4.0 – 8.0 Hz.
- Owing to the better noise conditions at ARCES and the better noise suppression due to the larger number of sensors, the detection threshold could be lowered to 4.0.

As for the Apatity infrasound array, all data recorded during 2005 were processed using the detector deployment for infrasound signals described above. This resulted in a total of 80,724 detections, which averages to 221.2 detections /day. However, one problem by using the seismic array ARCES for detection of infrasound signals is that many seismic signals are so strong that they still have significant onsets on the infrasound beams. These non-infrasound detections have to be sorted out during the fk-analysis.

Fk-analysis for ARCES array data

For estimating backazimuth and apparent velocity of the observed signals, the seismic array data processing as developed for ARCES with its data quality checks could be copied directly (Schweitzer, 2003). However, many sites of the seismic array are much less sensitive to infrasound signals than others. To obtain stable results, in particular also for weaker signals, data from these less sensitive sites (B5, C1, C2, C5, D2, D3, D6, D8) are not used during the further data processing.

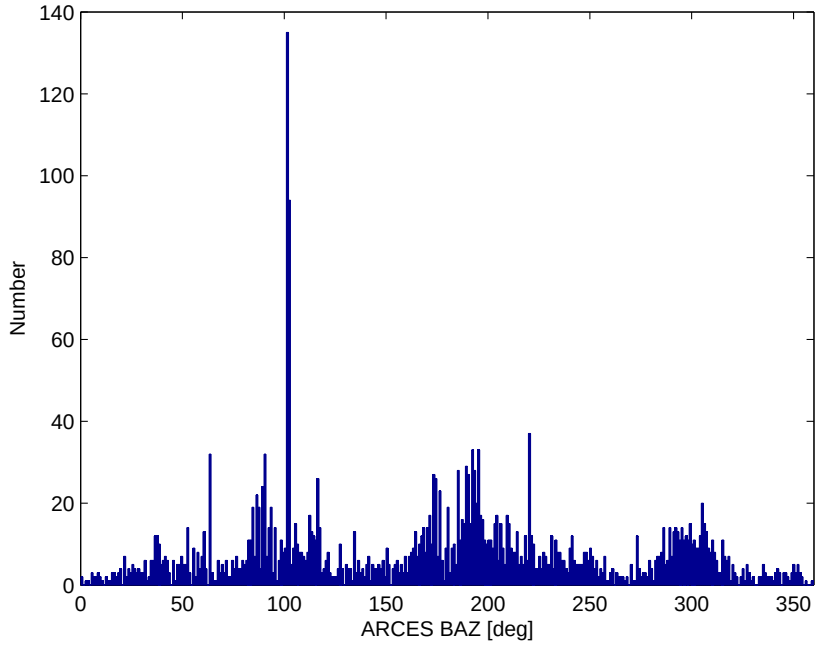

Fig. 6.3.9. Distribution of 2,768 backazimuth observations of infrasound signals observed with the Apatity infrasound array during 1st January – 17th December 2005.

The sensitivity for acoustic signals of the remaining sensors is still different and the observed signal amplitudes scatter over a large range. However, the signal coherence over the array is quite high and therefore, the most stable results are achieved by normalizing the traces before

fk-analysis. The fk-analysis is performed with a window-length for the signal of between 5 and 15 s and a noise window before the estimated onset time of 0.5 s.

The major problem in searching and analyzing infrasound signals with ARCES is that many seismic signals have so large amplitudes that they are still detected due to their relatively large SNR on the infrasound beams. Therefore, each fk-analysis is performed for 7 slightly changed window positions/length to find the best slowness estimate (i.e., the one with the highest relative power), and whenever the apparent velocity is between 0.27 and 0.66 km/s, the phase is assumed to be an infrasound (IS) observation.

Applying this data processing, 2,794 infrasound signals were found in the 2005 ARCES recordings, which corresponds to 7.6 detections per day. For the 2,768 infrasound signals detected until the 17th of December 2005, we show histograms with the distribution of apparent velocities (Fig. 6.3.9) and the backazimuth values (Fig. 6.3.10). It is obvious that the largest number of infrasound signals correlates with pronounced backazimuth directions and that most of the signals have apparent velocities between 0.3 and 0.4 km/s. However, the large number of apparent velocity observations around 0.44 km/s is surprising and will be further investigated in the future.

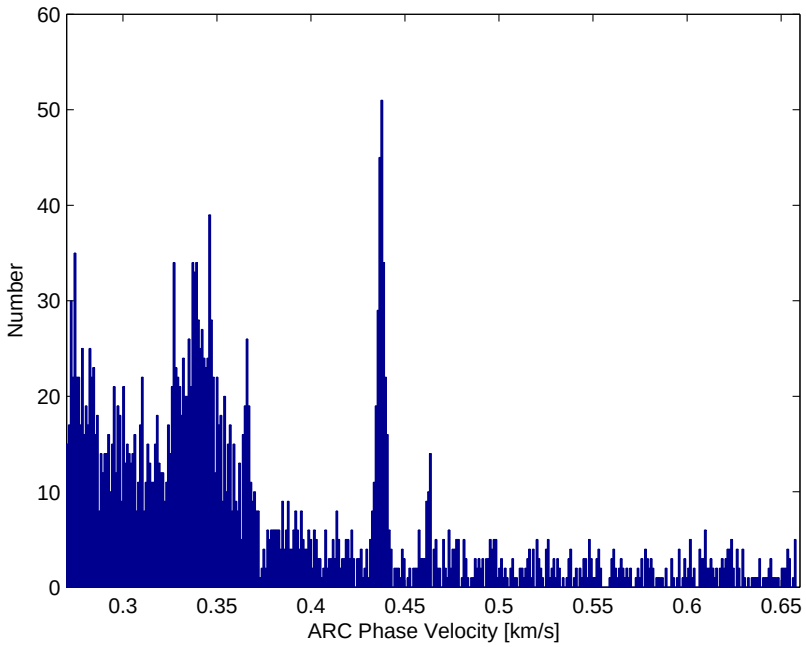

Fig. 6.3.10. Distribution of 2,768 apparent velocity observations of infrasound signals observed with the Apatity infrasound array during 1st January – 17th December 2005.

6.3.4 Comparing infrasound signals with seismic events in the GBF bulletin

On the average, 23.4 infrasound signals per day were observed with the Apatity infrasound array and 7.6 signals per day with the ARCES array. This number of observations results from the application of the data processing described above, which comprises only an initial set of infrasound signal processing rules. The question still open is; can these signals be associated to

sources already known from their seismic signals? To investigate this question in more detail the following test was performed:

The Generalized Beamforming (GBF) algorithm (Ringdal and Kvaerna, 1989) integrates automatically all observations of local and regional phases from all seismic arrays analyzed at the NORSAR data center in one common bulletin, associates these observations to their common sources, and locates these seismic sources. It can be assumed that this bulletin is quite complete and that it is representative for local and regional seismic events in Fennoscandia and the European Arctic with local magnitudes above 1.5 in on-shore regions and above 2.5 overall. At large distances from the arrays, the threshold could be higher. We searched the GBF bulletin for the first 351 days of the year 2005 (until the 17th of December) for seismic events at local or near regional epicentral distances to ARCES or the Apatity infrasound array. The following association criteria were used to correlate seismic events with presumed, corresponding infrasound signals:

- The epicentral distance of the event must be within 500 km from the array.
- The possible onset time of the infrasound signals was set to be within the time window spanned by group velocities between 0.2 and 0.7 km/s.
- The difference between the event backazimuth and the backazimuth observed for the infrasound signal should not be larger than 20 degrees.

BALTIC STATES-BELARUS-NW RUSSIA REGION

Origin time	Lat	Lon	Azres	Timres	Wres	Nphase	Ntot	Nsta	Netmag
2005-074:14.49.38.0	67.70	34.84	5.36	0.62	1.96	6	13	3	1.28

Sta	Dist	Az	Ph	Time	Tres	Azim	Ares	Vel	Snr	Amp	Freq	Fkq	Pol	Arid	Mag
APA	79.0	81.5	Pg	14.49.50.2	-0.5	87.3	5.8	7.3	31.0	494.1	4.32	1	1	743613	
APA	79.0	81.5	Lg	14.50.00.1	-0.5	81.4	-0.1	4.2	11.7	1577.1	3.67	1		743619	0.74
APA	79.0	81.5	s	14.50.03.0		83.2	1.7	3.4	6.4	1414.3	2.51	1		743620	0.87
APA	79.0	81.5	Ix	14.51.24.3		78.6	-2.9	0.325	14.2	5676.4	1.08	4		16005	
APA	79.0	81.5	Ix	14.54.24.6		73.3	-8.2	0.329	21.5	8792.5	9.88	6		16010	
APA	79.0	81.5	Ix	14.55.24.6		73.8	-7.7	0.338	116.5	66643.0	4.90	3		16015	
ARC	431.5	114.0	Pn	14.50.40.5	2.0	123.6	9.6	7.8	47.9	210.7	4.92	1		744345	
ARC	431.5	114.0	p	14.50.44.9		119.4	5.4	7.9	4.9	29.0	5.07	1		744348	
ARC	431.5	114.0	p	14.50.50.0		119.4	5.4	7.0	7.6	93.6	3.36	1	1	744349	
ARC	431.5	114.0	Sn	14.51.23.0	0.2	124.0	10.0	4.7	6.0	147.3	4.16	2	1	744357	1.25
ARC	431.5	114.0	s	14.51.27.2		116.4	2.4	3.7	3.5	80.1	4.28	3		744362	
ARC	431.5	114.0	s	14.51.33.6		111.3	-2.7	3.5	11.5	307.3	2.66	1	-3	744363	
ARC	431.5	114.0	s	14.51.38.1		129.2	15.2	4.6	11.3	378.2	3.90	1	-3	744369	1.69
ARC	431.5	114.0	Lg	14.51.41.5	0.3	117.9	3.9	5.1	4.7	216.0	2.74	1		744374	1.51
ARC	431.5	114.0	Ix	15.12.01.0		104.7	-9.3	0.319	10.7	130.4	4.17	2		97910	
ARC	431.5	114.0	Ix	15.12.52.6		104.0	-10.0	0.320	4.9	42.9	3.73	3		97915	
ARC	431.5	114.0	Ix	15.12.58.3		104.4	-9.6	0.319	4.3	59.1	3.45	3		97920	
ARC	431.5	114.0	Ix	15.13.54.4		102.3	-11.7	0.325	11.2	256.5	2.69	3		97925	
SPI	1304.8	143.5	p	14.52.21.8		163.0	19.5	5.6	6.4	72.3	5.89	2		743922	
SPI	1304.8	143.5	Pn	14.52.24.8	0.3	146.2	2.7	7.8	5.1	62.2	5.92	1		743925	

Fig. 6.3.11. GBF bulletin of an event in the Khibiny Massif, Kola Peninsula with associated infrasound signals (marked as Ix) observed at the Apatity infrasound array and at ARCES.

Applying these rules, 944 infrasound signals could be associated to 651 different events of the GBF bulletin. For these 651 events we obtained the following statistics:

- 333 events could be associated only with infrasound signals observed at the Apatity infrasound array (see Fig. 6.3.12).
- 250 events could be associated only with infrasound signals observed at the ARCES seismic array (see Fig. 6.3.12).
- 68 events could be associated with infrasound signals at both arrays, the ARCES seismic array and the Apatity infrasound array (Fig. 6.3.13).

Fig. 6.3.11 shows the GBF bulletin for an event in the Khibiny Massif, Kola Peninsula, for which infrasound signals were observed at both arrays. The source area is known for large explosions in open pit mines. The associated infrasound signals show quite small backazimuth residuals, the SNR of the observed infrasound signals at both arrays is of the same order as for the seismic signals, and at both arrays, the infrasound waves are arriving in different onset groups within a time window of 1 to 2 minutes.

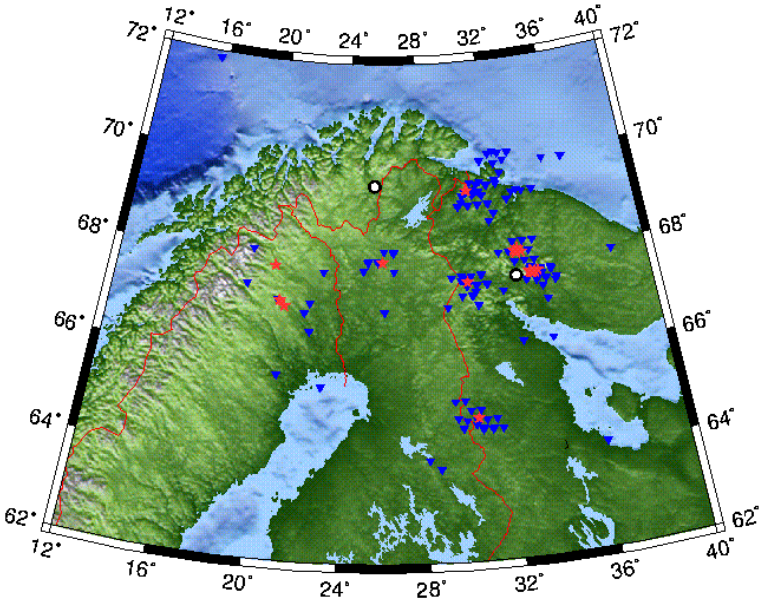

Fig. 6.3.12. The map shows automatically located events (GBF) for which either ARCES or the Apatity infrasound array observed infrasound signals. The blue triangles show the GBF event locations and the red stars show the location of known sites with explosions either at the Earth's surface or in the atmosphere. Note that the automatic GBF locations usually scatter over a larger area around these source regions.

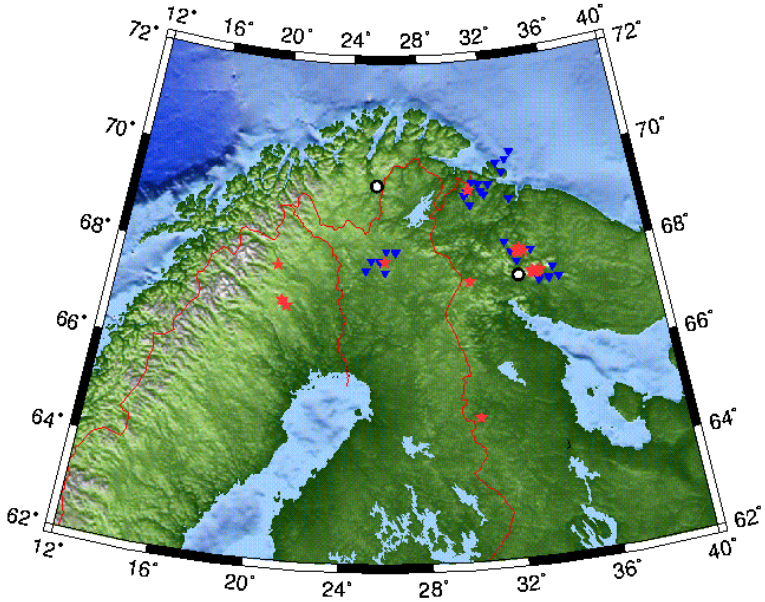

Fig. 6.3.13. The map shows automatically located events (GBF) for which both ARCES and the Apatity infrasound array observed infrasound signals. The blue triangles show the GBF event locations and the red stars show the location of known sites with explosions either at the Earth's surface or in the atmosphere.

On the map in Fig. 6.3.12 all reasonably well located GBF events for which either ARCES or the Apatity infrasound array have observed an infrasound signal are shown as blue triangles. The red stars show locations, known for regular explosions at the Earth's surface or in the atmosphere. Note that the automatic GBF locations usually scatter over a larger area around these source regions. Fig. 6.3.13 shows all of the 68 events for which infrasound signals were observed at both arrays.

We plan in the future to compare in more detail the infrasound observations with analyst reviewed event locations. This will require a review by an analyst of each infrasound signal, in order to confirm their validity and to identify possible misassociations if appropriate.

Acknowledgements

This paper is a summary of a quarterly report previously submitted to USASMDC under contract W9113M-05-C-0224.

Johannes Schweitzer
Frode Ringdal
Tormod Kværna
Vladimir Asming, KRSC
Yuri Vinogradov, KRSC

References

Baryshnikov, A.K. (2004). Research of infrasound background characteristics for estimation of threshold sensitivity of infrasound method for nuclear test monitoring. Final Technical Report ISTC 1341-01 (Part 1 of total 2), International Science and Technology Center (ISTC), Moscow, 255 pp.

Ringdal, F. and T. Kvaerna (1989): A multichannel processing approach to real time network detection, phase association and threshold monitoring. Bull. Seism. Soc. Am., **79**, 1927-1940.

Ringdal, F. & J. Schweitzer (2005). Combined seismic/infrasonic processing: a case study of explosions in NW Russia. Semiannual Technical Summary, 1 January – 30 June 2005, NORSAR Sci. Rep. **2-2005**, 49-60.

Schweitzer, J. (2003). Upgrading the ARCES (PS 28) on-line data processing system. Semiannual Technical Summary, 1 July – 31 December 2002, NORSAR Scientific Report **1-2003**, 33-43.

6.4 Seismic/Infrasonic Processing: Case Study of explosions in north Finland

6.4.1 Introduction

Each year between mid-August and mid-September, a series of explosions in the north of Finland is recorded by the stations of the Finnish national seismograph network and also by the seismic arrays in northern Fennoscandia and NW Russia. Based upon event locations given in the seismic bulletin of the University of Helsinki, the geographical coordinates of the explosion site are assumed to be approximately 68.00°N and 25.96°E. The explosions are carried out by the Finnish military in order to destroy outdated ammunition and are easily identified from the automatic seismic bulletins at NORSAR for several reasons. Firstly, they are always detected with a high SNR on the ARCES array, secondly they register very stable azimuth estimates on the detection lists, and thirdly they take place at very characteristic times of day (the origin time indicated by the seismic observations almost invariably falls within a few seconds of a full hour, or half-hour in the middle of the day). A preliminary list of candidate events was obtained by scanning the GBF (Kværna and Ringdal, 1989) automatic detection lists[1] for events which appeared to come from the correct region at appropriate times of day. A typical example is shown in Figure 6.4.1.

NORTHERN LAPLAND FINLAND

Origin time	Lat	Lon	Azres	Timres	Wres	Nphase	Ntot	Nsta	Netmag
2005-242:11.00.06.0	68.23	26.58	5.61	0.87	2.27	4	9	3	1.37

Sta	Dist	Az	Ph	Time	Tres	Azim	Ares	Vel	Snr	Amp	Freq	Fkq	Pol	Arid	Mag
ARC	151.7	163.0	p	11.00.28.3		177.1	14.1	6.1	128.8	615.0	5.36	1		530183	
ARC	151.7	163.0	Pg	11.00.30.3	-0.1	175.8	12.8	8.6	12.8	587.5	5.73	2		530190	
ARC	151.7	163.0	p	11.00.34.6		169.5	6.5	7.2	5.1	95.9	4.63	3		530197	
ARC	151.7	163.0	Lg	11.00.51.8	2.5	171.2	8.2	4.5	30.4	1486.9	4.77	2		530213	1.40
APA	278.5	287.6	Pn	11.00.47.2	-0.5	286.7	-0.9	9.4	4.2	236.4	5.00	1		530285	
APA	278.5	287.6	p	11.00.53.1		274.2	-13.4	8.6	5.8	268.1	4.00	1		530287	
APA	278.5	287.6	s	11.01.21.7		283.2	-4.4	4.1	8.7	566.5	6.09	2	-2	530289	1.34
APA	278.5	287.6	Lg	11.01.25.9	0.4	287.1	-0.5	3.2	4.4	426.7	4.89	3		530290	1.33
SPI	1155.1	158.5	p	11.02.45.7		166.2	7.7	7.0	7.6	287.1	6.01	1	1	535309	

Fig. 6.4.1. Automatic event location estimate from the GBF list http://www.norsar.no/NDC/bulletins/gbf/2005/GBF05242.html The event is characterised by a high SNR for the P- phase at the ARCES array, an S-P time of approximately 20 seconds for ARCES, and a backazimuth from ARCES of ~177°. The location estimate incorporates detections from the ARCES and Apatity arrays.

Between 2001 and 2005, a total of 108 events were found which appeared to fit the general attributes of explosions from this site; the GBF location estimates for these events are displayed in Figure 6.4.2. These fully automatic estimates display a somewhat surprisingly large geographical spread and, assuming that these events are in fact essentially co-located, the origin times will be correspondingly spurious. Before we proceed in attempting to detect and analyse infrasound signals produced from these explosions, we must first confirm that all of our candidate events are in fact from essentially the same location and then obtain the best possible origin time for each event.

1. See http://www.norsar.no/NDC/bulletins/gbf/

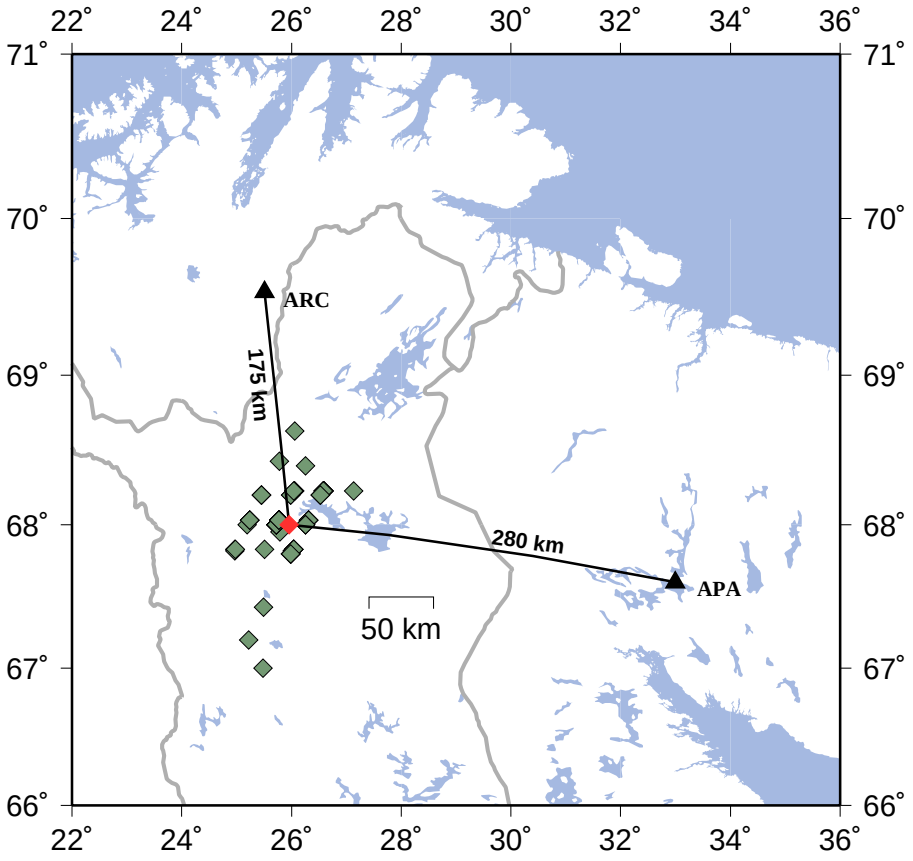

Fig. 6.4.2. Estimated location of the explosion site (orange diamond) in relation to the seismic arrays ARCES and Apatity together with the GBF fully automatic location estimates for 108 candidate events between August 2001 and September 2005 (green diamonds). The regular pattern of event location estimates is due to the fixed-grid trial epicenter procedure employed by the GBF.

6.4.2 Estimation of origin time for the explosions

It has been demonstrated by Gibbons et al. (2005) and Kværna et al. (2005) that far better location estimates can be obtained using one or more regional arrays by applying parameters which have been carefully calibrated for events confirmed to have taken place previously at a site of interest. However, the waveform similarity exhibited between these candidate events suggests that a process analogous to that described in Gibbons et al. (2005) may be circumvented in favour of a derivation of origin times based upon waveform similarity alone.

A single event is chosen as a master event (see Figure 6.4.3) from which an arrival time of the initial P-phase is picked manually. The **barey** model (see Schweitzer and Kennett, 2002) is currently deemed to be the best 1-dimensional velocity model for the region concerned and this predicts that an event occurring at 68.00^{o} N and 25.96^{o} E will result in a first arrival (the Pb phase) after 27.60 seconds. The site defined by these coordinates is 175 km from ARCES which is a difficult distance regarding the identification of phase types since Pb, Pg, and Pn are all predicted to arrive within 1.1 seconds of each other. However, if we assume that an event

has an origin time 27.6 seconds prior to the arrival of the first P-phase, the event displayed in Figure 6.4.3 can be assumed to have an origin time of 2005-244:10.30.00.438.

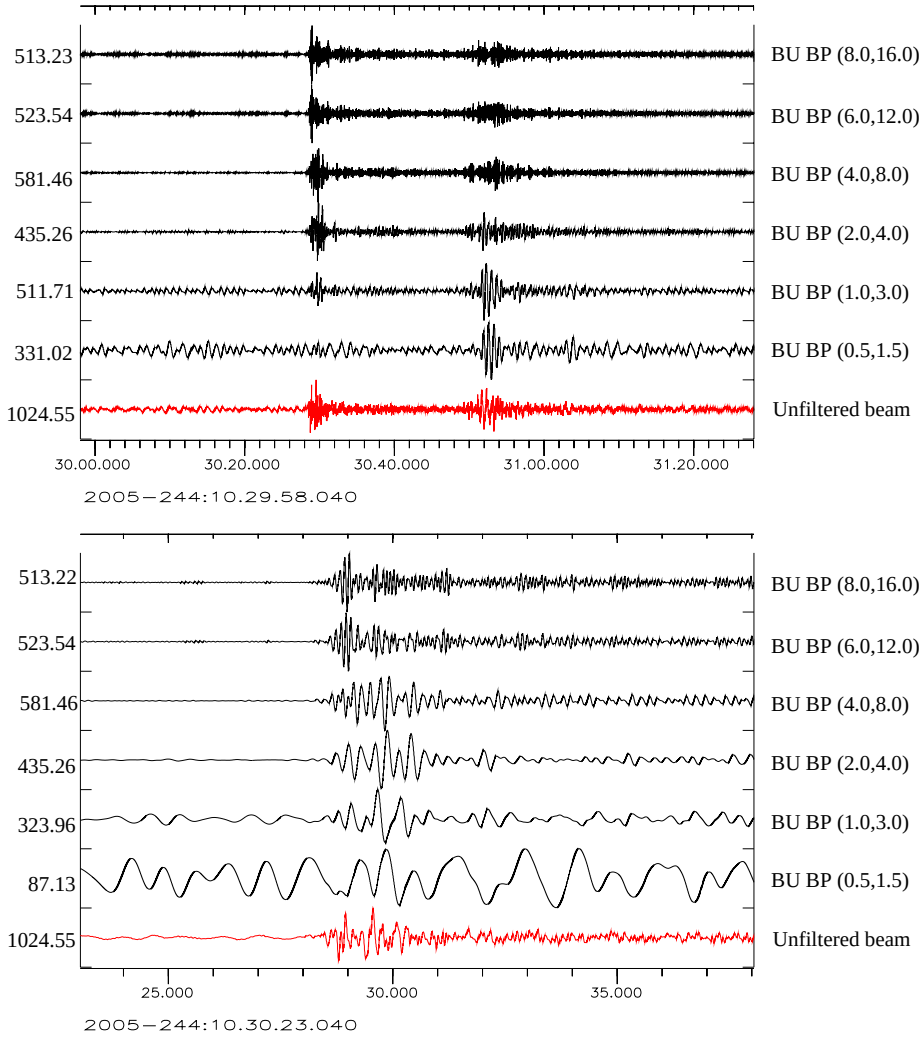

Fig. 6.4.3. Beam at ARCES of signals from an event in Northern Finland at approximately 10:30 GMT on September 1st 2005. The beam is steered with an apparent velocity of 6.72 km/s and a backazimuth of 173^{o}. The onset time of the initial P-arrival is estimated to be 2005-244:10.30.28.380.

We then need to create a waveform template specification for running cross-correlation calculations. We choose to create a template which begins 1.0 seconds prior to the predicted Pg arrival and which ends 40.0 seconds following the predicted Pg arrival. The waveforms are bandpass filtered between 4.0 and 16.0 and the time-series are resampled to 200 Hz. The waveform template is displayed for the ARA0_sz channel in Figure 6.4.4. Each of the short period vertical channels on the ARCES array was provided with the same template specification. The full array waveform template was correlated against data segments for each of the time intervals of interest as has been described in previous reports (e.g. Gibbons and Ringdal, 2004; Gibbons and Ringdal, 2005a,b). A typical cross-correlation detection is displayed in Figure 6.4.5. In fact, every one of the 108 candidate events displayed this degree of waveform similarity; the

lowest correlation coefficient obtained was 0.41 and even this value is significant given the length of the data segment and the high time-bandwidth product.

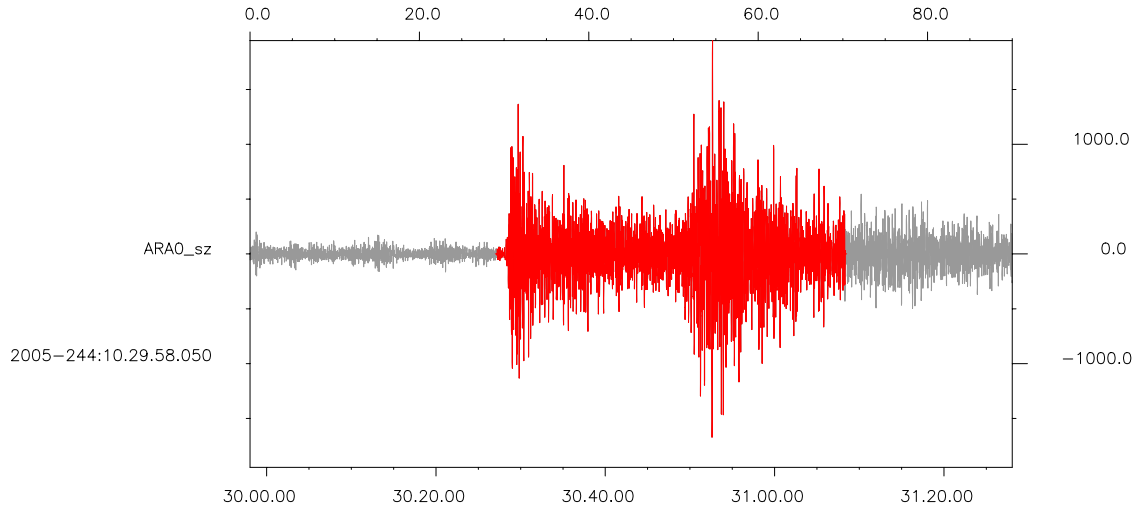

Fig. 6.4.4. Waveform template highlighted in red for the ARA0_sz channel for the 1st September 2005 ammunition destruction explosion in Northern Finland. The waveform is filtered between 4.0 and 16.0 Hz and resampled to 200 Hz.

The high correlation values observed for the event set is a strong indication that the explosions are very closely spaced, although we cannot specify the precise extent of the source area based on these data alone. If we use the 'quarter of the wavelength' criterion of Geller and Mueller (1980), we can, as a first approximation, state that the exlosions probably occurred within an area of less than 1 km in diameter.

That all of these explosions are thereby constrained to have occurred within such a small source region should make this data set a useful benchmark for future improvements to automatic event location algorithms aimed at improving the situation inferred from Figure 6.4.2. The time of maximum cross-correlation is obtained to the highest possible degree of accuracy using a spline interpolation and, by considering the definition of the waveform template relative to the manually read arrival time, we can estimate the origin times of each one of the 108 explosions recorded between August 2001 and September 2005. Since these origin times are all determined from the waveform semblance from event to event, any error in the origin time determination is almost certain to be dominated by error in the measurement of the arrival time, inadequacy of the velocity model, or error in the location of the explosion site. This is to say that the error is essentially identical for each event and that if, for a future explosion, it were possible to obtain an absolute GPS source location measurement and a precise origin time then all of the event origin times could be corrected simultaneously.

For reference, a list of the origin times for all of the events used in the current study is provided in Figure 6.4.6.

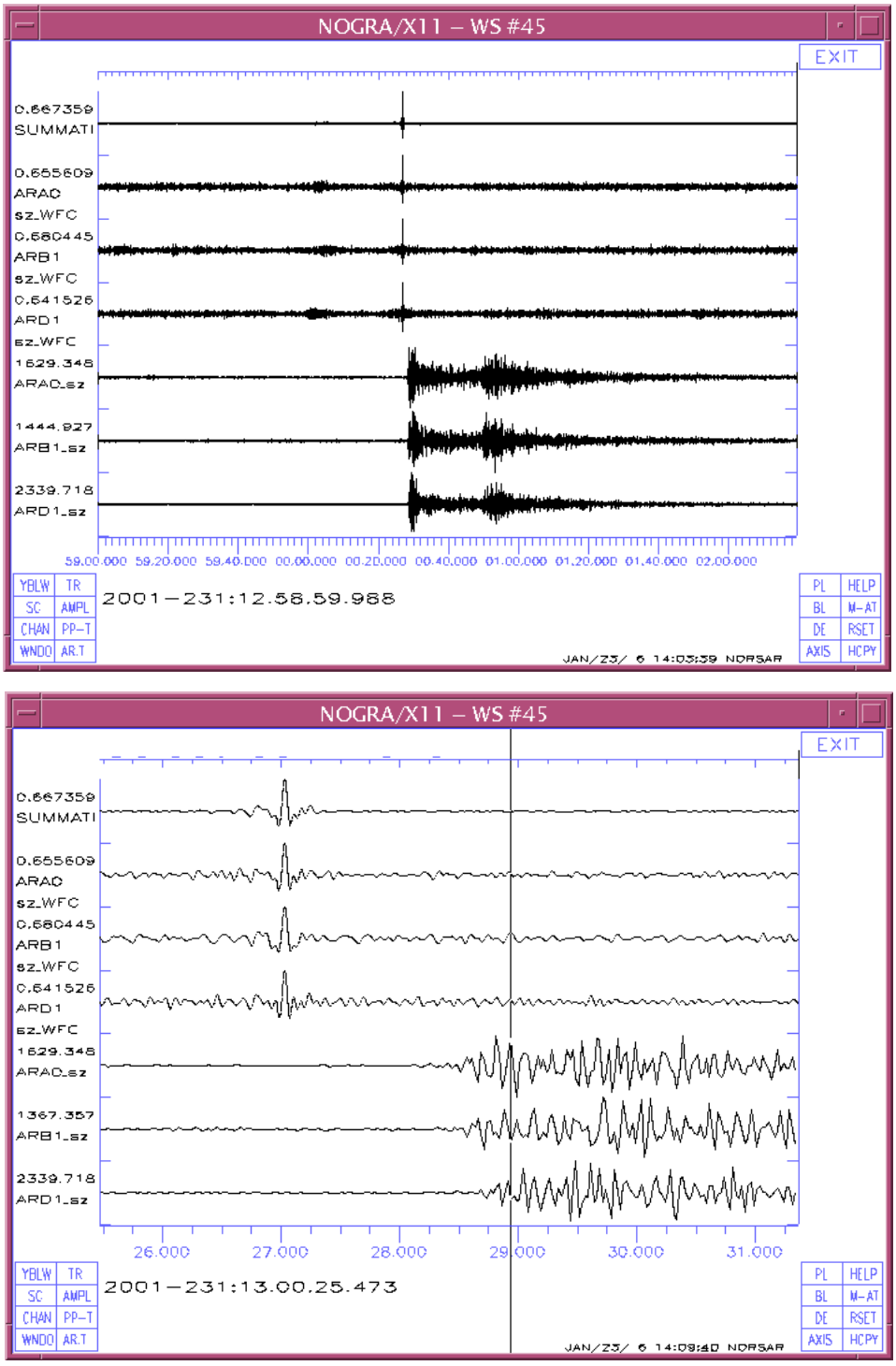

Fig. 6.4.5. Detection by waveform correlation of the August 19th 2001 ammunition destruction explosion in Northern Lapland using the master waveform template displayed in Figure 6.4.4. The 40 second long high-frequency master waveform records a correlation coefficient of 0.66 with the detected waveform, therefore guaranteeing an almost identical source location and type.

2001-228:13.59.59.505	2002-251:13.29.59.938	2004-242:11.30.03.553
2001-229:12.29.58.991	2002-252:11.59.59.483	2004-243:11.00.03.839
2001-230:13.29.58.192	2002-253:11.59.59.947	2004-244:11.00.03.986
2001-231:12.59.59.023	2002-254:11.44.59.738	2004-245:11.30.03.556
2001-232:10.59.59.045	2002-255:10.44.59.803	2004-246:11.00.00.846
2001-233:14.29.58.501	2002-256:10.44.59.615	2004-247:10.30.00.039
2001-234:11.29.59.331	2002-257:10.00.00.387	2004-248:10.00.00.883
2001-235:11.59.59.649	2002-258:10.00.00.087	2004-249:10.59.59.905
2001-236:11.29.59.104	2002-259:11.00.00.112	2004-250:10.00.00.207
2001-237:12.59.56.807	2002-260:10.14.59.787	2004-251:10.00.00.301
2001-238:11.59.56.607	2003-233:12.00.01.685	2004-252:10.30.01.126
2001-239:15.59.56.761	2003-234:11.00.01.756	2004-253:09.00.01.088
2001-240:13.29.56.924	2003-235:11.00.00.283	2004-254:09.00.00.480
2001-241:13.29.56.093	2003-236:10.30.00.027	2004-255:10.00.00.684
2001-242:12.44.56.485	2003-237:10.30.00.185	2004-256:08.59.59.571
2001-243:12.44.56.390	2003-238:11.59.59.930	2004-257:09.29.58.714
2001-244:12.29.56.414	2003-239:09.30.00.915	2004-258:09.00.01.861
2001-245:12.14.56.175	2003-240:10.59.59.804	2005-236:12.00.03.287
2001-246:12.59.59.983	2003-241:10.29.59.778	2005-237:11.00.03.265
2001-247:12.44.59.496	2003-242:10.29.59.588	2005-238:11.00.01.462
2001-248:11.44.59.142	2003-243:09.59.59.906	2005-239:10.00.02.689
2001-249:11.45.00.103	2003-244:11.59.59.408	2005-240:10.59.59.776
2001-250:11.59.56.659	2003-245:11.29.59.139	2005-241:10.59.59.828
2001-251:11.59.57.022	2003-246:10.44.58.987	2005-242:10.59.59.449
2001-252:10.29.56.870	2003-247:09.59.58.642	2005-243:11.59.59.870
2001-254:12.44.55.638	2003-248:09.59.58.486	2005-244:10.29.59.068
2002-241:13.29.59.647	2003-249:10.29.58.397	2005-245:10.59.59.022
2002-242:13.29.59.542	2003-250:11.29.58.247	2005-246:10.59.59.647
2002-243:13.30.00.118	2003-251:09.59.58.067	2005-247:11.00.03.608
2002-244:12.30.00.072	2003-252:10.29.57.973	2005-248:09.00.00.681
2002-245:12.29.59.664	2003-253:10.00.00.555	2005-249:10.00.00.401
2002-246:12.29.59.481	2003-254:11.29.59.883	2005-250:09.45.00.083
2002-247:12.59.59.211	2004-238:13.30.03.333	2005-251:09.45.00.086
2002-248:13.29.58.978	2004-239:12.00.03.518	2005-252:11.30.00.289
2002-249:12.29.58.839	2004-240:11.29.03.564	2005-253:10.45.00.017
2002-250:12.59.58.477	2004-241:11.29.04.079	2005-254:09.59.59.828

Fig. 6.4.6. List of estimated origin times for the 108 events from the Finnish explosion site used in this study.

6.4.3 Data analysis

Ringdal and Schweitzer (2005) presented a case study of seismic and infrasonic recordings of six presumed surface explosions in Pechenga, Russia, near the Norwegian border. The explosions in northern Finland described in this paper have many of the same characteristics, although the infrasonic signals are not as large as those observed for the Pechenga explosions. Nevertheless, the SNR is sufficient to provide slowness estimates at the ARCES array for the seismic signals (in all cases) and for infrasonic signals (in the majority of cases). We will use various subconfigurations of the ARCES array (see Figure 6.4.7) in our further analysis of these signal characteristics.

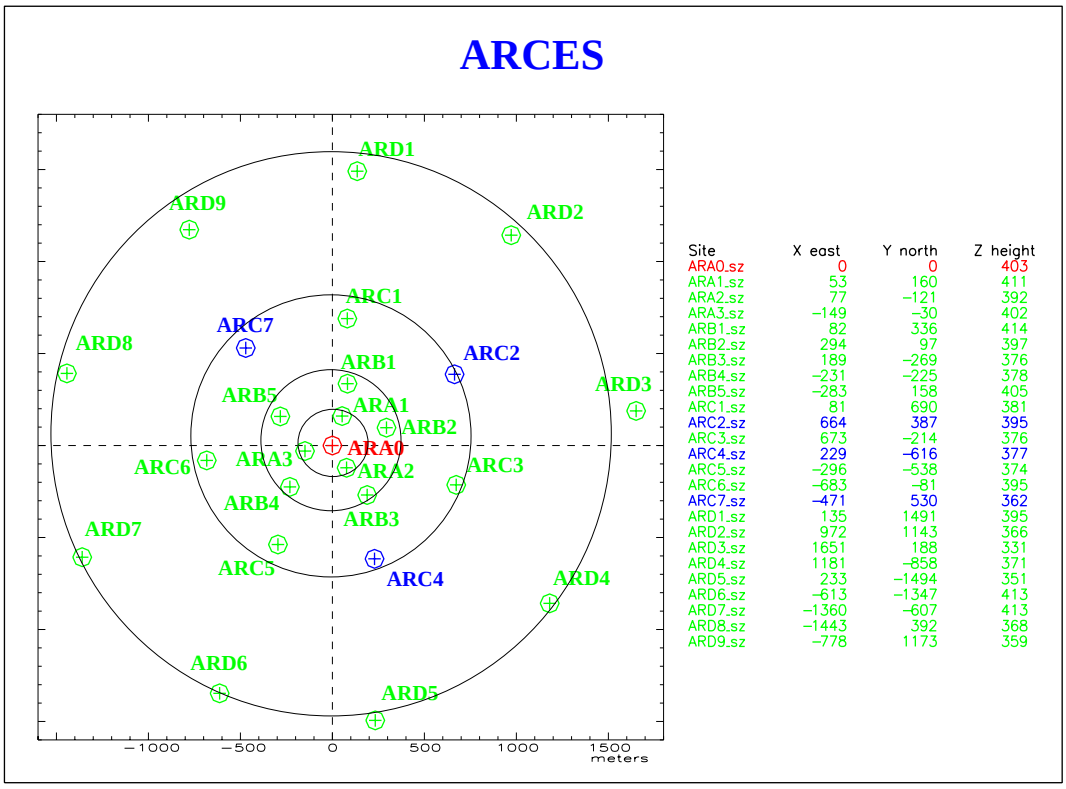

Site	X east	Y north	Z height
ARA0.sz	0	0	403
ARA1.sz	53	160	411
ARA2.sz	77	−121	392
ARA3.sz	−149	−30	402
ARB1.sz	82	336	414
ARB2.sz	294	97	397
ARB3.sz	189	−269	376
ARB4.sz	−231	−225	378
ARB5.sz	−283	158	405
ARC1.sz	81	690	381
ARC2.sz	664	387	395
ARC3.sz	673	−214	376
ARC4.sz	229	−616	377
ARC5.sz	−296	−538	374
ARC6.sz	−683	−81	395
ARC7.sz	−471	530	362
ARD1.sz	135	1491	395
ARD2.sz	972	1143	366
ARD3.sz	1651	188	331
ARD4.sz	1181	−858	371
ARD5.sz	233	−1494	351
ARD6.sz	−613	−1347	413
ARD7.sz	−1360	−607	413
ARD8.sz	−1443	392	368
ARD9.sz	−778	1173	359

Fig. 6.4.7. ARCES array configuration. The four circles correspond to the A, B, C and D-rings as discussed in the text.

Figure 6.4.8 shows an example of such a recording at selected ARCES sensors for one of the explosions. In fact, this is one of the explosions which had the largest infrasound signals; in most cases, the infrasound phase was hardly visible on single sensor traces, even though f-k analysis could nevertheless be carried out.

Thus, this data set of more than 100 surface explosions in almost exactly the same place recorded by the ARCES array provides an excellent opportunity to investigate the stability of slowness estimates, both for the seismic and infrasonic recordings, as presented in the following. We will do such analysis investigating both the effects of filter frequency band, array aperture and number of sensors. In this respect, we will use various sub-configurations of ARCES to simulate array configurations of various diameters and number of sensors.

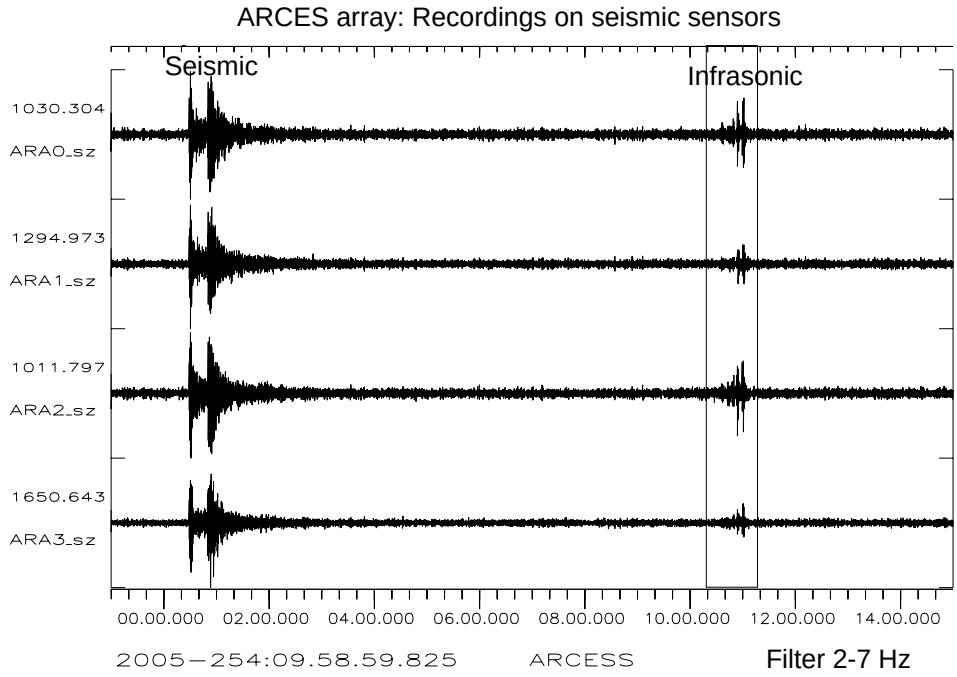

Fig. 6.4.8. ARCES waveforms for one of the explosions discussed in the text (Event 108 in the table). Note the clear recording of both the seismic P and S waves and the infrasonic waves, which appear about 10 minutes later. The 60-second interval used for the infrasonic f-k analysis is marked on the plot.

6.4.4 Seismic P-phases

Figure 6.4.9 shows the ARCES slowness estimates for the 108 events in four different frequency bands. As has been observed by Gibbons et. al. (2005) and Kværna et. al. (2005), such estimates are very stable when fixed frequency bands are applied, and, not surprisingly, this figure confirms this stability. The standard deviation in azimuths is as small as 0.3 degrees for the best filter (3-5 Hz), and is 1 degree or lower for all the filters shown. The average values of the azimuth estimates varies by up to 5 degrees among the filters, and these differences are highly significant in view of the small scatter in each population (The standard deviations of the mean values range from 0.03 to 0.1 degrees).

We note that the length of the f-k window (10 seconds) used in the present study is somewhat longer than the traditional 2-3 seconds used in standard detection processing. This may have provided some increased stability in the slowness estimates, but we have not investigated this question in any detail.

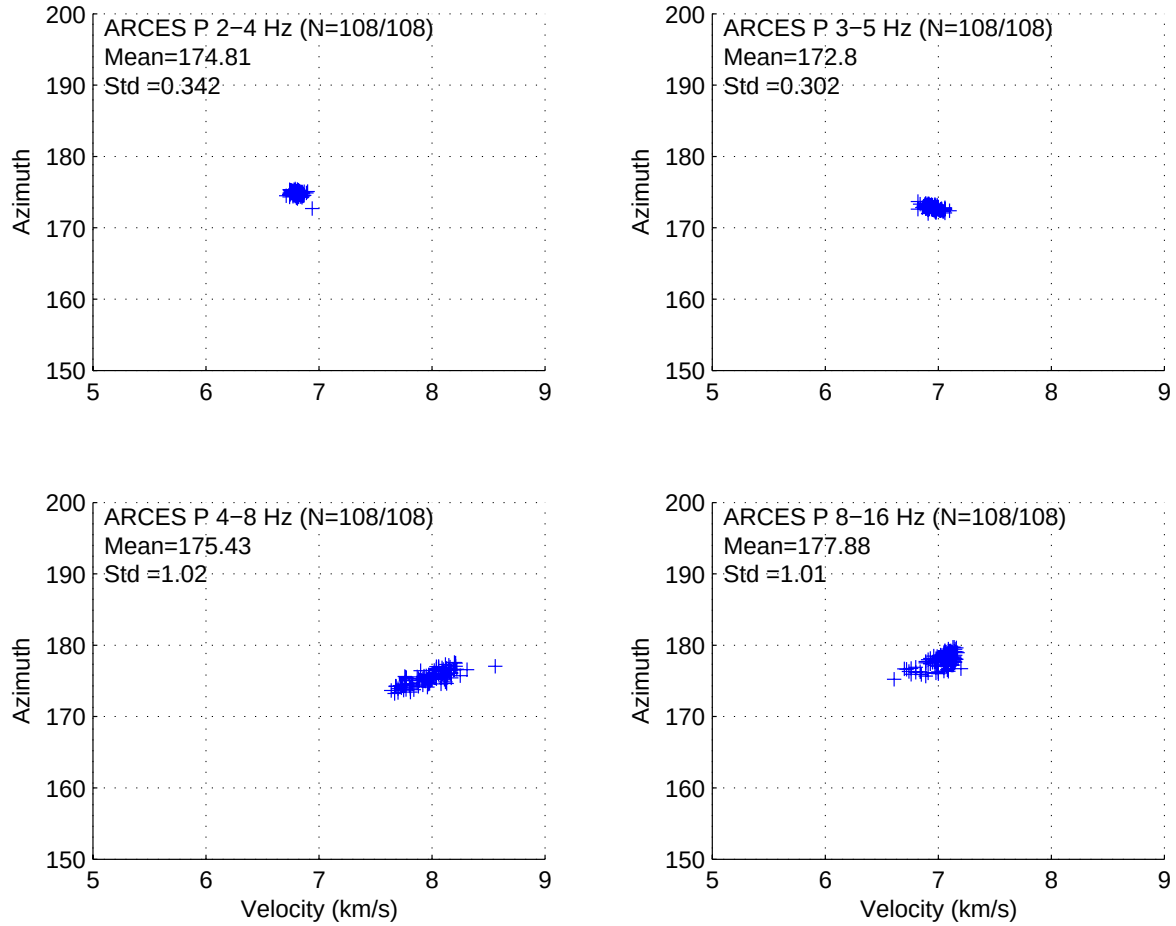

Fig. 6.4.9. Slowness estimates of the 108 events in the data base. The figure corresponds to estimates for the seismic P-phase (25-35 seconds after the event origin time), in four different filter bands. For each filter band, the mean and standard deviation of the azimuth estimates are indicated.

Fig. 6.4.10 shows the ARCES slowness estimates for the event set as a function of various sub-configuration of vertical-component seismometers. These are, in increasing sizes:

- The 4-element A-ring configuration (seismometers A0, A1, A2, A3)
- The 9-element A,B-ring configuration (by adding the seismometers B1-B5)
- The 16-element A,B,C-ring configuration (by adding the seismometers C1-C7)
- The 25-element A,B,C,D-ring configuration (comprising the full ARCES vertical-component array)

As expected, the scatter of the estimates decreases as the array size and number of seismometers increases, and the amount of decrease in the standard deviations is about proportional to the increase in array diameter. Again, we see that the mean azimuth estimates show significant differences among the array configurations, even if we are applying the same bandpass filter (3-5 Hz) throughout.

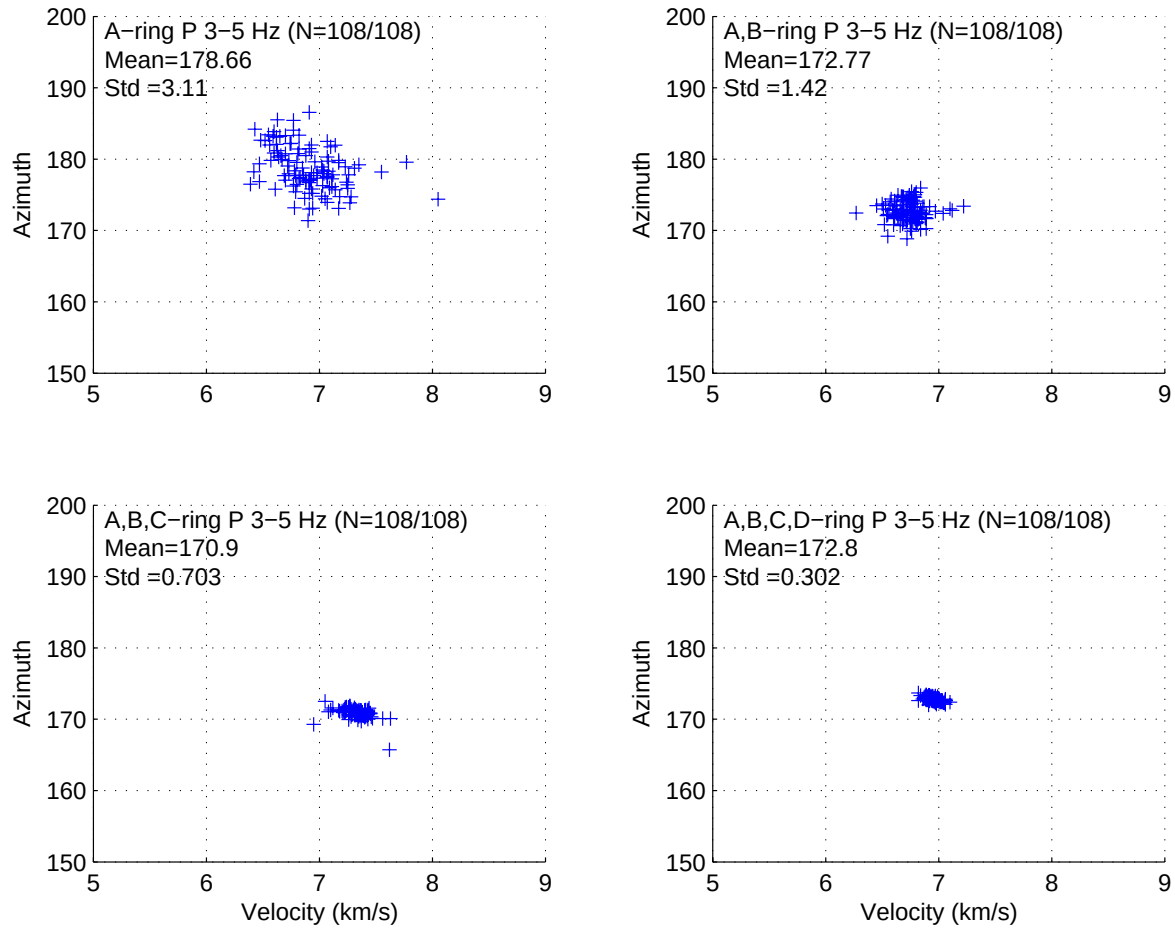

Fig. 6.4.10. Slowness estimates of the 108 events in the data base. The figure corresponds to estimates for the seismic P-phase (25-35 seconds after the event origin time), in the filter band 3-5 Hz. The four subconfigurations are as described in the text. For each subconfiguration, the mean and standard deviation of the azimuth estimates are indicated.

To investigate how much of this observed decrease in scatter is due to array aperture, and how much is due to increased number of seismometers, we made some experiments by selecting only 4 seismometers (in the outermost ring) for each of the four subconfigurations. The results from one such experiment is shown in Figure 6.4.11. The reduction in scatter is quite similar to that in Figure 6.4.10. This indicates that the array aperture is the most important factor in order to obtain variance reduction, whereas the number of sensors in each configuration is not essential in this regard. Nevertheless, an increased number of sensors is useful so as to reduce the possibility of side lobes, and it also adds redundancy which would be important if one or more seismometers malfunction.

An interesting observation is that the adding or removal of a single seismometer in a 4-sensor configuration can have significant effect on the average azimuth (but not much effect on the stability of the estimates). This is an observation that needs to be taken into consideration when doing slowness analysis and location estimation by regional arrays, since the outage of one or more sensors could influence the expected azimuth estimates for any given source region.

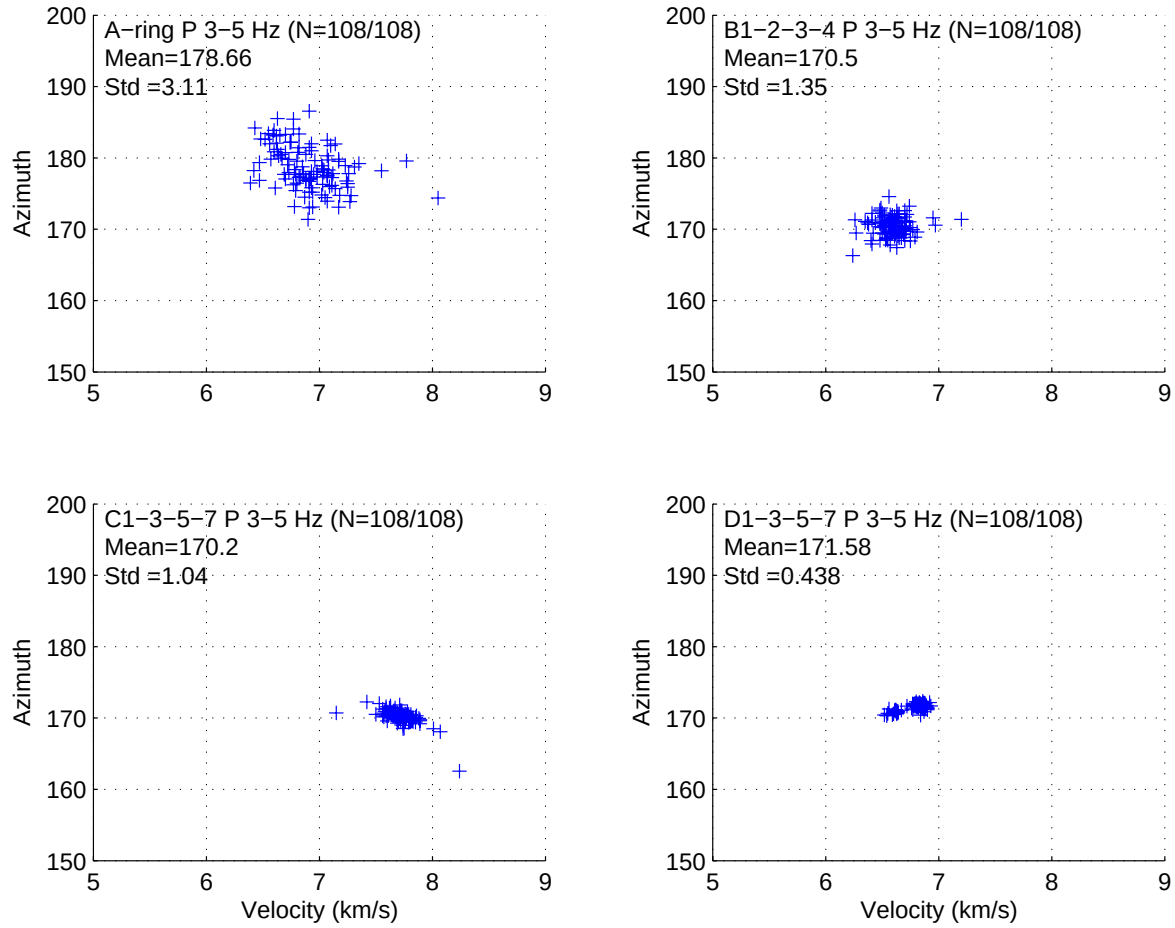

Fig. 6.4.11. Slowness estimates of the 108 events in the data base. The figure corresponds to estimates for the seismic P-phase (25-35 seconds after the event origin time), in the filter band 3-5 Hz. In contrast to Figure 6.4.10, the four subconfigurations now comprise only four seismometers each, as indicated on the plots. Note the similarity to Figure 6.4.10.

6.4.5 Infrasonic waves

In our study of slowness estimates for infrasonic waves recorded at the ARCES seismic array, we have used throughout a 60 second window beginning 620 seconds after the event origin time. Fig. 6.4.12 shows the ARCES slowness estimates for the infrasonic phases (named Ix) as a function of the same sub-configuration of vertical-component seismometers as used in our studies of P-waves described earlier.

In contrast to the P-wave analysis, we were not able to make reliable slowness estimates for the infrasonic phases of all the events. This is mainly due to low infrasonic SNR for a number of the events in the database. This makes a comparison between the performances of different filters and subconfigurations more complicated, and we need to consider both the number of successful estimates and the variance reduction when evaluating the results.

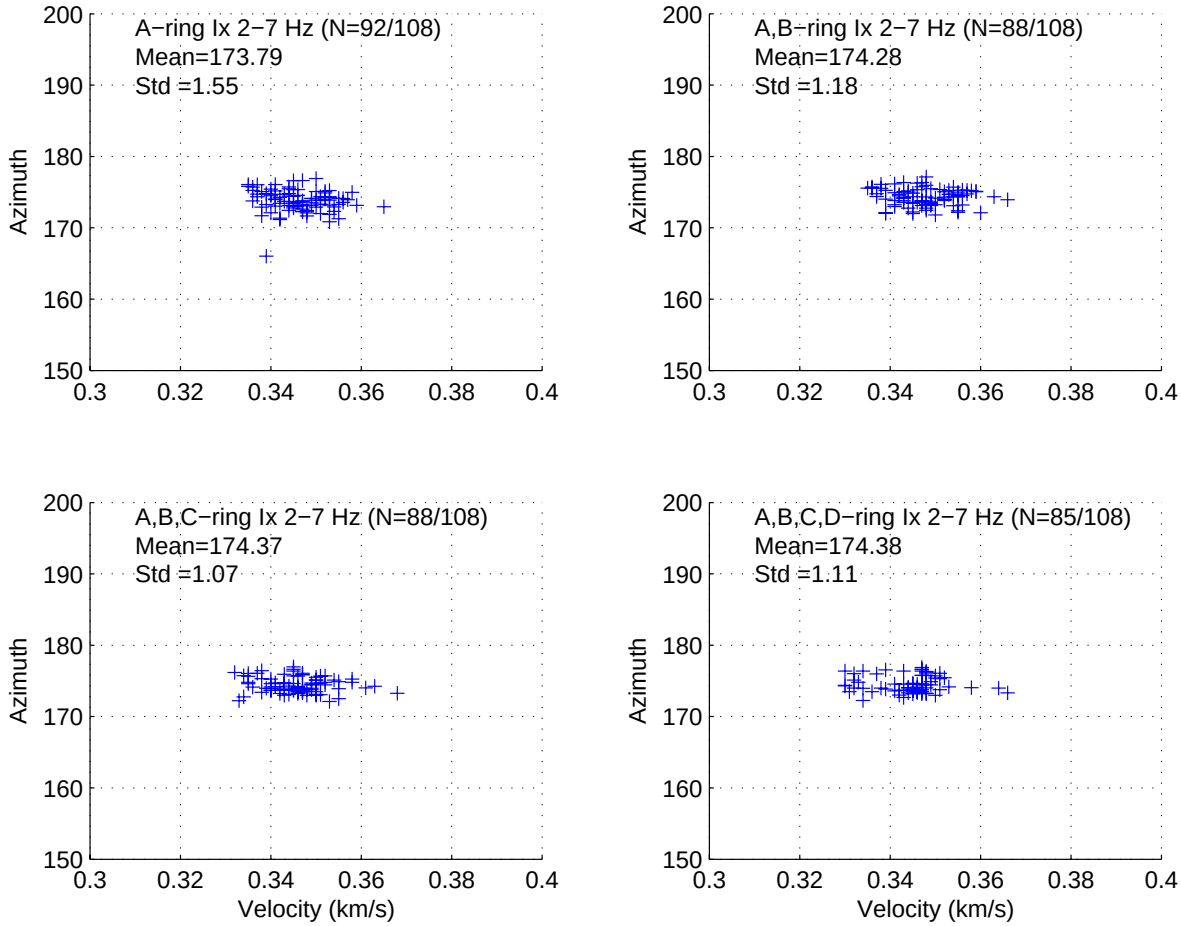

Fig. 6.4.12. Slowness estimates of the 108 events in the data base. The figure corresponds to estimates for the infrasonic phase (620-680 seconds after the event origin time), in the filter band 2-7 Hz. The number of events for which reliable estimates could be made is indicated on each plot. The four subconfigurations are as described in the text. For each subconfiguration, the mean and standard deviation of the azimuth estimates are indicated.

When comparing the results to those obtained for seismic P-waves, we see some interesting differences. For example, we see no significant variance reduction as the array aperture and number of sensors increases. Although there appears to be a slight reduction in the standard deviations, the largest number of successful estimates were in fact made using the smallest configuration. Therefore we consider that there is essentially no difference in the stability of the slowness estimates for these four configurations. It is of course possible that other estimation techniques could show such improvements, but it may also be that the variance in estimates is dominated by factors such as varying atmospheric conditions over the 5 years covered by this study. Another important observation is that the average azimuth values are essentially independent of the subconfiguration chosen. This also contrasts to our observations from seismic P-waves.

In order to study the frequency dependency for infrasonic waves, we found that the SNR of ARCES infrasonic observations were not sufficient to enable us to do a meaningful study. For this purpose, we therefore used data recorded by the microbarographs installed at the Apatity seismic/infrasound array. A description of this array is presented in the paper by Schweitzer et. al. in this issue. Examples of recording and processing of some of these same Finnish

explosions using Apatity infrasonic data have earlier been presented by Vinogradov and Ringdal (2003). In the study presented here, we used a 60 second window starting at 970 seconds after the event origin time for the f-k analysis. Note that we selected for analysis only one of the three infrasonic phases observed at Apatity and desribed in the above publication.

Fig. 6.4.13 shows the Apatity slowness estimates for the infrasonic phase (named Ix) for the events in four different frequency bands. Again, the contrast to the seismic observations is striking. The average azimuth estimates of the infrasonic phases are virtually independent on the frequency band, and there is thus no observable systematic differences in infrasonic slowness estimates as a function of frequency within the bands processed in this study.

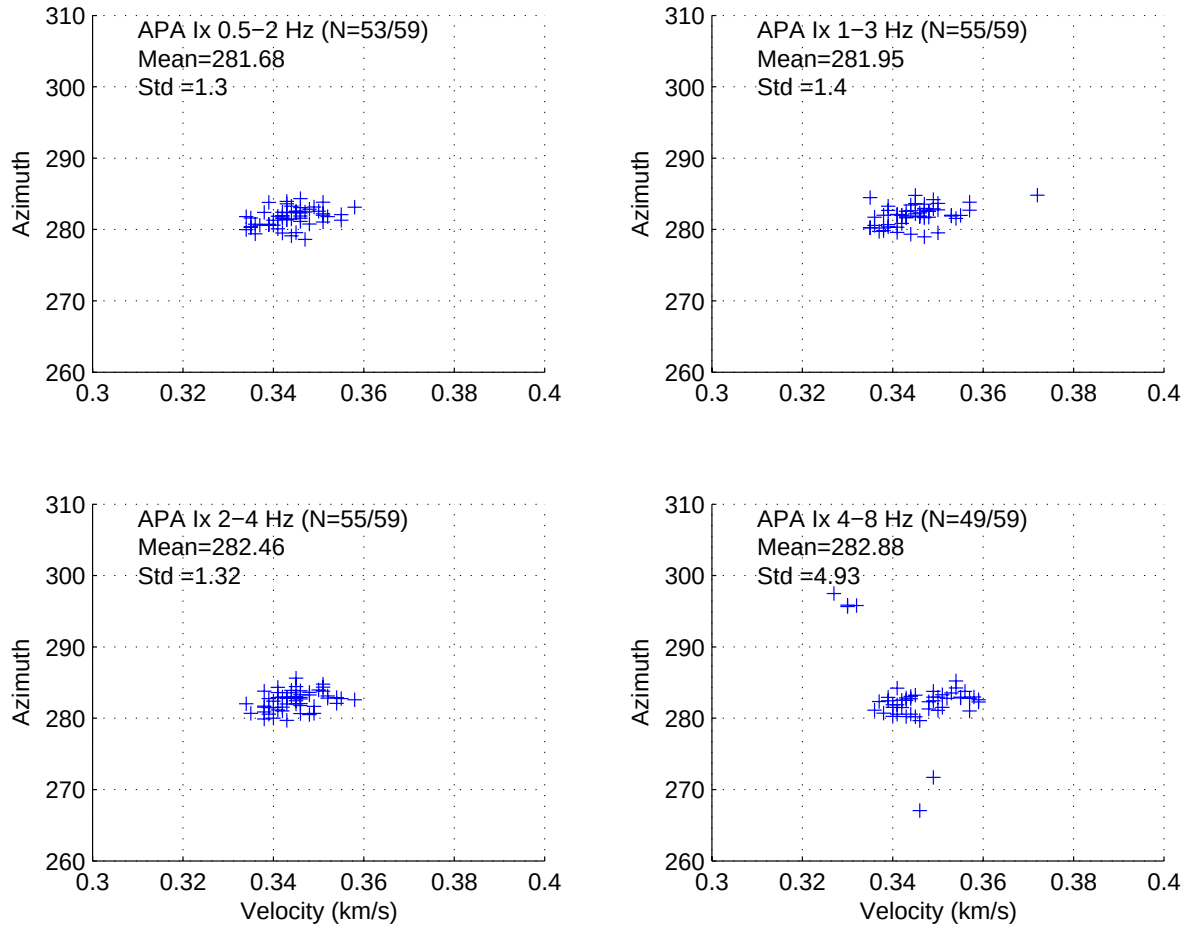

Fig. 6.4.13. Slowness estimates of the 59 events in the data base for which Apatity infrasonic recordings were available. The figure corresponds to estimates for the infrasonic phase (970-1040 seconds after the event origin time), in four different filter bands. The number of events for which reliable estimates could be made is indicated on each plot. For each filter band, the mean and standard deviation of the azimuth estimates are indicated.

6.4.6 Conclusions

We have used waveform cross-correlation to determine very accurate origin times for a data-base of 108 explosions, at a site in northern Finland, presumably carried out for the purpose of destroying old ammunition. The extremely high correlation coefficients observed for this data set indicates that these explosions are all very closely spaced, probably within an area of some hundreds of meters in diameter. This database will be highly valuable for various studies

related to obtaining improved accuracy in detecting and characterizing seismic events using regional array recordings at local distances.

In the present paper, we have used this database to study the stability of slowness estimates for both seismic and infrasonic phases, using ARCES and Apatity array recordings. Our analysis of seismic P-phase observations confirm the stability of fixed-frequency band f-k analysis previously noted e.g. by Gibbons et. al. (2005) and Kværna et. al. (2005). Furthermore, by analyzing various subconfigurations of the ARCES array, we find that the scatter (standard deviation) in the azimuth estimates for the explosions is about inversely proportional to array aperture.

When carrying out a similar analysis of infrasonic data, we find some interesting differences. In contrast to the case for the seismic P-waves, the azimuth scatter found by our f-k estimation process does not decrease when the array aperture increases. Furthermore, the average azimuth remains the same both with varying array aperture and with varying filter bands. This is also in contrast to what we have observed for the seismic P-waves.

In future work we plan to expand upon these studies by analyzing data from other source regions. Whe the infrasound array near ARCES becomes operational (expected in 2006), we will obtain important supplementary data to carry out such expanded studies.

References

Geller, R.J. and Mueller, C.S. (1980). Four similar earthquakes in Central California, *Geophys. Res. Lett.*, **7**, pp. 821-824.

Gibbons, S. J., Kværna, T., and Ringdal, F. (2005). Monitoring of seismic events from a specific source region using a single regional array: a case study, *J. Seism.*, **9**, pp. 277-294.

Gibbons, S. J. and Ringdal, F. (2004). A waveform correlation procedure for detecting decoupled chemical explosions, NORSAR Scientific Report: Semiannual Technical Summary No. 2 - 2004. NORSAR, Kjeller, Norway. pp. 41-50.

Gibbons, S. J. and Ringdal, F. (2005a). The detection of rockbursts at the Barentsburg coal mine, Spitsbergen, using waveform correlation on SPITS array data, NORSAR Scientific Report: Semiannual Technical Summary No. 1 - 2005. NORSAR, Kjeller, Norway. pp. 35-48.

Gibbons, S. J. and Ringdal, F. (2005b). Detection of the aftershock from the 16 August 1997 Kara Sea event using waveform correlation, NORSAR Scientific Report: Semiannual Technical Summary No. 2 - 2005. NORSAR, Kjeller, Norway, 24-31.

Kværna, T., Gibbons, S. J., Ringdal, F., and Harris, D. B. (2005). Integrated Seismic Event Detection and Location by Advanced Array Processing. In *Proceedings of the 27th Seismic Research Review, Rancho Mirage, California, September 2005. "Ground-based Nuclear Explosion Monitoring Technologies"*. pp. 927-936.

Ringdal, F., and Kværna, T. (1989). A multi-channel processing approach to real time network detection, phase association, and threshold monitoring, *Bull. seism. Soc. Am.*, **79**, pp. 1927-1940.

Schweitzer, J. and B. L. N. Kennett (2002). Comparison of Location Procedures - The Kara Sea event of 16 August 1997, NORSAR Scientific Report: Semiannual Technical Summary No. 1 - 2002. NORSAR, Kjeller, Norway. pp. 97-103.

Vinogradov, Yu. and F. Ringdal (2003). Analysis of infrasound data recorded at the Apatity array, NORSAR Scientific Report: Semiannual Technical Summary No. 1 - 2003. NORSAR, Kjeller, Norway. pp. 68-77.

Acknowledgements

This research has been supported partly under contract W9113M-05-C-0224.

Frode Ringdal
Steven J. Gibbons

6.5 Moment tensor (MT) inversion for regional events in Fennoscandia and adjacent areas

6.5.1 Introduction

The reliable determination of earthquake epicenters and focal mechanisms, *i.e.*, centroid moment tensor solutions, is an important objective of earthquake seismology. Centroid moment tensors are fundamental input data for fast hazard estimation of aftershocks, quantitative simulation of tsunamis in case of submarine earthquakes, and seismo-tectonic evaluation and creation of seismic hazard maps.

Although moment tensor (MT) inversion is routinely applied by miscellaneous institutions for teleseismic events, it is rarely exerted in the case of weaker regional events with magnitudes of about 4.0. The reason for this is that regional earthquakes possess higher frequencies and reliable regional velocity models of the crust and upper mantle are required (Bruhns, 2003).

T. Dahm (University of Hamburg) and F. Krüger (University of Potsdam) developed algorithms to accomplish robust MT inversions for regional events with magnitudes of 4.0 – 4.5 (Dahm *et al.*, 1999; Dahm & Krüger, 1999; Krüger & Dahm, 2002). In this study, we applied these programs to regional earthquakes observed in Fennoscandia.

6.5.2 Moment tensor theory

During MT inversion, the focus lies on the information that data provide about earthquake mechanisms. The location of the earthquake as well as the focal time are assumed to be known. Amplitudes and shape of radiated waves depend on kinematics of faulting, and reflect the geometry of the fault and the motion on it. The concept is to model seismic waves generated by an earthquake by solving the equation of motion with faulting represented as equivalent body forces that result in the same seismic radiation pattern (Stein & Wysession, 2003). A seismic MT is a general concept, describing in a first order approximation the equivalent forces of a variety of seismic point sources (Jost & Herrmann, 1989).

The first MT inversions (calculation of MT elements from observed seismograms) were conducted by Gilbert (1973) in the frequency domain using the linearity between MT and Green's function elements. The concept of seismic MTs was taken up by Backus & Mulcahy (1976) and Backus (1977a, 1977b). An overview is given by Jost & Herrmann (1989).

In the far-field, ground motion displacement $\vec{u}$ can be expressed as (see *e.g.*, Dahm *et al.*, 2004):

$$u_n(\vec{x}, t) = \int_0^\infty M_{pq}(t) \frac{\delta}{\delta \xi_q} G_{np}(\vec{x}, t-\tau; \vec{\xi}, 0) d\tau \ , \qquad (1)$$

where $\vec{x}$ is pointing to the station, $\vec{\xi}$ is directed towards the moment centroid in the origin of the coordinate system and G_{np} is the *n*-th component of ground movement at the station in response to a unit-force excitation in *p*-direction at the source (a Green's function).

M_{pq} is no longer time-dependent if a step function is assumed as source time function.

Further, it holds that

$$\frac{\delta}{\delta\xi_q} G_{np}(\vec{x}, T) = \frac{\delta G_{np}}{\delta x_j}\frac{\delta x_j}{\delta\xi_q} + \frac{\delta G_{np}}{\delta t}\frac{\delta T}{\delta\xi_q} \tag{2}$$

with the retardation time $T = t - \frac{r}{c}$, including $r = \sqrt{(x_1-\xi_1)^2 + (x_2-\xi_2)^2 + (x_3-\xi_3)^2}$, and c being the wave velocity. The first part of Equ. (2) can be neglected in the far-field, thus leaving

$$u_n(\vec{x}, t) \approx M_{pq}\int_0^\infty \dot{G}_{np}(\vec{x}, t-\tau)\frac{\delta T}{\delta\xi_q}d\tau = M_{pq}G_{np}(\vec{x}, t)\frac{\delta T}{d\xi_q}, \tag{3}$$

which can be used to infer radiation patterns for a general MT source.

The meaning of a MT is clearest when examining its eigenvalues and eigenvectors in the principal axis transformation (Jost & Herrmann, 1989; Dahm *et al.*, 2004):

$$M = \begin{bmatrix} a_{1x} & a_{2x} & a_{3x} \\ a_{1y} & a_{2y} & a_{3y} \\ a_{1z} & a_{2z} & a_{3z} \end{bmatrix} \begin{bmatrix} e_1 & 0 & 0 \\ 0 & e_2 & 0 \\ 0 & 0 & e_3 \end{bmatrix} \begin{bmatrix} a_{1x} & a_{1y} & a_{1z} \\ a_{2x} & a_{2y} & a_{2z} \\ a_{3x} & a_{3y} & a_{3z} \end{bmatrix}, \tag{4}$$

where a_i is the orthonormal eigenvector to the eigenvalue e_i. The eigenvalues e'_i of the deviatoric MT are defined by $e'_i = e_i - tr$ with the trace $tr = \frac{e_1 + e_2 + e_3}{3}$.

Assuming that $|e'_3| \geq |e'_1| \geq |e'_2|$, the MT can be decomposed in the following way:

$$\begin{bmatrix} e_1 & 0 & 0 \\ 0 & e_2 & 0 \\ 0 & 0 & e_3 \end{bmatrix} = tr \underbrace{\begin{bmatrix} 1 & 0 & 0 \\ 0 & 1 & 0 \\ 0 & 0 & 1 \end{bmatrix}}_{\text{isotropic}} + (e_1 - e_2) \underbrace{\begin{bmatrix} 1 & 0 & 0 \\ 0 & 0 & 0 \\ 0 & 0 & -1 \end{bmatrix}}_{\text{dev.: best DC}} + (e_2 - tr) \underbrace{\begin{bmatrix} 1 & 0 & 0 \\ 0 & 1 & 0 \\ 0 & 0 & -2 \end{bmatrix}}_{\text{dev.: CLVD}}. \tag{5}$$

The sum of the eigenvalues is related to the volume change in the source (isotropic part). If it is zero, only the deviatoric part exists. It represents a pure double couple (DC) source, if one of the eigenvalues vanishes. If this is not the case, the deviatoric MT can be decomposed either after Kanamori & Given (1981) into a major and minor DC or after Knopoff & Randall (1970) into a DC and a compensated linear vector dipole (CLVD).

Often, the minor DC or the CLVD reflect lateral heterogeneities in the Earth, noise in the data and the deviation of the earthquake from a point source, but in some cases, it may result from physical conditions as simultaneous ruptures on nearby faults with different orientations. Sources with large CLVD components have been observed in several complicated tectonic environments, *e.g.*, volcanic areas (Stein & Wysession, 2003).

Equ. (3) can be written in the simple matrix form (*e.g.*, Dahm *et al.*, 2004):

$$\vec{u} = \boldsymbol{GM} \tag{6}$$

which in time domain results in the linear inversion

$$\boldsymbol{m} = \boldsymbol{G}^{-1}\vec{u} \tag{7}$$

where $\boldsymbol{G}^{-1}$ is the generalized inverse. In frequency domain, the inversion becomes nonlinear due to the nonlinear dependence of the observed amplitude spectra on the MT elements. Equations have to be linearized by Taylor series expansions around a starting solution and iterative inversion schemes have to be used. The same holds true for certain constraints on the MT, *e.g.*, a constraint to a DC or a tensile crack.

Since the focal depth is not very well constrained, inversions can be performed for several depths, where the most probable depth will minimize the quadratic error between observed and theoretical waveforms, since differences in source depth influence the relative excitation of normal modes (Jost & Herrmann, 1989). The connection between source depth and results of MT inversion was analyzed by Sipkin (1982).

6.5.3 Program package MTINVERS

A program package called MTINVERS has been developed to perform MT inversion. The work steps include data pre-processing, picking of phases, calculation of Green's functions and finally the amplitude spectra inversion and inversion in time domain. The Green's functions are calculated applying the reflectivity code *refgreen* by Ungerer (1990). The program for MT inversion *mtinvers* has been provided by T. Dahm (University of Hamburg) and F. Krüger (University of Potsdam). A description of the code is given in Dahm *et al.* (2004). Seismic data processing is done using *EP* (Fyen, 2004). C-shell scripts and Fortran programs are employed as intermediary steps between codes, to construct input files and to direct the program flow.

Thus, the user has to fill in only one input file (called *input.list*) and to run only one script file (*input.csh*) to perform the whole process. Additionally, routines to test filtering and resampling have been developed along with GMT scripts (Wessel & Smith, 2003) for plotting of results and documentation has been prepared. Input parameters are:

For the pre-processing:

- time and location of earthquake, length of data extraction, filter parameters and sampling rate for body and surface waves individually

For the calculation of Green's functions:

- velocity model, depth range, slowness range, duration of earthquake as well as frequency range, sampling rate (same as for data) and number of integration points for body and surface waves individually

For the amplitude spectra inversion:

- inversion constraints, taper window, weight with distance and possibly a restricted frequency range for body and surface waves individually

For the inversion in time domain:

- depth of earthquake (result of amplitude spectra inversion).

Data pre-processing comprises broadband filtering, restitution to ground motion, resampling and rotation in 2-D. In principle, all kinds of phases can be picked. We confined the search to P-, SV-, SH-, Rayleigh and Love waves (P- and Rayleigh wave on vertical (z) component, SV- and Rayleigh wave on the radial (r) component and SH- and Love wave on the transverse (t)

component). Green's functions are calculated by the reflectivity method (e.g., Müller, 1985) in form of 8 elementary seismograms for z, r and t components. They are determined for a whole depth range, which is conserved for amplitude spectra inversion and only restricted to one depth during inversion in time domain by searching for the lowest misfit between observed and synthetic seismograms during amplitude spectra inversion. Other indicators for a stable solution can be a high DC percentage and the visual comparison of observed and calculated amplitude spectra and seismograms. After time domain inversion, the resulting MT is decomposed in isotropic and deviatoric parts. The deviatoric part is further split in best DC and CLVD.

Both amplitude spectra inversion and inversion in time domain have some assets and drawbacks. Amplitude spectra inversion is more complicated in a mathematical sense, since equations are non-linear. Further, since no phase information is used, the method cannot distinguish between compressive and dilatational quadrants. On the other hand, amplitude spectra inversion is more stable than time domain inversion if the data are not yet aligned to the synthetic seismograms and it is also more stable in the cases of wrong velocity models or source depths. Since time domain inversion is less stable for high frequencies, it is also less stable for inversion of body waves. Many institutes which routinely apply MT inversions use only surface waves for inversions in the time domain or filter the signal at very low frequencies. For the inversion of regional events as presented here, the frequency content is generally higher and cannot be neglected.

When using data from a broadband array, the automatic processing routine treats each array station individually and a weighting factor can be introduced before inversion. Additionally, it is possible to calculate the beam manually and insert it as a seismogram pretending that it comes from a single station. The first case is suitable for the NORSAR array where the interstation distance is large enough to record differences in waveforms (especially for the 07 April 2004 Flisa event), the second approach can be used for the Spitsbergen array to enhance the signal-to-noise ratio. Until now, only the first approach has been applied.

In the following, results of the application of the MT inversion in amplitude and time domain to regional events are presented. Since the focus lies on testing of the method, only little or no interpretation of the MT solutions is given.

6.5.4 Results

Observed seismograms and theoretically calculated Green's functions are strongly depending on the velocity structure seen by the seismic waves. In Fig. 6.5.1, the different velocity models applied in this study are plotted and the PREM model is shown for comparison.

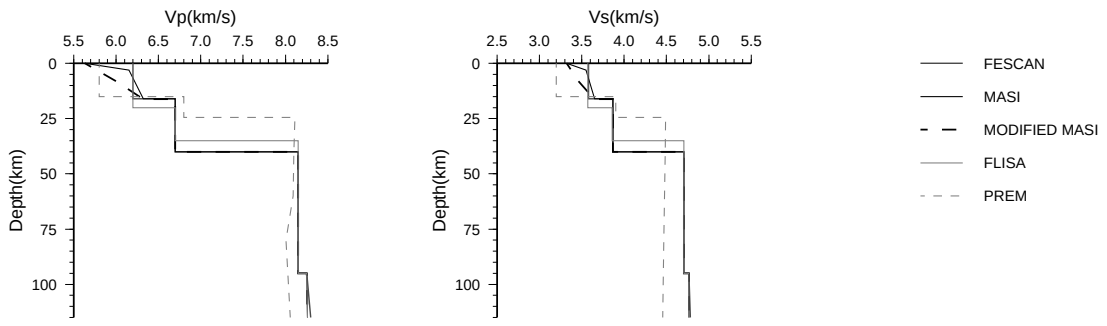

Fig. 6.5.1. Velocity models applied in this study.

At first, Green's functions have been calculated according to the standard velocity model used at NORSAR (FESCAN). Since this model does not sufficiently reproduce the surface wave dispersion, the MASI model by Roth & Bungum (2003) was also tested. Results were satisfactory for the Svalbard event, but not for the Jan Mayen event. Therefore, the MODIFIED MASI model was developed by trial-and-error resulting in lower velocity gradients in the upper crust. For the Flisa event, the velocity model by Schweitzer (2005) is used. The depth extent of the models is larger than displayed in Fig. 6.5.1.

The 14 April 2004 Jan Mayen earthquake

The 14 April 2004 Jan Mayen earthquake as well as the 04 July 2003 Svalbard earthquake were used for calibration of the parameters used during the calculation of Green's functions and inversion, especially the velocity models. The Jan Mayen event has a magnitude of Mw= 5.9 (HRVD, Harvard CMT catalog, 1998) and the epicenter is located at 7.747˚W and 71.067˚N. Fig. 6.5.2 shows the epicenter as a black star and the stations, which recorded data (APZ9, ARE0, FIA1, HFC2, KBS, NOA, and VSU), are shown as as grey triangles to give an impression of the azimuthal coverage.

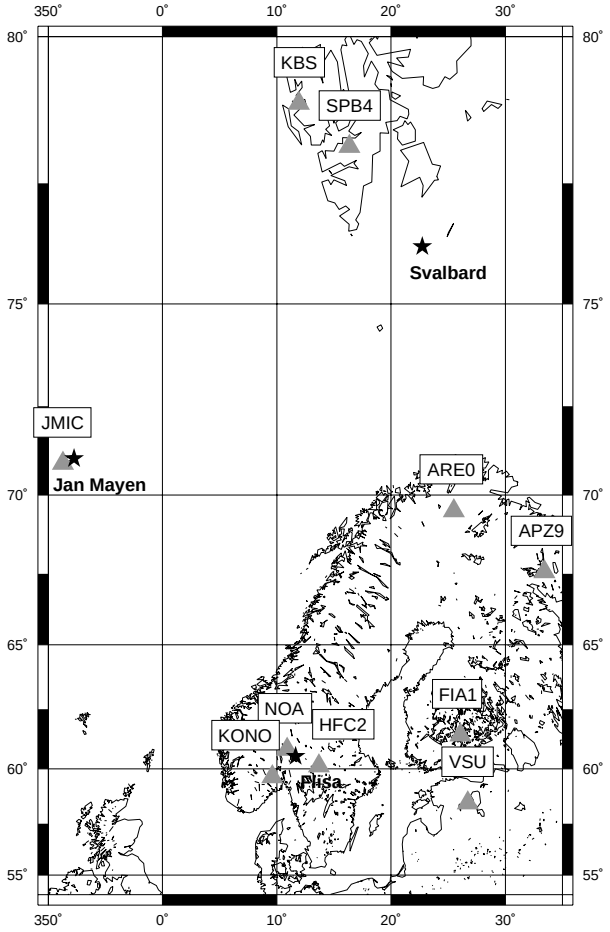

Fig. 6.5.2. Epicenters of the investigated earthquakes (Jan Mayen, Svalbard and Flisa) are shown as black stars and seismic stations (arrays) for which data have been used in this study are shown as grey triangles.

Fig. 6.5.3 shows the broadband filtered, restituted, resampled and rotated data as used in the inversion process; the filter parameters were chosen according to the surface wave analysis.

For the amplitude spectra inversion, the whole frequency range of 0.01 – 0.3 Hz was used for body waves and 0.01 – 0.07 Hz for surface waves, respectively. The MASI velocity model was used for the calculation of Green's functions, since the firstly applied FESCAN model proved inappropriate to excite surface waves sufficiently. The inversion results are displayed in Fig. 6.5.4 for a depth range from 2 to 8 km. Isotropic and DC percentage are of the same order for all depths, but the focal solution is rotated slightly and the misfit has a clear minimum at a depth of 5 km.

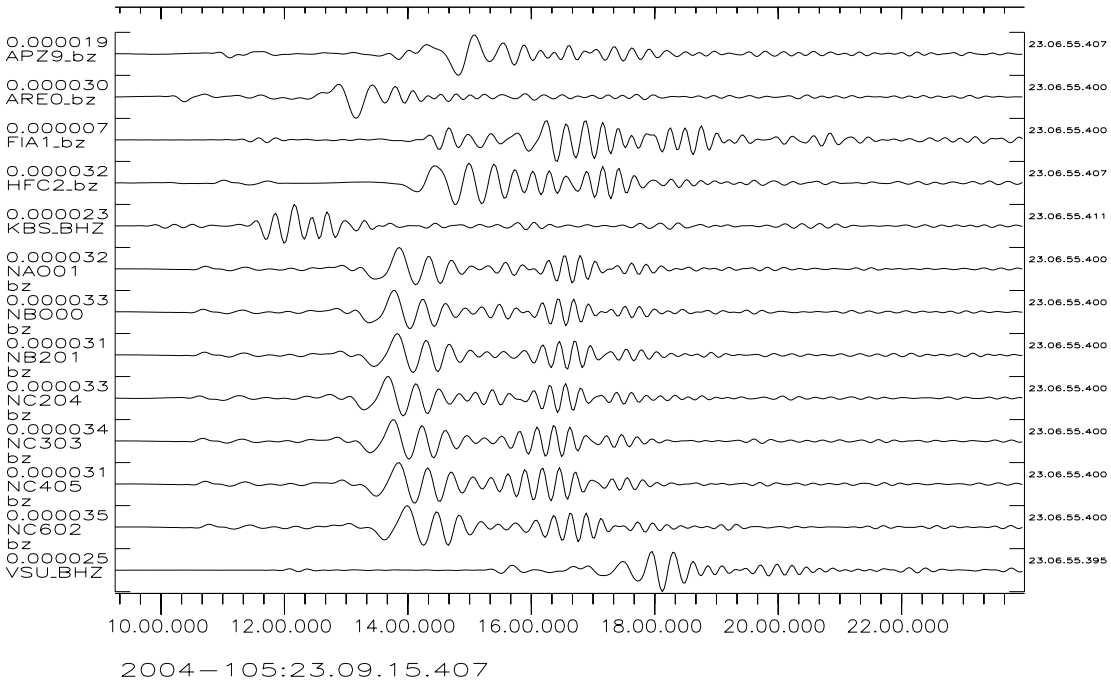

Fig. 6.5.3. Broadband filtered, restituted, resampled and rotated data; the data are prepared for surface wave analysis (filtered by 0.01 – 0.07 Hz); only z components are displayed.

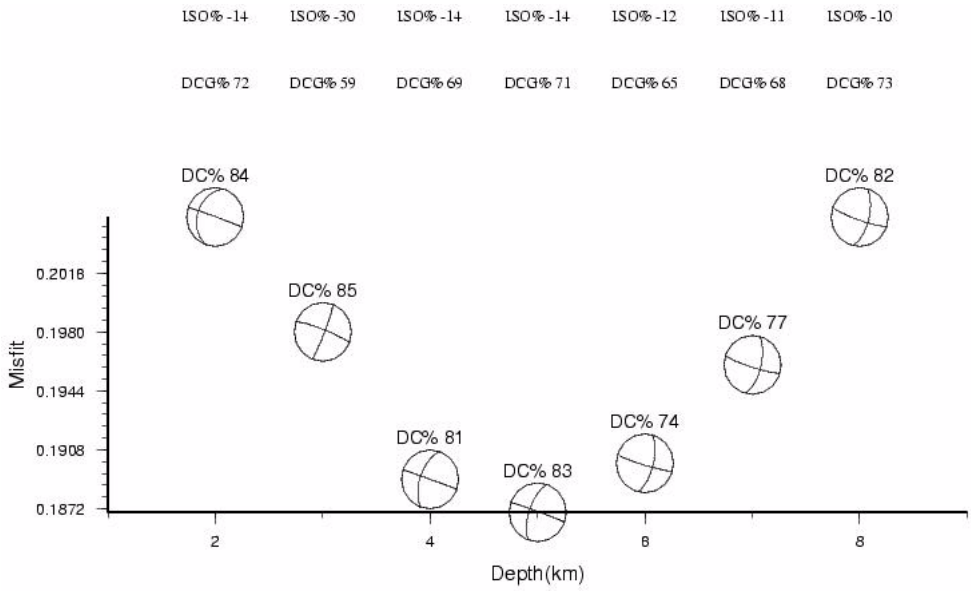

Fig. 6.5.4. Results of the amplitude spectra inversion: misfit and focal solutions for different depths.

The inversion in time domain was carried out in three steps of increasing frequency content. At first, body waves were filtered prior to inversion at 0.01 – 0.05 Hz and surface waves at 0.01 – 0.03 Hz, resulting in a misfit of 0.220. Next, the body wave frequency range amounted to 0.01-0.15 and the surface frequency range to 0.01 – 0.05 Hz with a misfit of 0.428. Finally, the frequency content covered the whole range of the pre-processed data between 0.01 – 0.3 Hz for body waves and 0.01 – 0.07 Hz for surface waves, yielding a misfit of 0.579.

In Fig. 6.5.5, the deviatoric MT and DC produced by MTINVERS are compared to the solutions of Harvard (HRVD, Harvard CMT catalog, 1998) and ETH Zürich (ZUR_RMT, Bernardi *et al.*, 2004), respectively. Further parameters produced by the MT inversion are listed in Table 6.5.1.

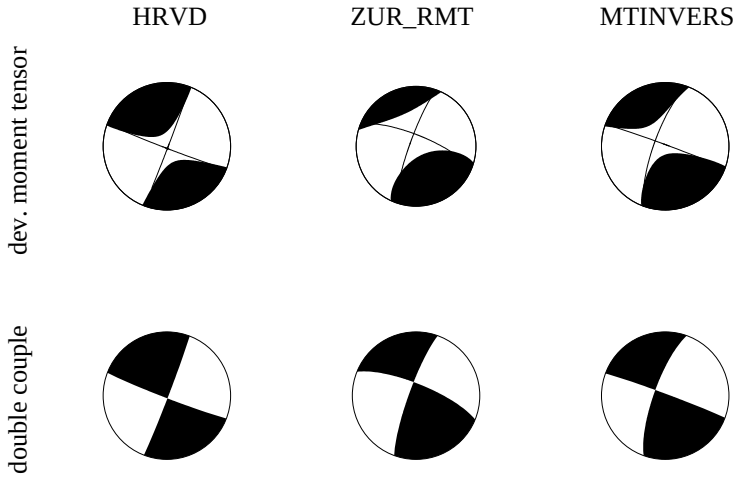

Fig. 6.5.5. Comparison of the deviatoric MTs (top) and DC parts (bottom) of the investigated Jan Mayen event as inverted with MTINVERS and as published by Harvard (Harvard CMT catalog, 1998) and ETH Zürich (Bernardi et al., 2004).

Table 6.5.1. Seismic moment, focal depth and fault plane solution as derived by MTINVERS and as published by Harvard (Harvard CMT catalog, 1998) and ETH Zürich (Bernardi *et al.*, 2004).

	HRVD	ZUR_RMT	MTINVERS
M0 (Nm)	7.90E+17	1.00E+18	3.40E+17
Depth (km)	12	12	5
Strike 1	111	200	199.8
Dip 1	87	81	75.7
Rake 1	2	165	177.6
Strike 2	21	292	290.4
Dip 2	88	75	87.6
Rake 2	177	9	14.3

Although the misfit provided by MTINVERS is rather high, the agreement between MT and the solutions determined by Harvard and ETH Zürich is good, the MTINVERS solutions for deviatoric MT and DC giving the visual impression of lying between the other two. The focal depth (given in Table 6.5.1) differs, but is still in the same range. The isotropic part amounts to 15%, the DC percentage is 70%.

The fit between observed and synthetic seismograms can be seen in Fig. 6.5.6. The MT solution in Fig. 6.5.5 was assumed as source signal. On the left, body wave cutouts are presented, surface waves cutouts are visible on the right. Time scales (in samples) are the same for each column. Columns from left to right show phases from the vertical, radial and transverse com-

ponent. Unfortunately, no body waves were detected on the transverse component. Observed data are plotted by black lines, calculated seismograms are displayed as grey lines. Stations and maximum amplitudes are indicated for each trace.

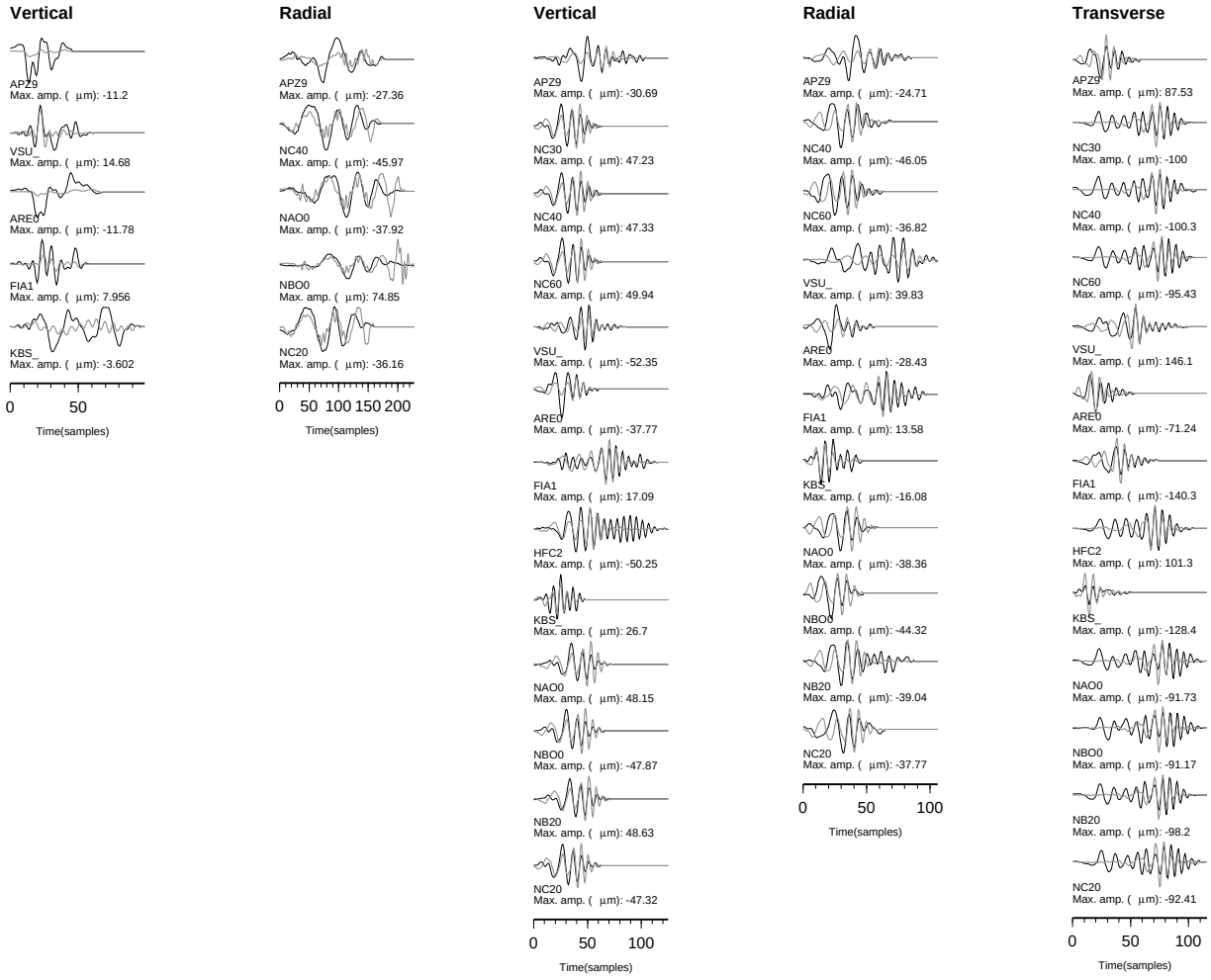

Fig. 6.5.6. Fit between observed data (black lines) and synthetic seismograms (grey lines) with the MT source assumed as in Fig. 6.5.5; left: body waves, right: surface waves.

Surface wave fits are much better than body wave fits, since lower frequencies were used for inversion. Nevertheless, the seismograms are approximated sufficiently in most of the body wave cases, even if the observed seismograms are smoother. The poor fit at station KBS can be explained by the fact that in this case the seismic waves propagate exclusively through an oceanic crust and uppermost mantle, whereas the velocity model is designed for a continental crust and uppermost mantle. Synthetic seismograms at stations APZ9 and ARE0 also differ from the observations, but agree very well at the NORSAR array.

The 04 July 2003 Svalbard event

The second event used for calibration is the 04 July 2003 Svalbard event with a magnitude of Mw = 5.4 (HRVD, Harvard CMT catalog, 1998). Its location is at 22.745˚E and 76.253˚N. The azimuthal coverage with recording broadband stations (APZ9, ARE0, FIA1, HFC2, JMI, KBS, KONO, and NOA) is better than in the case of the Jan Mayen event, where all stations were situated east of the epicenter (see Fig. 6.5.2). The pre-processed data shown (Fig. 6.5.7) are filtered with parameters, suitably chosen for body wave analysis.

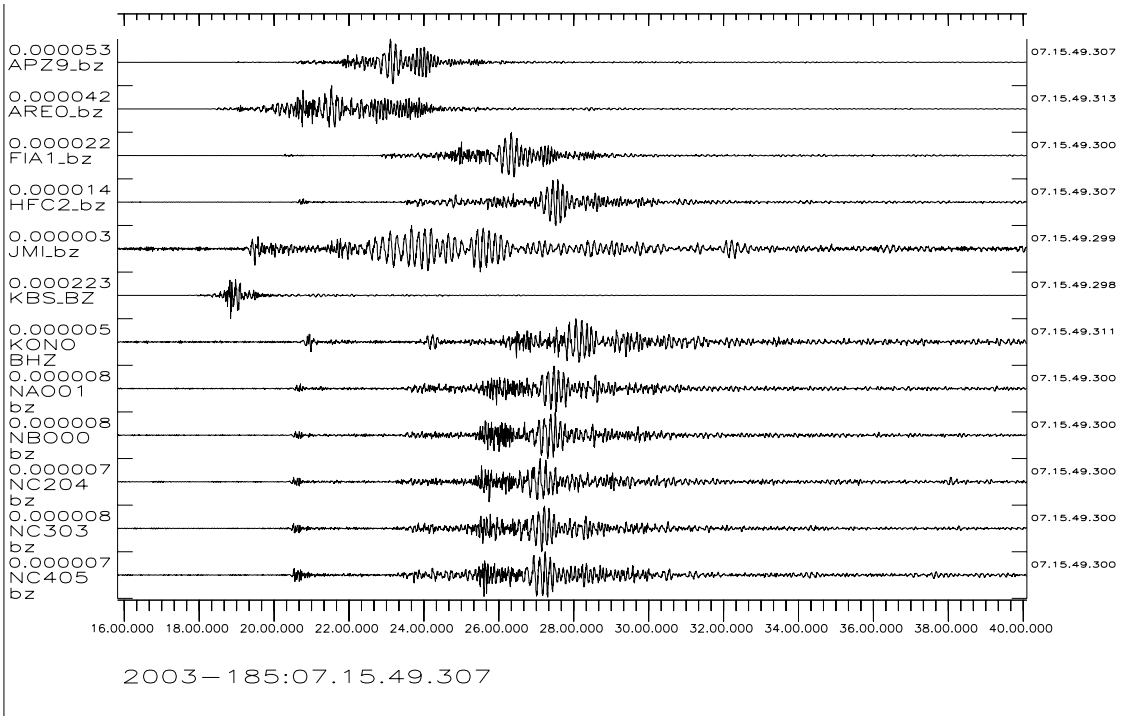

Fig. 6.5.7. Broadband filtered, restituted, resampled and rotated data; data are prepared for body wave analysis (filtered by 0.1 – 0.5 Hz); only vertical components are displayed.

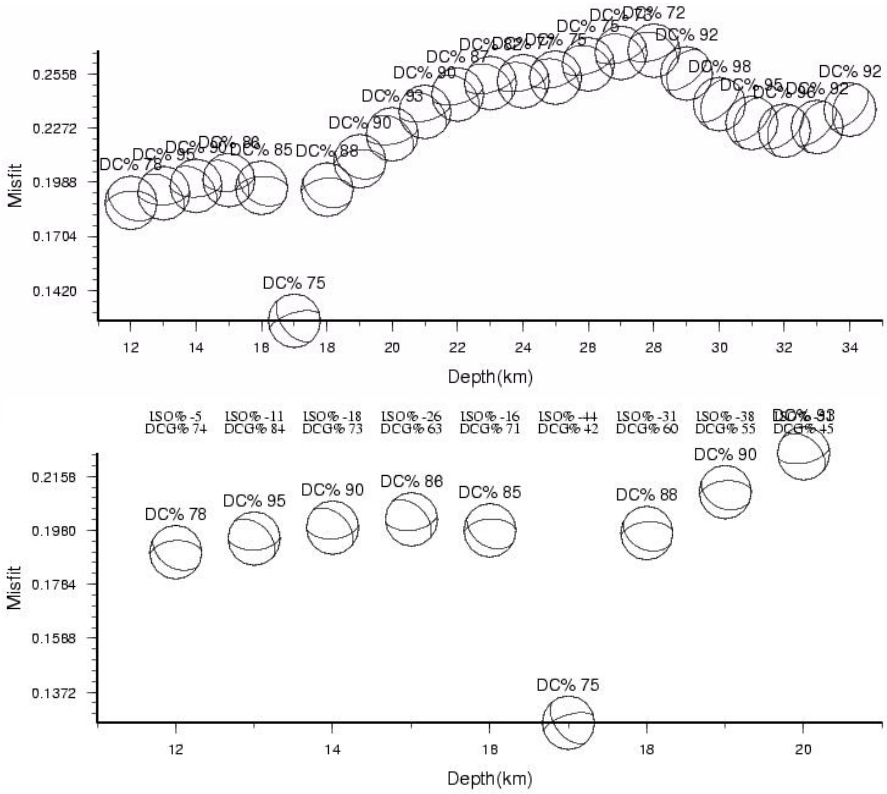

Fig. 6.5.8. Results of amplitude spectra inversion: misfit and focal solution plotted against depth; the bottom picture is a cutout of upper graphic.

In contrast to the Jan Mayen event, only higher frequencies could be used for body wave analysis (0.1 – 0.5 Hz) for the Svalbard event, whereas the frequency range used for surface waves is similar (0.01 – 0.05 Hz). Since the hypocenter depth has been calculated to be 33 ± 13 km by Stange & Schweitzer (2004), amplitude spectra inversions were computed for a broad depth range from 10 – 60 km. As can be seen in Fig. 6.5.8, the misfit increases towards higher depths, although a second minimum can be detected around 32 km. However, all solutions in the depth range of 12 – 20 km are quite similar (exept for some rotation) but a clear minimum can be found at a depth of 17 km, even if featuring a smaller DC percentage.

For inversion in the time domain, the following filter steps were applied: a) 0.1 – 0.23 Hz for body and 0.01 – 0.023 Hz for surface waves, b) 0.1 – 0.36 Hz for body and 0.01 – 0.036 for surface waves and c) 0.1 – 0.5 Hz for body and 0.01 – 0.05 Hz for surface waves, resulting in misfits of 0.240, 0.291 and 0.342 respectively, which is better than the misfit obtained for the Jan Mayen event. To successfully model the surface-wave dispersion, Green's functions were calculated by using the modified MASI model (Fig. 6.5.1). Both the deviatoric MT and the DC are presented in Fig. 6.5.9 for comparison with solutions from Harvard (Harvard CMT catalog, 1998) and ETH Zürich (Bernardi *et al.*, 2004). Table 6.5.2 provides all parameter values.

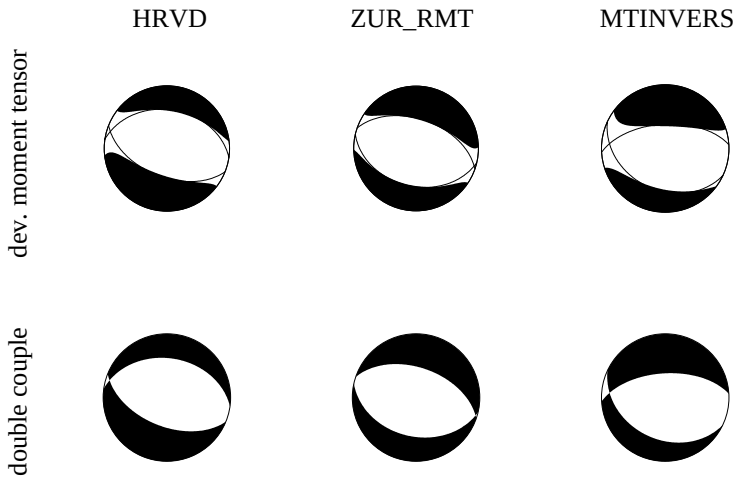

Fig. 6.5.9. Comparison of the deviatoric MTs (top) and DC parts (bottom) of the investigated Svalbard event as inverted with MTINVERS and as published by Harvard (Harvard CMT catalog, 1998) and ETH Zürich (Bernardi et al., 2004).

Table 6.5.2. Comparison of seismic moment, focal depth and fault plane solution produced by MTINVERS with results from Harvard and ETH Zürich.

	HRVD	ZUR_RMT	MTINVERS
M0 (Nm)	2.20E+17	1.80E+17	1.30E+17
Depth (km)	15	15	17
Strike 1	278	289	266.6
Dip 1	38	51	58.7
Rake 1	-101	-86	-105.9
Strike 2	112	103	115.2
Dip 2	53	39	34.8
Rake 2	82	-95	-65.8

The solutions are very similar, but the deviatoric tensor and the DC computed by MTINVERS are a little bit rotated. The depth is consistent and the seismic moment is in the same order of magnitude. The isotropic part amounts to 37% of the complete MT, the DC percentage is only

59%. The parameter "DC percentage" should not be overrated, since it is not well resolved by this type of inversion. The hypocentral depth of 17 km is probable, since Stange & Schweitzer (2004) state that recorded seismograms indicate a hypocenter within the crust. The fit between the observed data and synthetic seismograms is displayed in Fig. 6.5.10. In the surface wave frequency range, the fit between observed and calculated seismograms is extraordinarily good. Even for the high frequency body waves, the similarity is high. Synthetic seismograms and observations disagree the most at stations ARE0, JMI, KBS and SPB4.

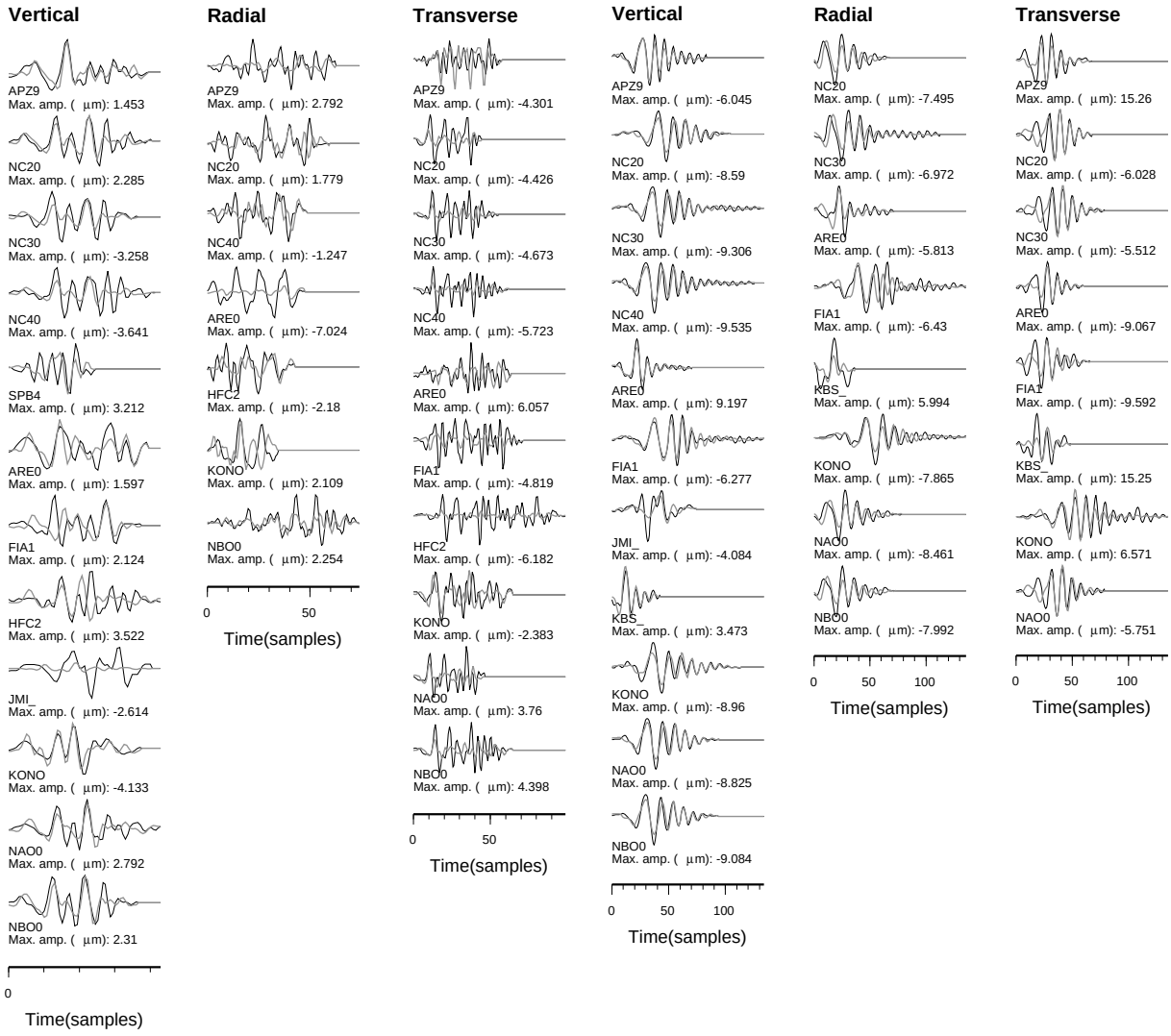

Fig. 6.5.10. Fit between observed data (black lines) and synthetic seismograms (grey lines) with MT source assumed as in Fig. 6.5.9; left: body waves, right: surface waves.

The 07 April 2004 Flisa event

The 07 April 2004 Flisa event affords the unusual opportunity to analyze an event occurring close to the NORSAR array with a magnitude of 3.5. The closest epicentral distance is less than 20 km. Its coordinates were 11.6526˚E and 60.5511˚N (Schweitzer, 2005; Fig. 6.5.11). The azimuthal coverage is enhanced by the recordings of station HFS. Because of the proximity to the epicenter, no surface waves can be observed (Fig. 6.5.12).

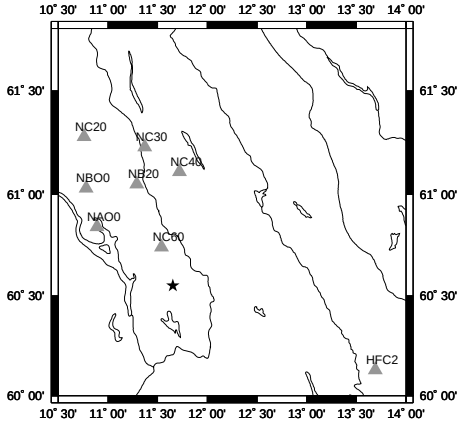

Fig. 6.5.11. The Flisa event epicenter (star) and the stations used for MT inversion (triangles).

The data are filtered by 0.5 – 1.0 Hz. For this event, only an amplitude spectra inversion has been performed so far. Instead of trying to isolate single phases, the wave train is included as a whole. For calculations, the FLISA velocity model by Schweitzer (2005) is used. In Fig. 6.5.13, the misfit-against-depth curve is reproduced.

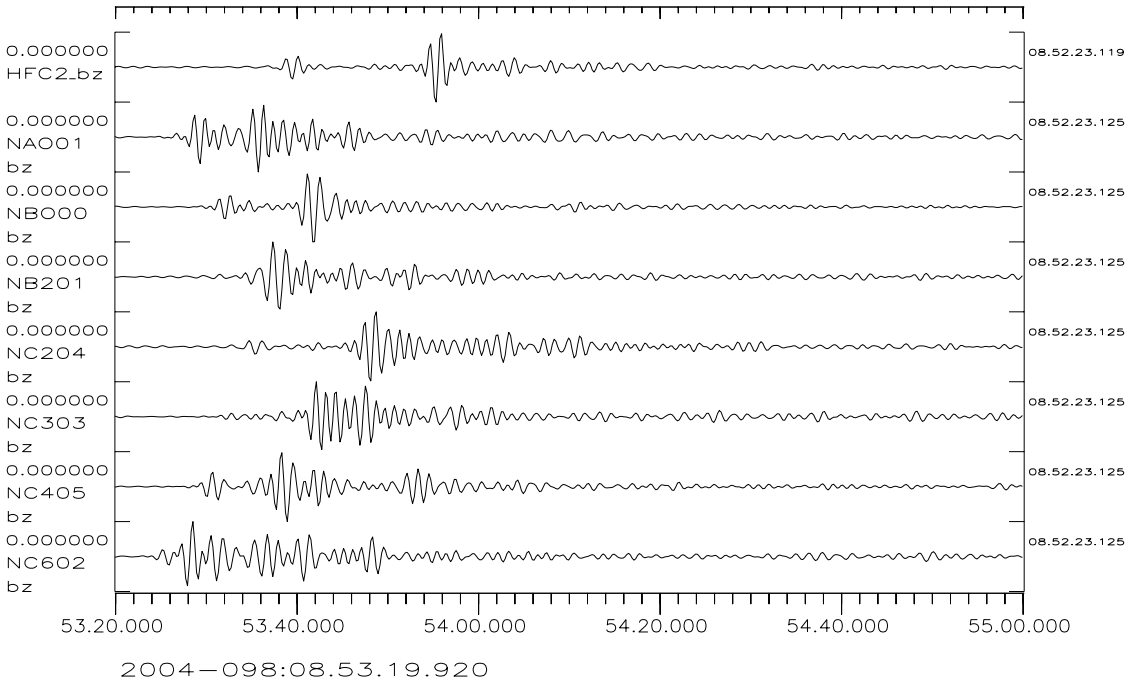

Fig. 6.5.12. Broadband filtered, restituted, resampled and rotated data (filtered by 0.5 – 1.0 Hz).

Two minima can be distinguished, the broader of which is at a depth of 20 km and has a slightly lower misfit of 0.247. The isotropic part amounts to 32% and the DC percentage is 52%. The seismic moment is computed to be 2.2E+14 Nm. The DC solutions are quite stable over a large depth range.

The DC solution given by Schweitzer (2005; Fig. 6.5.14) resulting from polarities of first onsets is extraordinarily constrained by a polarity change of P onsets across the NORSAR array, which is not as clear if one only looks at the broadband stations used for MT inversion. Further, stations from whole Fennoscandia and Estonia were included in the analysis and PmP

polarities at the vertical components of the subarray NC2 were incorporated to restrict the number of possible solutions. These are probably also distinguishable at the central broadband station, but since the seismogram was included as a whole, small amplitudes are attached less importance, so that the PmP onsets might not be of help during an eventual inversion in the time domain.

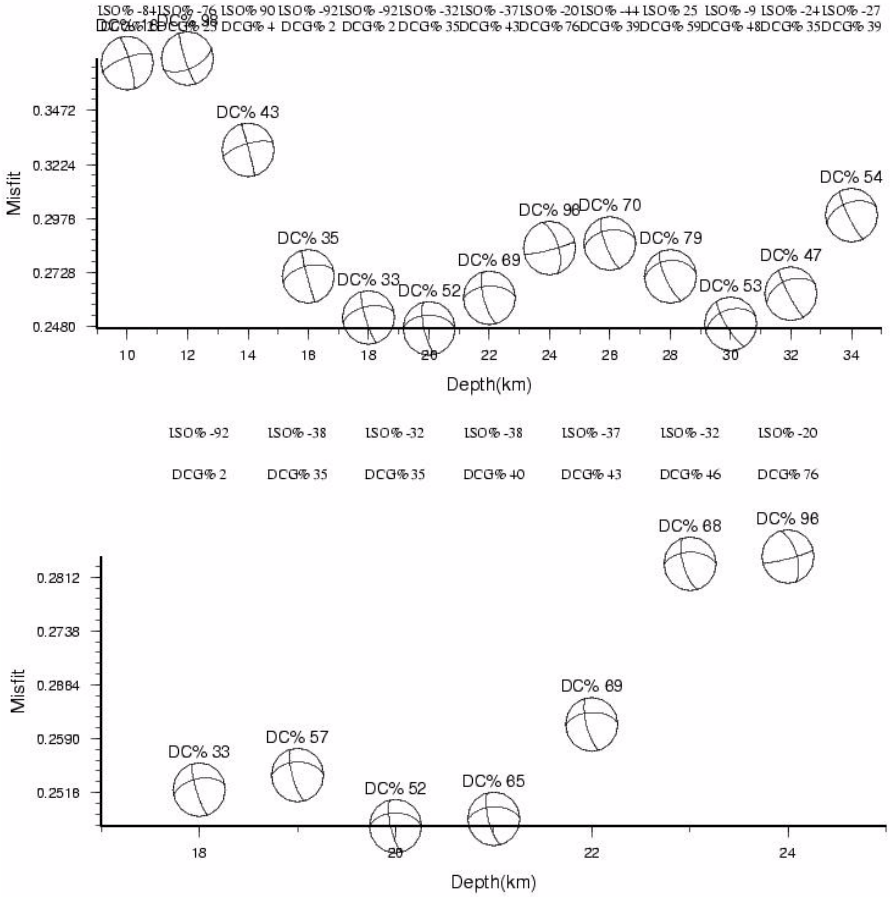

Fig. 6.5.13. Results of the amplitude spectra inversion: misfit and focal solution are plotted against depth; the bottom picture is a cutout of upper graphic.

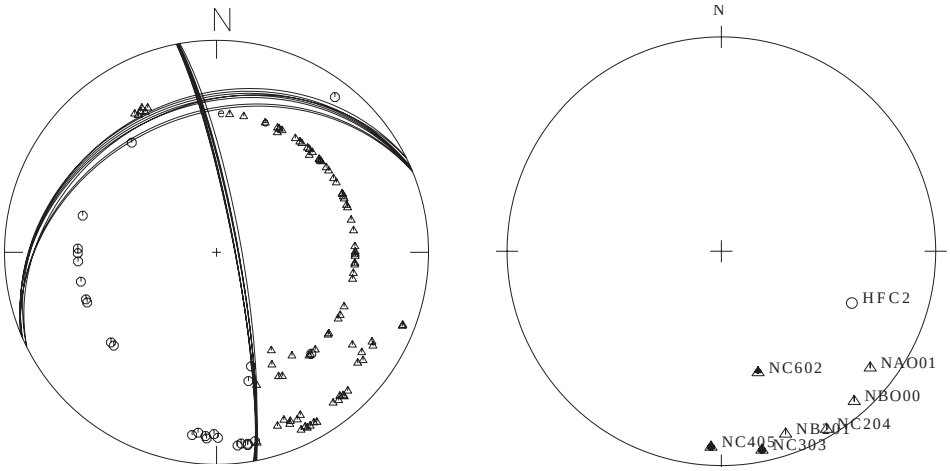

Fig. 6.5.14. Comparison of station distribution; left: stations used by Schweitzer (2005), right: broadband stations available for MT inversion by MTINVERS.

Schweitzer (2005) interprets the steep, north-south striking plane as fault plane consistent with other earthquakes in the Oslo Graben area. The focal depth was determined to be 22.5 km. Fig. 6.5.14 displays a comparison of the station distribution as used by Schweitzer (2005) on the left and the broadband stations available for MT inversion by MTINVERS.

The steep, north-south striking fault plane can be identified as well in the MTINVERS DC solutions. The strike and dip of the auxiliary plane is different, but as can be seen clearly in Fig. 6.5.14, no data were available to constrain its position. Including more stations would clearly improve the solution as well as data from relevant short period stations.

In Fig. 6.5.15, a comparison between observed data and synthetic seismograms is shown. The MT resulting from amplitude spectra inversion is used as source function. Especially for shorter signals, the fit is surprisingly good. Since seismograms have not yet been aligned in time, offsets between both traces can be identified in some cases (*e.g.*, vertical components of NC3 and NC4, radial components of HFC2 and NC3). This may also cause the problem in modelling the radial component of NC4: a wrong cutout which does not even contain the desired signal may have been used for the inversion. In general, the synthetic seismograms tend to be shorter than the observed wave trains, which may be caused by too simple velocity model not correcting for station or scattering effects.

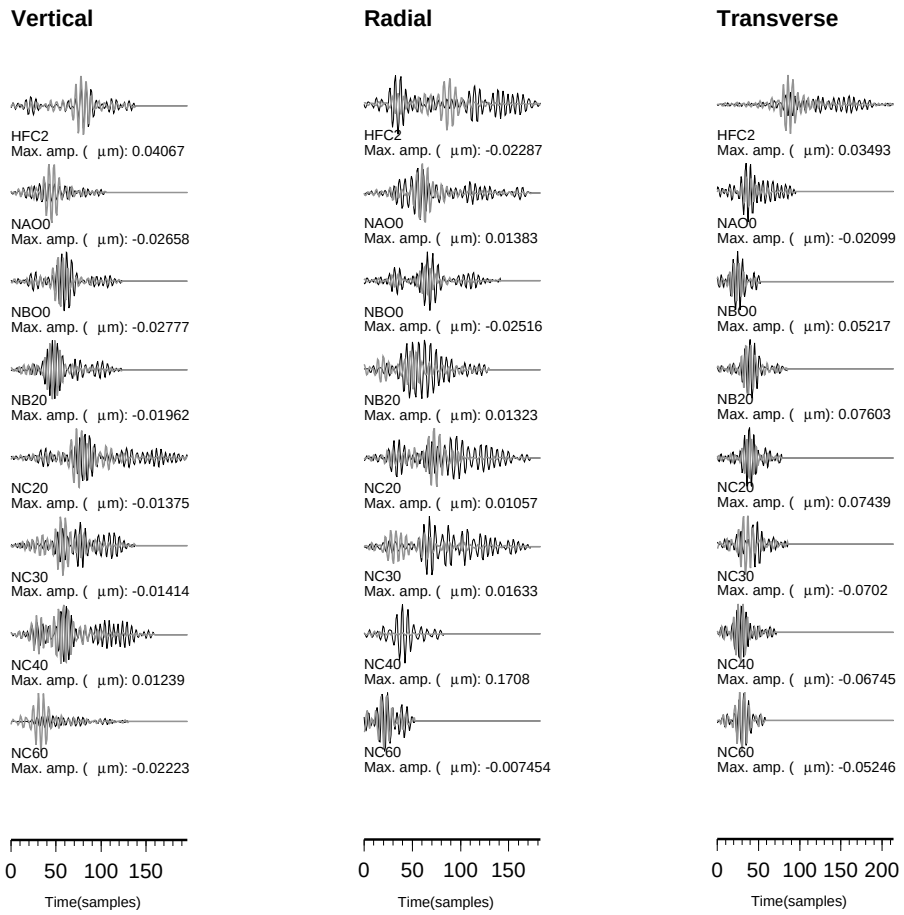

Fig. 6.5.15. Fit between observed data (black lines) and synthetic seismograms (grey lines) with MT source assumed as in Fig. 6.5.13; from left to right: vertical, radial and transverse component.

6.5.5 Conclusions

In general, surprisingly good results were obtained for the regional MT inversion of the 14 April 2004 Jan Mayen and the 04 July 2003 Svalbard event, although the azimuthal coverage is generally not very good when using only regional data directly available at NORSAR. The most critical working step is the alignment of seismograms and Green's functions along with determining the length of the phase analysis window. The longer the phase analysis window, the more information is contained, but at the same time, the risk of overlapping with further phases not aligned correctly in time due to an insufficient velocity model is larger.

The velocity model FESCAN used at first turned out to be too simple for this regional inversion and had to be adjusted by trial-and-error fitting of synthetic to observed seismograms to inprove the modelling of surface wave dispersion.

For regional events, a higher impact in velocity model differences between source and receiver region is noticeable (*e.g.*, oceanic/continental crust, amount of sediments). The larger high-frequency energy content compared to teleseismic events demands a higher accuracy of the velocity model. The oceanic microseismic noise peak in the range of 0.1 – 0.2 Hz overlaps with the body wave frequency spectrum. A judgement of the fit of observed and synthetic seismograms considering the misfit alone is sometimes insufficient (*e.g.,* a bad misfit can be caused by a poor fit at one single station, explainable by an incorrect velocity model). Since the misfit is no objective measure, depending *e.g.,* on time length of the phase analysis window and the frequency content, a comparison to other studies is difficult. Nevertheless, it is a useful tool to compare MT results for individual earthquakes.

In more special cases as that of the 07 April 2004 Flisa event, MT inversions are more difficult. Maybe more stations have to be used to better constrain the auxiliary plane. Even short-period stations may be included, since due to its small size, the high-frequency content of the earthquake is unusually large compared to the Jan Mayen and Svalbard event.

In general, a good velocity model is crucial. It can either be prepared elaborately by incorporating results from other geological or geophysical studies or it can be adapted by hand, which is a very time consuming process.

Another possibility is the application of "pseudo 2-D" velocity models. Raypaths for various source-receiver geometries can be classified in more oceanic or more continental pathways and different 1-D velocity models can be used to calculate the Green's functions for each pair. Besides, other reflectivity codes exist which allow for variable underground models for source and receiver region.

Theoretically, it is possible to apply a 3-D velocity model, but new programs have to be developed. Then, the reflectivity method cannot be applied to compute Green's functions, and *e.g.*, finite-differences or pseudo-spectral codes must be used. MTINVERS has to be adapted, since at the moment, 8 Green's functions are introduced, whereas in the more general 3-D case, 27 Green's functions are required.

Acknowledgments

This project was financially supported by the DAAD (Deutscher Akademischer Austauschdienst, German Academic Exchange Service). Daniela Kühn would like to thank Torsten Dahm and Frank Krüger for e-mail support.

Daniela Kühn, University of Hamburg
Johannes Schweitzer

References

Aki, K. & Richards, P.G. (1980). *Quantitative Seismology: Theory and Methods*. W. H. Freeman and Co., New York, San Francisco.

Backus, G.E. & Mulcahy, M. (1976). Moment tensors and other phenomenological descriptions of seismic sources – I. Continuous displacements. *Geophys. J. R. A. S.*, **46**, 341-361.

Backus, G.E. (1977a). Interpreting the seismic glut moments of total degree two or less. *Geophys. J. R. A. S.*, **51**, 1-25.

Backus, G.E. (1977b). Seismic sources with observable glut moments of spatial degree two. *Geophys. J. R. A. S.*, **51**, 27-45.

Bernardi, F., Braunmiller, J., Kradolfer, U. & Giardini, D. (2004). Automatic regional moment tensor inversion in the European-Mediterranean region. *Geophys. J. Int.*, **157**, 703-716.

Bruhns, C. (2003). *Momententensoren hochfrequenter Ereignisse in Südchile*. PhD Thesis, Universität Potsdam.

Dahm, T. & Krüger, F. (1999), Higher-degree moment tensor inversion using far-field broad-band recordings: theory and evaluation of the method with application to the 1994 Bolivia deep earthquake. *Geophys. J. Int.*, **137**, 35-50.

Dahm, T., Manthei, G. & Eisenblätter, J. (1999). Automated moment tensor inversion to estimate source mechanisms of hydraulically induced micro-seismicity in salt rock. *Tectonophys.*, **306**, 1-17.

Dahm, T., Krüger, F., Stammler, K. & Yuan, X. (2004). Moment tensor inversion – a practical for beginners. ESC Young Scientist Trainings Course, 09-12 September 2004, Potsdam, Germany.

Fyen, J. (2004). *EP – Command Reference and User Guide*. NORSAR.

Gilbert, F. (1973). Derivation of source parameters from low-frequency spectra. *Phil. Trans. Roy. Soc. London*, **A**(274), 369-371.

Harvard CMT catalog (1998). CMT catalog search. Available from World Wide Web: http://www.seismology.harvard.edu, Department of Earth and Planetary Sciences, Harvard University, United Kingdom.

Jost, M.L. & Herrmann, R.B. (1989). A student's guide to and review of moment tensors. *Seis. Res. Lett.*, **60**(2), 37-57.

Kanamori, H. & Given, J. (1981). Use of long-period surface waves for rapid determination of earthquake-source parameters. *Phys. Earth Plan. Int.*, **27**, 8-31.

Knopoff, L. & Randall, M.J. (1970). The compensated linear-vector dipole: a possible mechanism for deep earthquakes. *J. Geophys. Res.*, **75**, 4957-4963.

Krüger, F. & Dahm, T. (2002). The 1992 Roermond earthquake, a regional event study. In Senate Commission for Geoscience, Editor, *Ten Years of German Regional Seismic Network (GRSN)*, Report 25, DFG.

Müller, G. (1985). The reflectivity method: a tutorial. *J. Geophys. Res.*, **58**, 153-174.

Roth, M. & Bungum, H. (2003). Waveform modeling of the 17 August 1999 Kola Peninsula earthquake. *Bull. Seis. Soc. Am.*, **93**(4), 1559-1572.

Schweitzer, J. (2005). The 7 April 2004 Flisa, Southern Norway earthquake sequence – eight hypocenter determinations and one focal mechanism. *NORSAR Sci. Rep.*, **1-2005**, 62-76.

Sipkin, S.A. (1982). Estimation of earthquake source parameters by the inversion of waveform data: synthetic waveforms. *Phys. Earth Plan. Int.*, **30**, 242-255.

Stange, S. & Schweitzer, J. (2004). Source depths at regional distances: an example from the Western Barents Sea/Svalbard Region. *NORSAR Sci. Rep.*, **1-2004**, 45-50.

Stein, S. & Wysession, M. (2003). *An Introduction to Seismology, Earthquakes and Earth Structure*. Blackwell Publishing.

Ungerer, J. (1990). Berechnung von Nahfeldseismogrammen mit der Reflektivitätsmethode. Institut für Geophysik, Universität Stuttgart. Diplomarbeit.

Wessel, P. & Smith, W.H.F. (2003). *GMT – Technical Reference and Cookbook*. School of Ocean and Earth Science and Technology. Version 3.4.3.